SALT TECTONIC CONTROLS ON FACIES AND SEQUENCE STRATIGRAPHY OF THE TRIASSIC CHINLE FORMATION, GYPSUM VALLEY SALT WALL, COLORADO

ELIZABETH ANNE HENESS

Master's Program in Geological Science

APPROVED:

Richard P. Langford, Ph.D., Chair

Katherine A. Giles, Ph.D.

Carl Lieb, Ph.D.

Charles Ambler, Ph.D.
Dean of the Graduate School

Copyright ©

by

Elizabeth Anne Heness

2016

Dedication

For my neighbor Len, many summers were spent in his garden learning about the earth.

SALT TECTONIC CONTROLS ON FACIES AND SEQUENCE STRATIGRAPHY OF THE TRIASSIC CHINLE FORMATION, GYPSUM VALLEY SALT WALL, COLORADO

by

ELIZABETH ANNE HENESS, B.S.

THESIS

Presented to the Faculty of the Graduate School of

The University of Texas at El Paso

in Partial Fulfillment

of the Requirements

for the Degree of

MASTER OF SCIENCE

Department of Geological Science

THE UNIVERSITY OF TEXAS AT EL PASO

May 2016

ProQuest Number: 10118803

All rights reserved

INFORMATION TO ALL USERS
The quality of this reproduction is dependent upon the quality of the copy submitted.

In the unlikely event that the author did not send a complete manuscript
and there are missing pages, these will be noted. Also, if material had to be removed,
a note will indicate the deletion.

ProQuest 10118803

Published by ProQuest LLC (2016). Copyright of the Dissertation is held by the Author.

All rights reserved.
This work is protected against unauthorized copying under Title 17, United States Code
Microform Edition © ProQuest LLC.

ProQuest LLC.
789 East Eisenhower Parkway
P.O. Box 1346
Ann Arbor, MI 48106 - 1346

Acknowledgements

I would like to thank my professors, family, and friends who supported me, through good and bad times. Many of us do not realize the impact that we have on each other, for those who have impacted me I am truly blessed.

Abstract

This study focuses on mapping the facies geometry and depositional sequences of the Chinle Formation adjacent to the Gypsum Valley Salt Wall (GVSW). Interactions between salt tectonics and fluvial systems can affect sediment distribution. The upper Triassic Chinle Formation was deposited across the western U.S. in an intra-cratonic, fluvial environment. Throughout the Paradox Basin in Utah and Colorado, deformation associated with rising salt anticlines and subsiding minibasins coincided with Chinle deposition. In most areas, only small and isolated remnant Chinle outcrops actually expose the contact between Chinle sediments and the salt diapir. In Gypsum Valley three study areas were mapped and sampled based on proximity to the GV diapir, and a fourth location, 12 km from the diapir was chosen as a standard to compare and contrast with Chinle facies documented proximal to the diapir. Fifteen correlated stratigraphic sections illustrate the stratigraphy and the distribution of the Chinle facies.

Near the diapir, conglomeratic facies contain clasts predominately composed of carbonate eroded from the diapir caprock. The carbonate conglomeratic lenses disappear within 0.7 km of the diapir. Individual sandstone channels are 0.5 – 1.0 m thick and extend roughly 2.0 m on outcrop. Channels are laterally stacked and, in some units, vertically stacked. Red siltstones, over 16 m thick form overbank deposits, that separate channel complexes. Within the expanse of overbank deposits, paleosols 0.5 meters in thickness consist of blocky clay peds, and in some instances exhibit extensive sand-rich lateral rooted horizons. Along strike channels, overbank deposits and lacustrine deposits are traceable for ~3.5 km. Lacustrine units contain abundant septerian nodules and sandstone concretions. Debris flows are restricted to areas where the Chinle Formation is in contact with the underlying diapir caprock. By contrast, 12 km from the diapir, ~50 meters of coarse to medium grained sandstone predominate, no caprock conglomerates occur, indicating that the material either breaks down before traveling far, or the presence of a depositional barrier to the diapir derived carbonate clast/grain dispersal. Petrographic analysis indicates a complex cement history that changes with proximity to the diapir. A fourth Halokinetic Sequence is reported that records angular unconforities of 3-10 degrees.

Table of Contents

Acknowledgements v

Abstract vi

Table of Contents vii

List of Tables ix

Chapter 1: Introduction 1

1.1 Background and Geological Setting: 3

1.2 Salt Tectonism and Sedimentation: 10

1.3 Regional Setting of Gypsum Valley: 11

1.4 Previous Work: Salt Tectonism and Chinle Stratigraphy: 14

1.5 Study Areas: 16

1.6 Methods (Analysis): 16

Chapter Two: Chinle Lithofacies and Facies Associations of the late Triassic Chinle Formation 19

2.1 Lithofacies 25

2.2 Facies Associations 30

2.3 Differences in Facies Association by Locality 51

Chapter Three: Petrographic Facies and Diagenesis 56

3.1 Petrofacies Association (PFA) 58

3.2 Petrofacies Interpretation 76

3.3 Diagenetic Sequences 79

Chapter Four: Sequence Stratigraphy 88

4.1 Halokinetic Sequence Stratigraphy 88

4.2 Fluvial Sequence Stratigraphy 89

Chapter Five: Discussion 104

5.1 Discussion 104

Chapter Six: Conclusion 111

References 114

Appendix 1 122

Appendix 2 123

Appendix 3 124

Appendix 4 125

Vita 126

List of Tables

Table 1: Lithofacies table with corresponding codes, grain size, abundance, and geometry. 28

Table 2: Facies Associations with corresponding Miall facies.....50

Table 3: Facies Association Percentages by Stratigraphic Section. 51

List of Figures

Figure 1: Map of study area and surrounding salt structures of Utah and Colorado.2

Figure 2: Geologic Map of Gypsum Valley. 5

Figure 3: Lithostratigraphic Members of the Late Triassic Chinle Formation. 8

Figure 4: Stratigraphic Distribution of Facies Associations of Bridge Canyon. 20

Figure 5: Stratigraphic Distribution of Facies Associations of the Box Canyon Transect.....22

Figure 6: Stratigraphic Distribution of Facies Associations of Summit Canyon.....24

Figure 7: Lithofacies as seen in outcrop. 30

Figure 8: Facies Association 1.....33

Figure 9: Facies Association 2.....35

Figure 10: Facies Association 3.....37

Figure 11: Facies Association 4.....39

Figure 12: Facies Association 5.....43

Figure 13: Facies Association 6.....45

Figure 14: Facies Association 7.....47

Figure 15: Facies Association 8.....49

Figure 16: Ternary Diagram after Folk (1980). 57

Figure 17: Locations of thin sections and thin section labels, excluding Summit Canyon.....58

Figure 18: Thin Section BMS1 from Bridge Canyon Section S1.....60

Figure 19: Thin Section LS3 from Bridge Canyon.....61

Figure 20: Sample S4S3 from Bridge Canyon. 62

Figure 21: Sample S5S5 from close proximity to the diapir in Bridge Canyon.....63

Figure 22: Sample GVEH5 is from Chinle Strata that overlapped the SW in Bridge Canyon. 65

Figure 23: Sample 3.9.4 from Mustache Canyon. 68

Figure 23.b: Sample 3.10.1 from Mustache Canyon. 69

Figure 24: Sample 3.8.7 from Summit Canyon. 71

Figure 24.b: Sample 3.8.5 from Summit Canyon. 71

Figure 25: Sample 3.8.2 from Summit Canyon. 72

Figure 26: Conglomerate sample-displaying signs of dedolomitization. 73

Figure 27: Calcite rich conglomerate sample. 74

Figure 28: Map displaying locations of Petrofacies. 75

Figure 29: Major sediment sources around the Chinle depositional basin, adapted from Cater (1970). 78

Figure 30: Diagenesis event chart for sandstone samples in Bridge and Summit Canyon. 79

Figure 31: Conglomeratic sample 3.7.4. 83

Figure 32: Conglomerate sample GVEH4. 84

Figure 33: Conglomerate sample 3.3.4. 84

Figure 34: Conglomerate sample 3.3.12. 85

Figure 35: Map displaying distribution of cement types. 86

Figure 36a: Bridge Canyon photopan with annotated HS 92

Figure 36b: Illustrated Bridge Canyon stratigraphic sections with annotated HS. 93

Figure 37a: The Box Canyon transect with annotated photopanarama and HS. 98

Figure 37b: Illustrated Box Canyon transect sections with annotated HS. 99

Figure 38: Outcrop highlighting HS. 102

Chapter 1: Introduction

A limited number of studies have documented how the distribution of facies changes proximal to salt diapirs (Giles and Lawton, 2002; Prochnow et al., 2006; Matthews et al., 2007). Documenting the distribution and morphology of fluvial channels is fundamental in understanding how salt tectonism shaped paleoenvironments and potential hydrocarbon reservoir distribution (Giles and Lawton, 2002). Interactions of sediment distribution with salt diapirs and salt tectonics are currently of interest, not only because of the poorly understood nature of salt-sediment controls but because of petroleum companies' interest in their utility to generate hydrocarbon traps (Cater, 1970, Matthews et.al. 2007, Banaham and Mountney, 2013). This study aids in elucidating how salt tectonism and deposition interact to create these reservoirs.

Gypsum Valley is a collapsed salt structure in the Paradox Basin of Southwest Colorado that provides exceptional 3D exposures of salt-sediment interactions of the Triassic fluvial Chinle Formation (Figure 1). The walls of the valley have several exposures of the Paradox Formation evaporites in contact with the Chinle strata and exposures that extend a kilometer from the exposed Gypsum Valley salt wall (GVSW), providing an excellent opportunity to document the fluvial facies variation in different horizons at varing distances from the GVSW. Previous studies on salt-related depositional changes within the Chinle Formation occur northwest of Gypsum Valley around Moab, Utah, are distant from the margins of diapirs and do not provide information on depositional interactions at the salt-sediment interface (Baars and Doelling, 1987; Prochnow et al., 2006; Hazel, 1994; Matthews et al., 2007). This study is the first that documents facies and stratigraphic relationships of exposed Chinle strata directly onlapping the exposed salt wall in Paradox Basin and correlates them to facies far out into the adjacent minibasin.

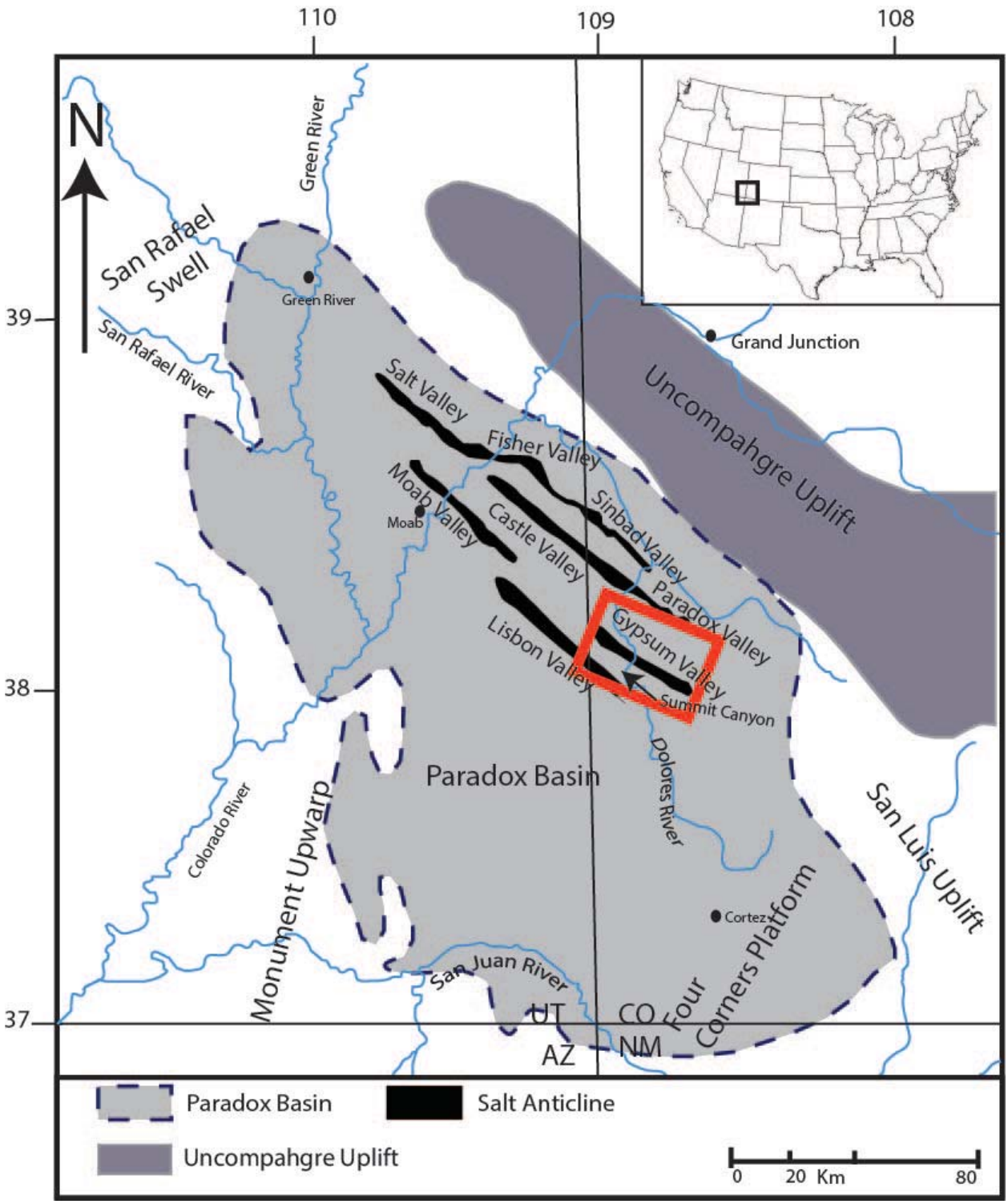

Figure 1: Map of Paradox Basin tectonostratigraphic features, the location of the study area and surrounding salt structures of Utah and Colorado. Red box outlines the location of study area in Gypsum Valley and Summit Canyon. Modified from Cater, 1970.

1.1 Background and Geological Setting:

The Chinle Formation was deposited during the Upper Triassic, covering large portions of Colorado, Utah, New Mexico and Arizona. Herbert Gregory (Gregory, 1917) named the Chinle Formation for Chinle Valley in Arizona. Major John Wesley Powell named the Shinarump Member of the Chinle, first to call it the Shinarump Group on a Geologic Survey Expedition (Powell, 1876). The lateral equivalent of the Chinle Formation and overlying lower Wingate Formation is the Dolores Formation farther east in the area of Ouray, Colorado (Stewart et al., 1972). In Texas the age equivalent to the Chinle Formation is the Dockum Group (Stewart et al., 1972; Dubiel et al.,1991).

The Chinle Formation overlies the Tr-3 unconformity, separating it from older units such as the Triassic Moenkopi, Permian Cutler Group and Pennsylvanian Paradox Formation within the Paradox Basin (Stewart et al., 1972; Pipiringos and O'Sullivan, 1978; Dubiel et al., 1991) In eastern Utah and southwestern Colorado, the upper most Triassic to Jurassic Wingate Sandstone overlays the Chinle Formation forming the J0 unconformity. In Gypsum Valley, the exposed Chinle overlies the Cutler Formation and Paradox Salt diapir and the Moenkopi is absent. However the Moenkopi is present in wells drilled in the adjacent minibasin (Figure 2). Onlap and erosion thin the Chinle stratigraphy against the Gypsum Valley diapir, overlapping, and partially burying the salt on the northwest end. The formation pinches out against older upturned Permian Cutler and Pennsylvanian Honaker Trail strata on the southeast end of the diapir.

Sediments of the Upper Triassic were deposited in a continental backarc setting, derived from multiple sources including: the Cordilleran magmatic arc, Ancestral Rocky Mountains, Appalachian Mountains, and rock assemblages south of the Colorado Plateau (Blakey and

Gubitosa, 1983; Howell and Blakey, 2013; and Riggs et al., 2013). Dynamic subsidence of the Cordilleran magmatic arc likely controlled fluvial deposition within the backarc basin (Stewart et al., 1972; Blakey and Gubitosa, 1983; Lawton, 1994; Howell and Blakey, 2013). The overall pattern is that older units are confined to near the source, and younger units step progressively farther to the north, resulting in an offstepping pattern of deposition (Hazel, 1994; Kluth and DuChene, 2009).

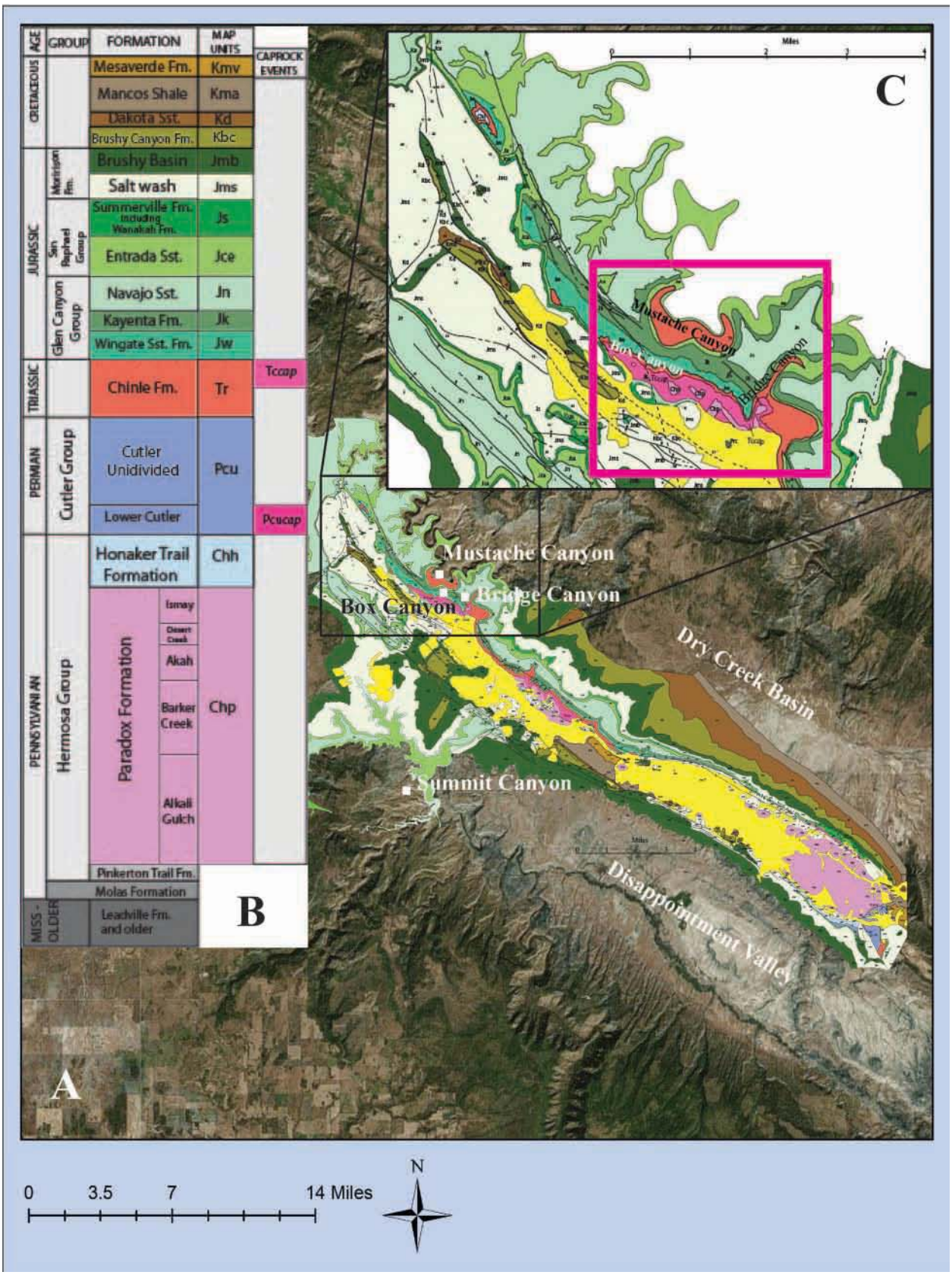
AGE
GROUP
FORMATION
MAP UNITS
CAPROCK EVENTS
CRETACEOUS
Mesaverde Fm.
Kmv
Mancos Shale
Kma
Dakota Sst.
Kd
Brushy Canyon Fm.
Kbc
JURASSIC
Morrison Fm.
Brushy Basin
Jmb
Salt wash
Jms
San Rafael Group
Summerville Fm. including Wanakah Fm.
Js
Entrada Sst.
Jce
Glen Canyon Group
Navajo Sst.
Jn
Kayenta Fm.
Jk
Wingate Sst. Fm.
Jw
TRIASSIC
Chinle Fm.
Tr
Tccap
PERMIAN
Cutler Group
Cutler Unidivided
Pcu
Lower Cutler
Pcucap
PENNSYLVANIAN
Hermosa Group
Honaker Trail Formation
Chh
Paradox Formation
Ismay
Desert Creek
Akah
Barker Creek
Alkali Gulch
Chp
Pinkerton Trail Fm.
Molas Formation
MISS - OLDER
Leadville Fm. and older
B
C
Mustache Canyon
Bridge Canyon
Box Canyon
Dry Creek Basin
Summit Canyon
Disappointment Valley
A
0
3.5
7
14 Miles
N

Figure 2: Geologic Map of Gypsum Valley. A.) An overlay for the geologic map of Gypsum Valley (Stokes and Phoenix, 1948) on top of an EsriGIS base map with study locations and basins to the north and south. B.) The Chinle Formation is displayed as a coral-orange color. C. Study locations are highlighted on the map. Locations of stratigraphic sections within pink box can be found in Appendix 2.

The depositional setting of the Chinle Formation consisted of large braided streams, flowing from southeast to the northwest (Hazel, 1994). Lithologies range from polymictic conglomerates to silt and mudstones. Redbeds dominate over other heterolithic lithologies. Baars and Doelling (1987) describe the Chinle Formation in the Moab region as a multicolored, heterolithic "slope and ledge former" underlying the Wingate. Throughout the Chinle Formation there have been many diverse fossils and trace fossils reported including lungfish, crayfish and petrified wood (Dubiel et al., 1991), but few fossils have been found in the Gypsum Valley area. The Chinle Formation expresses a multitude of colors from purple to tan, developed in paleosols and wetting/drying climatic cycles in shallow lakes (Dubiel et al., 1991).

The climate of the early Triassic turned wet and humid in contrast to the arid settings of the Permian and Jurassic. During the Late Triassic (Norian-Rhaetian Epoch) Pangea moved north from the humid tropics to an arid paleoenvironment (Kent and Tauxe, 2005; Martz et al. 2014). Hazel (1994) provides a good regional setting and tectonic history of the deposition of the Chinle Formation at the Cane Creek Anticline near Moab, Utah (Figure 1). Dubiel et al. (1991) describes the paleogeography and climate of the Chinle while the supercontinent Pangea existed as having a humid atmosphere and abundant fluvial systems.

The colorful and variable Chinle Formation lends itself into division into numerous members in different parts of the Colorado Plateau and eastern Plains (Hazel, 1994). However, in general, the Chinle Formation consists of two major groupings of members. The lower units in the Chinle contain bentonitic clayey red beds, full of volcanic detritus from the Mogollon

Highlands to the south and a small contribution of detritus from the Uncompahgre Highlands to the north (Riggs et al., 2013). The upper unit coarsens to silty-sand and pebble conglomerates. Both units can be divided further into members, the lower unit consists of: Monitor Butte, Petrified Forest, Shinarump and the Moss Back members. The upper unit includes: Owl Rock, Church Rock and related members (Figure 3; Stewart et al. 1972). A recent regional correlation of stratigraphy across the study area correlates the members of the upper unit with the Dolores Formation in western Colorado (Figure 3; Lucas et al., 1997; Martz et al., 2014).

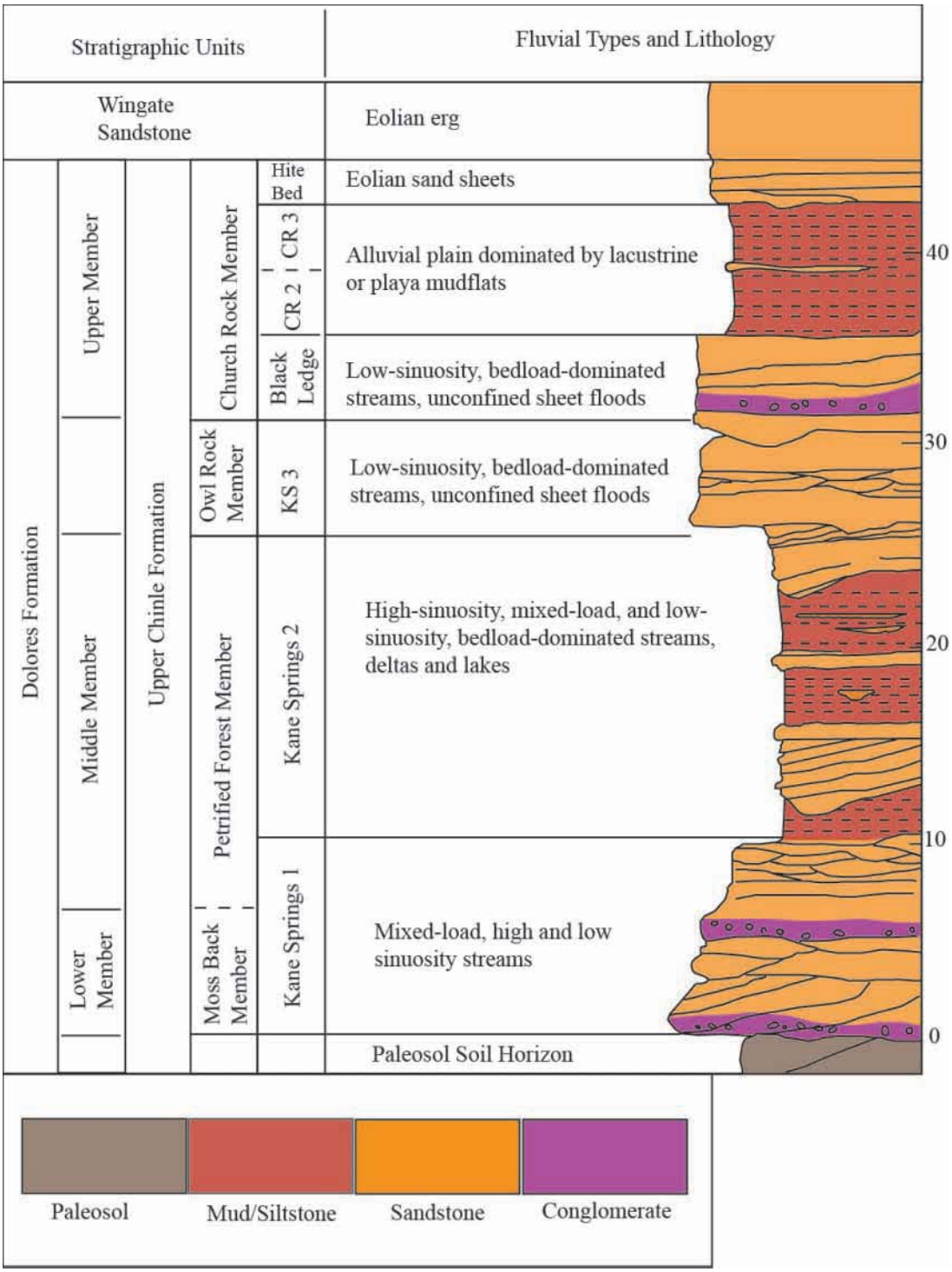

Figure 3: Lithostratigraphic Members of the Late Triassic Chinle Formation. Modified from Hazel (1994) and Shawe et al. (1968), the subdivision of the Upper Chinle Formation into its members found in the study area. Thicknesses on right of figure are means.

The lower members of the Chinle are not present in southwestern Colorado, including the study area around Gypsum Valley (Stewart et al., 1972; Hazel, 1994; Lucas et al., 1997). Shawe et al. (1968) notes the Temple Mountain, Shinarump, Moniter Butte, and Owl Rock members of the Chinle Formation are not present in the Slick Rock District. Beds thicken in the south in northeastern Arizona and northwestern New Mexico to over 400 meters and include the lower members that are absent in the study area (Stewart, 1957; 1972). Units within the formation best match the descriptions of the Mossback, Petrified Forest and Church Rock members. (Figure 3) These include the Black Ledge Member, and the middle and upper members of the Church Rock. The normal Chinle section consists of two sandstone and conglomerate channel fill units, the Mossback and the unit equivalent to the Black Ledge (Shawe et al. 1968) (Figure 3). The Mossback and Black Ledge are separated by the slope forming, mud-rich Petrified Forest Member. A similar red slope-forming mud-rich unit, the middle member of the Church Rock, separates the Black Ledge and the upper member of the Church Rock (Figure 3). From the literature such as (Stewart et al., 1972) and from the stratigraphic sections measured in this study, the study area Chinle strata can tentatively be correlated with the upper units of the Chinle Formation (Upper Mossback Member, the Petrified Forest Member, and the Church Rock Member), which includes the Black Ledge.

The Dolores/Chinle strata in the region of Gypsum Valley include the predominant Siltstone member (Stewart et al., 1972) and upper members that are tentatively correlated with the Church Rock member of the Chinle (Shawe et al., 1968). These authors also correlated three units of the Church Rock member toward the study area. These include the Black Ledge member of Shawe et al., 1968, and the middle and upper members of the Church Rock.

Shawe et al. (1968) provided a detailed stratigraphic cross section across most of the study area in San Miguel and Dolores counties. Units within the formation best match the descriptions of the Mossback, Petrified Forest and Church Rock members. The normal Chinle section consists of two sandstone and conglomerate channel fill units, the Mossback and the unit equivalent to the Black Ledge (Figure 3). The Mossback and Black Ledge are separated by the slope forming, mud-rich Petrified Forest Member. A similar red slope-forming mud-rich unit, the middle Member of the Church Rock, separates the Black Ledge and the upper Member of the Church Rock (Figure 3). Martz et al. (2014) and Blakey and Gubitosa (1983, 1984) described and recognized units in Lisbon Valley that also match the lithostratigraphic units of Gypsum Valley. In Lisbon Valley the nomenclature of the units is different but equivalent,as the Kane Spring Beds 1-3 are equivalent to Mossback, Petrified Forest and Owl Rock Member (Martz et al. 2014)(Figure 3).

Salt tectonism has locally disrupted the stratigraphy in Gypsum Valley. Distinctly absent from the normal section are the green and orange clay-rich shales, below the Moss Back member, that normally make up the bulk of the lower part of the Chinle Formation. Shawe et al. (1968) measured sections approximately 175 m thick (580 ft) within the Chinle. In the Bridge Canyon area, the thickest section measured is 150 m thick and lies adjacent to exposed salt caprock. Cole et al. (2009) measured Chinle thickness in wells at the Double Eagle Unit in the Andy's Mesa Field to be 131.1 m (Fossil Federal 5st1 well). In Lisbon Valley the thickness of the Chinle measures between 110 and 125 meters (Martz et al., 2014).

1.2 Salt Tectonism and Sedimentation:

Unlike siliciclastics and carbonates salt behaves in a ductile rather than brittle fashion when responding to regional tectonic stresses, differential loading, and a wide range of geologic conditions (Hudec & Jackson, 2007). Regional tectonics can therefore enhance the movement and shape of salt diapirs (Trudgill, 2011).

The process of passive diapirism can result from a number of drivers but in the Paradox Basin the main driver occurs from sediment loading, from the Cutler Formation, resulting in salt structures such as rising diapirs and sinking mini-basins (Trudgill, 2011). Minibasins form through salt withdrawal and often contain a complex stratigraphy that are the result of changes in the rate and distribution of migrating salt. Passive diapiric rise occurs with the salt near the surface (Giles and Lawton, 2002). The diapir may be buried under a thin layer of sediments, but renewed rise folds and deforms beds (Giles and Lawton, 2002). Diapirs can impact deposition by forming topographic highs and subsidence in minibasins that contain localized facies reflecting restricted and confined depositional systems that differ substantially from the regional surrounding environments (Hazel, 1994; Giles and Lawton, 2002).

1.3 Regional Setting of Gypsum Valley:

Gypsum Valley is a part of a group of salt structures within the Paradox Basin in southeast Utah and western Colorado (Figures 1 and 2). Gypsum Valley is a large, northeast-trending collapsed valley shaped by dissolution and collapse of the top of the salt diapir. In general strata dip away from the diapir at angles that range from 5 degrees to vertical caused by the rising salt flanks and subsidence of salt peripheral to the basin (Stokes and Phoenix, 1948; Shawe et al., 1968; Hazel, 1994).

The Paradox Basin formed during the Ancestral Rocky Mountain (ARM) orogeny. It is

flanked on the northeast by the Uncompahgre uplift, and on the southeast by the Four Corners platform (Hanshaw and Hill, 1969; Matthews et al., 2007). Subsidence began during the Pennsylvanian when salt was deposited as the Paradox Formation (Elston et al., 1962). The Uncompahgre uplift played a major role in the formation of the salt anticlines (Elston et al., 1962; Ohlen and McIntyre, 1965; Banham and Mountney, 2013). Beginning in the Pennsylvanian to Permian, salt diapirs rose as the Paradox Basin was rapidly filled with sediments derived from evolving stacked thrust faults of the the Uncompahgre uplift (Cater, 1970; Mack and Rasmussen 1984; Kluth and DuChene, 2009). As the proximal minibasins filled with sediment, the depositional locus moved to the southwest with the youngest diapirs also to the southwest. These salt anticlines and accompanying synclines trend northwest, paralleling the Uncompahgre Plateau's orientation and probably parallel the orientation of basement faults that began after salt deposition (Shawe et al. 1968; Kluth and DuChene, 2009; Trudgill and Paz, 2009). Formations predating the late Jurassic Morrison Formation were rotated and thinned by onlapping, and erosion of salt-cored anticlines (Cater, 1970; Mack and Rasmussen 1984). Synclines adjacent to Gypsum and Paradox Valleys provided salt for the cores of these anticlines by flowage (Cater, 1970). In the latest Jurassic, most of the diapirs were buried by the Morrison Formation and diapiric rise ceased (Trudgill and Paz, 2009). In the Late Cretaceous the Sevier orogeny in central Utah resulted in subsidence in the area associated with the Sevier Foreland Basin (Trudgill and Paz, 2009). The study area was buried under approximately 1.5 km of strata of the Cretaceous Dakota Sandstone, Mancos Shale and Mesa Verde Group. The Laramide deformation of the Colorado Plateau occurred during the Latest Cretaceous and the Paleogene; the salt walls were squeezed as the region underwent shortening (Ohlen and McIntyre, 1965). Reactivation of several basement faults is also thought to have occurred during the shortening of

the Laramide Orogeny, which tilted Mesozoic strata (Kluth and DuChene, 2009). Tectonic features associated with the Laramide Orogeny, that frame the Paradox Basin include: the Monument Upwarp to the southwest, the San Rafael Swell and Henry Basin to the west, and to the south and southeast margins are the Defiance Plateau and San Juan Basin (Dubiel et al., 2009). Little Laramide deformation is noted in the Paradox Basin itself, with the possible exception of the Glade and Dolores Fault Zones (Stevenson and Baars, 1986; Shawe et al., 1968). During the late Tertiary, San Juan volcanism occurred along with uplift of the Colorado Plateau, which resulted in unroofing, incision, and collapse of the diapirs (Cater, 1970; Ohlen and Mcintyre, 1965). Gypsum and anhydrite of the Paradox Formation are exposed mostly rimming the valley in Gypsum Valley. As is typical of most of the Paradox Salt anticlines, a large part of the diapir is buried under large collapsed roof blocks of Jurassic and Cretaceous strata (Ohlen and Mcintyre, 1965). This has generally been ascribed to dissolution of salt in axes of anticlines that caused collapse of the roofs of the diapirs (Ohlen and Mcintyre, 1965; Shawe et al., 1968). Solution and collapse is visible where disjointed blocks of Morrison Formation solution collapse are exposed. In Gypsum Valley, strata, including the Chinle Formation overlap part of the diapir rim, and are un-faulted, or offset only on minor faults along the periphery of the salt. However, isolated blocks of strata as young as Late Cretaceous Mesa Verde Group are found in the diapir.

Gas production has occurred in a southeastward plunging rim syncline, Dry Creek Basin, on the northeast flank of Big Gypsum Valley. Hydrocarbons are produced primarily from the arkosic sandstones within the Pennsylvanian Cutler and Honaker Trail Formations in the Andy's Mesa Field, and the Double Eagle units (Amador et al., 2009; Cole et al., 2009).

1.4 Previous Work: Salt Tectonism and Chinle Stratigraphy:

There are few existing studies that focus on interactions between fluvial systems and salt tectonics. Accommodation changes on a regional scale affect facies architecture causing lateral facies changes (Blakey and Gubitosa,1984; Lucas et al., 1997; Matthews et al., 2007). Blakey and Gubitosa (1983, 1984) described two major fining-upward sequences within the Chinle Formation with possible smaller cycles related to salt tectonism. Thickness variation and lateral facies changes are attributed to subsidence and accommodation space variation (Matthews et al., 2007). The Cane Creek Anticline that shows variation in Chinle thickness related to salt evacuation early in its history (Hazel, 1994; Matthews et al., 2007). The lower Chinle Formation thins onto the Moab Valley Salt Wall while the upper units thicken towards the salt wall onto the flanks, suggesting passive diapirism during depositions of these upper units. The opposite was observed for the Big Bend minibasin, lower Chinle units thicken towards its center but no discernable thickening occurred for the upper units, indicating salt withdrawl during deposition of the lower units (Matthews et al., 2007).

Matthews et al. (2007) described lateral variation, facies architecture changes, and stratigraphic changes of the Chinle Formation at the Cane Creek and Moab salt walls, and Big bend mini-basin. The facies associations that Matthews et al. (2007) recognized are: 1) Fluvial channel-fill sandstones, 2) Fluvial channel-fill mudstones, 3) Lacustrine mudstones, 4) Moderately to completely bioturbated sandstone and mudstones, 5) Paleosols, 6) Eolian sandstones, and 7) Disrupted beds. Disrupted beds were a result of faulting, folding, or fracturing of previous facies associations and could be interpreted as local events that occurred near the time of deposition and relate to a steep paleoslope.

Hazel (1994), Miall and Arush (2001), and Matthews et al. (2007) all observed lateral stratigraphic pinchouts and erosional unconformities between Chinle bedding contacts near salt anticlines in the Moab area. Hazel (1994) used the Chinle Formation to tie intrabasinal tectonism of the Cane Creek anticline to terrestrial sedimentology by examining sandstone body geometries, linking salt tectonism to alluvial architectural changes and regional uplift rather than climate or sediment supply rates. Channel morphology consisted of broad multistory sand sheets, linked to uplift of salt and decreased subsidence in the basin. Within the Big Bend minibasin in Castle Valley, the lithofacies and paleosols of the Chinle Formation were studied and used for the identification of fluvial aggradational cycle (FAC) sets for fluvial sequence stratigraphy (Prochnow et al., 2006). Within the minibasin a greater number of FAC's and paleosol horizons indicates higher sedimentation rates within the basin, while areas away from the axis appear to form fewer but more mature paleosols.

McFarland (2016) documented a structure related to the diapir called the shoulder. The shoulder can be divided into inboard and outboard components separated by an anticline. The inboard margin of the shoulder is named the collar and the outboard is termed the lateral. Within the area of the shoulder McFarland (2016) documented three wedge halokinetic sequences, (WHS-1, WHS-2, WHS-3). Each sequence is locally bounded by angular unconformities less than 5º. Each halokinetic sequence contains FA1 caprock bearing conglomerates within a broad single story sheet (3-5 meters thick and150 meters wide) (McFarland, 2016) that grade into FA3 overbank deposits as they onlap the salt shoulder (Figure 36). The FA3 overbank strata are in turn onlapped by broad multistory FA1 channel complexes; fewer conglomeratic lenses reach the crest of the shoulder and fine to sandstone-dominated channels (Figure 36). Disorganized conglomerates suggest that this exposure was near the edge of the rising diapir during the

subsequent Chinle deposition (McFarland, 2016). Thick overbank deposits are punctuated by small ribbon channels near the diapir (Figure 36) and away from the diapir forms amalgamated channels stacking into broad sheets.

1.5 Study Areas:

The three areas chosen for this study are Bridge Canyon, Box Canyon and Summit Canyon (outside GV) (Figure 2). Bridge Canyon provides a cross-sectional view of the Chinle Formation as it onlaps the GVSW and dips below the surface towards the Dry Creek minibasin. Box Canyon provides study of along strike variation, the stratum onlaps and eventually dips below the ground surface into minibasins topographic lows. Summit Canyon, located 10 km from the diapir margin, acts as a control area to illustrate regional Chinle facies and stratigraphy away from the influence of GVSW. In Summit Canyon, broad unconfined sheets dominate over single and amalgamated channels, which are dominant closer in proximity to the diapir. An additional area near Box Canyon and Bridge Canyon (refered to as the mustache) had samples collected for thin sections and a stratigraphic section was measured there.

1.6 Methods (Analysis):

Three locations were chosen to study the stratigraphy of the Chinle Formation at different distances from the Gypsum Valley Diapir (Figure 2, Appendix 2). Two of these locations (Bridge Canyon and Box Canyon) expose Chinle strata in direct contact with the salt. The third area is in Summit Canyon, 10 km from the margin of the diapir. Each location had one outcrop panel, 1 to 5 km long, (Figures 4-6). Bridge Canyon is a unique outcrop that extends from the

minibasin onto the diapir, straddling the wall. The second outcrop panel at Box Canyon parallels the diapir, just inboard of the margin, and the third panel, Summit Canyon, is about 10 km from the margin of the diapir.

A total of fifteen stratigraphic sections were measured ranging from 40-200 m in thickness. Stratigraphic sections were measured and correlated using a Jacob staff, Brunton Compass, located using handheld GPS, physcially correlated across each outcrop panel through tracing marker horizons, transferred to photomosaic panoramas, and then made into cross-sections for analysis. Sections included measurements of sedimentary structures, bedding geometries, contact types, and fossils, including petrified wood, trace fossils, and bivalves. Foreset dips, climbing-ripple orientations, and the azimuth of trough and channel axes were used to reconstruct paleocurrent directions. A complimentary study done by Josh McFarland (McFarland, 2016) mapped internal angular unconformities in three dimensions using GPS and satellite imagery. Bedding contacts were mapped to understand how a salt diapir would effect the distribution of depositional environments within the Chinle Formation. These observations were used to help interpret depositional environments. Depositional environments were interpreted from associations of genetically related facies. Changes in grain size, facies percentages, and other sedimentary factors are compared from section to section in order to determine the effects the evolving GVSW had on Chinle deposition. Localities were also compared, to determine if the diapir consistently rose or if each area had a different history of diapirism and salt evacuation.

Hand samples were taken from each major facies, up stratigraphic sections, and located with GPS coordinates. From Bridge Canyon, along strike of Box Canyon and Summit Canyon

more than 60 samples were collected from stratigraphic intervals measured. Rock samples were cut into billets and then sent to Spectrum Petrographic Inc. Vancouver Washington.

Thin sections were prepared with stains for calcite, potassium feldspar, and vacuum impregnated with blue-dyed epoxy. For mineralogy, 20 slides were stained for potassium feldspar and 44 were stained for carbonates and ferrous iron carbonates. Point counting of +300 points within 22 thin sections was done to determine mineralogy (Ingersoll et al., 1984); also thin sections were examined for porosity, compaction, and cement types. Diagenetic facies were determined based on the cements present within each sample. Relative diagenetic histories were inferred from thin sections observations. Crosscutting relationships and superposition were used to give relative timing of the sequences of cementation, dissolution, and compaction.

Chapter Two: Chinle Lithofacies and Facies Associations of the late Triassic Chinle Formation

Eleven lithofacies were identified in the measured sections and outcrop panels in Gypsum Valley and Summit Canyon (Table 1 and Figure 7). Miall's (1978) facies codes were added for better definition and ease in description. These were grouped into eight facies associations (Table 2). Lithofacies identified include: Poorly lithified siltstone (Fh, Fl, Fc), climbing ripple cross-stratified sandstone (Sr), ripple cross-stratified sandstone (Sr), trough cross-bedded sandstone (St), planar –tabular cross-stratified sandstone (Sp), massive sandstone (Sm), unsorted conglomerate (Gmm), chert bearing conglomerate (Gt, Gp), caprock bearing conglomerate (Gt, Gp), rip-up clast conglomerate (Gt, Gp) and mudstone (Fm). The most complete section of the Chinle in Gypsum Valley occurs in Bridge Canyon (Figure 4) where Chinle Formation rests on caprock and dips to the northeast into the Dry Basin minibasin. This section also exposes the lithofacies in closest proximity to the diapir. Facies in the Chinle Formation form cycles that grade from ledge forming conglomerate/sandstone lithofacies and form a sharp contact with the overlying siltstone lithofacies. Three main cycles of this facies alteration are present at Bridge Canyon and are fully exposed in outcrop.

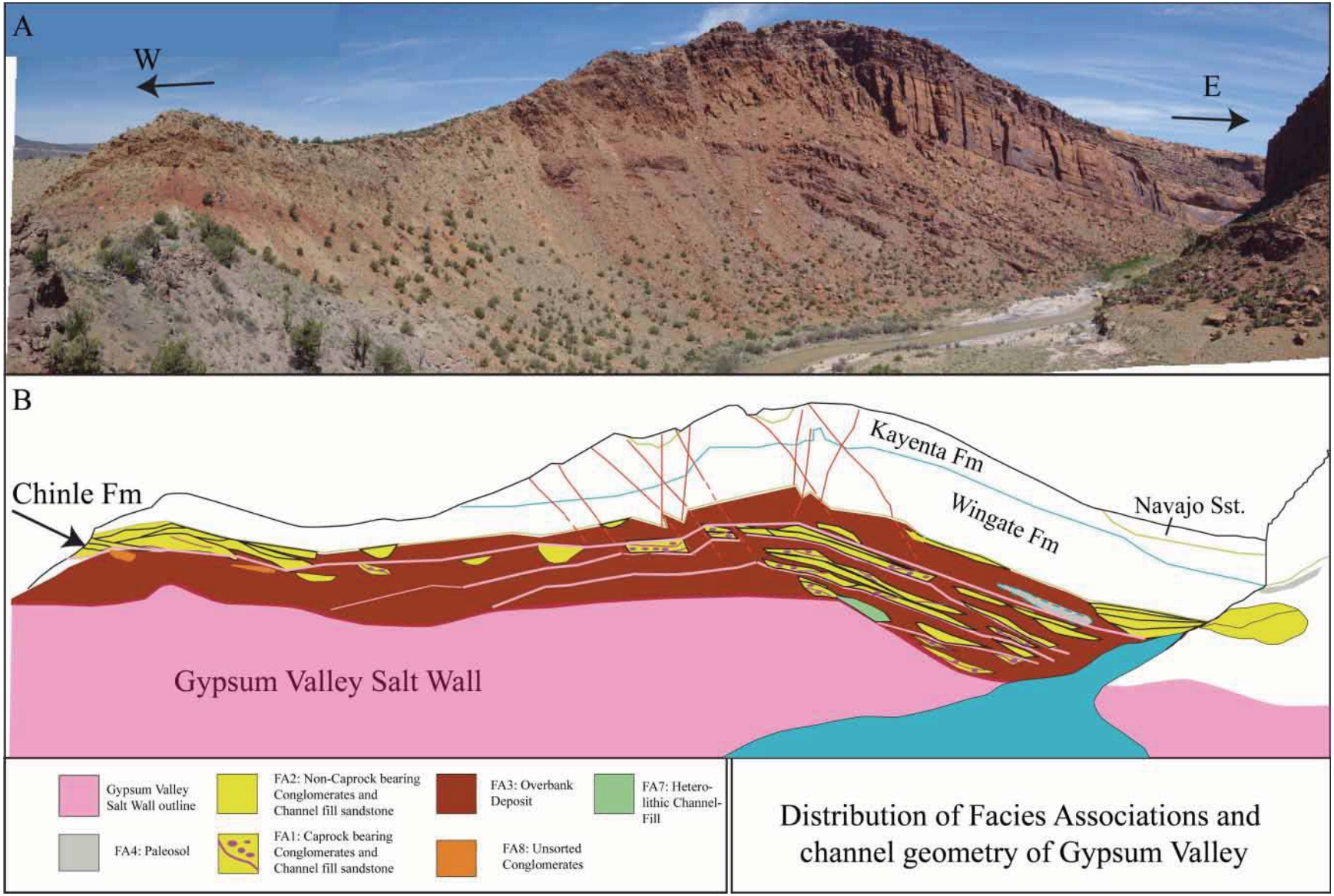

Distribution of Facies Associations and channel geometry of Gypsum Valley

Figure 4: Stratigraphic Distribution of Facies Associations in Bridge Canyon. A.) A panoramic view of Bridge Canyon, notice beds dip away from the GVSW. B.) Illustrated interpretation of the locations of contacts, and extent of mapped facies associations. Pink lines separate halokinetic sequences, three wedge halokinetic sequences appear in Bridge Canyon.

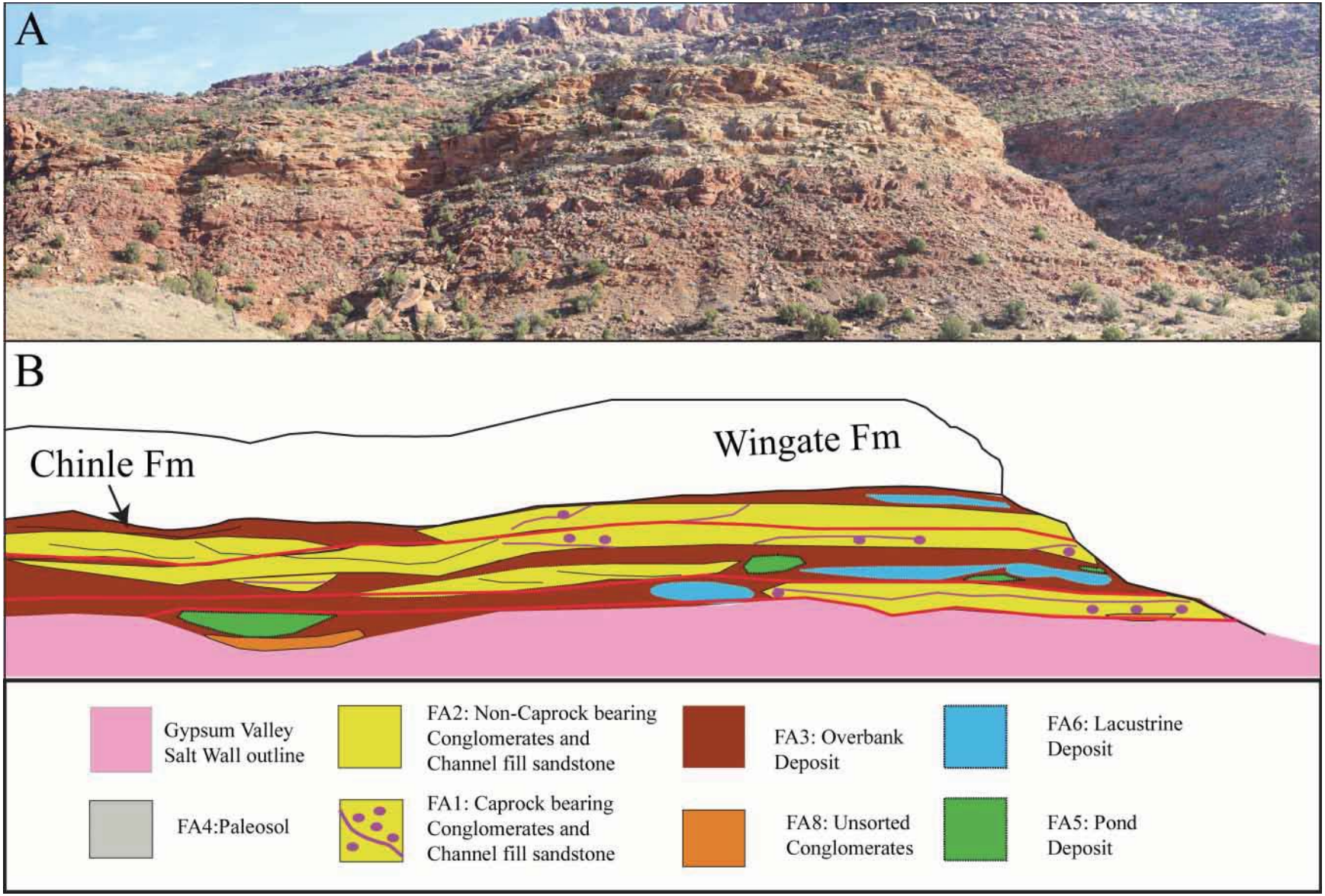
A
B
Chinle Fm
Wingate Fm
Gypsum Valley Salt Wall outline
FA2: Non-Caprock bearing Conglomerates and Channel fill sandstone
FA3: Overbank Deposit
FA6: Lacustrine Deposit
FA4:Paleosol
FA1: Caprock bearing Conglomerates and Channel fill sandstone
FA8: Unsorted Conglomerates
FA5: Pond Deposit

Figure 5: Stratigraphic Distribution of Facies Associations of the Box Canyon Transect. A.) Along strike view of the Box Canyon transect. B.) Interpreted distribution of facies associations.

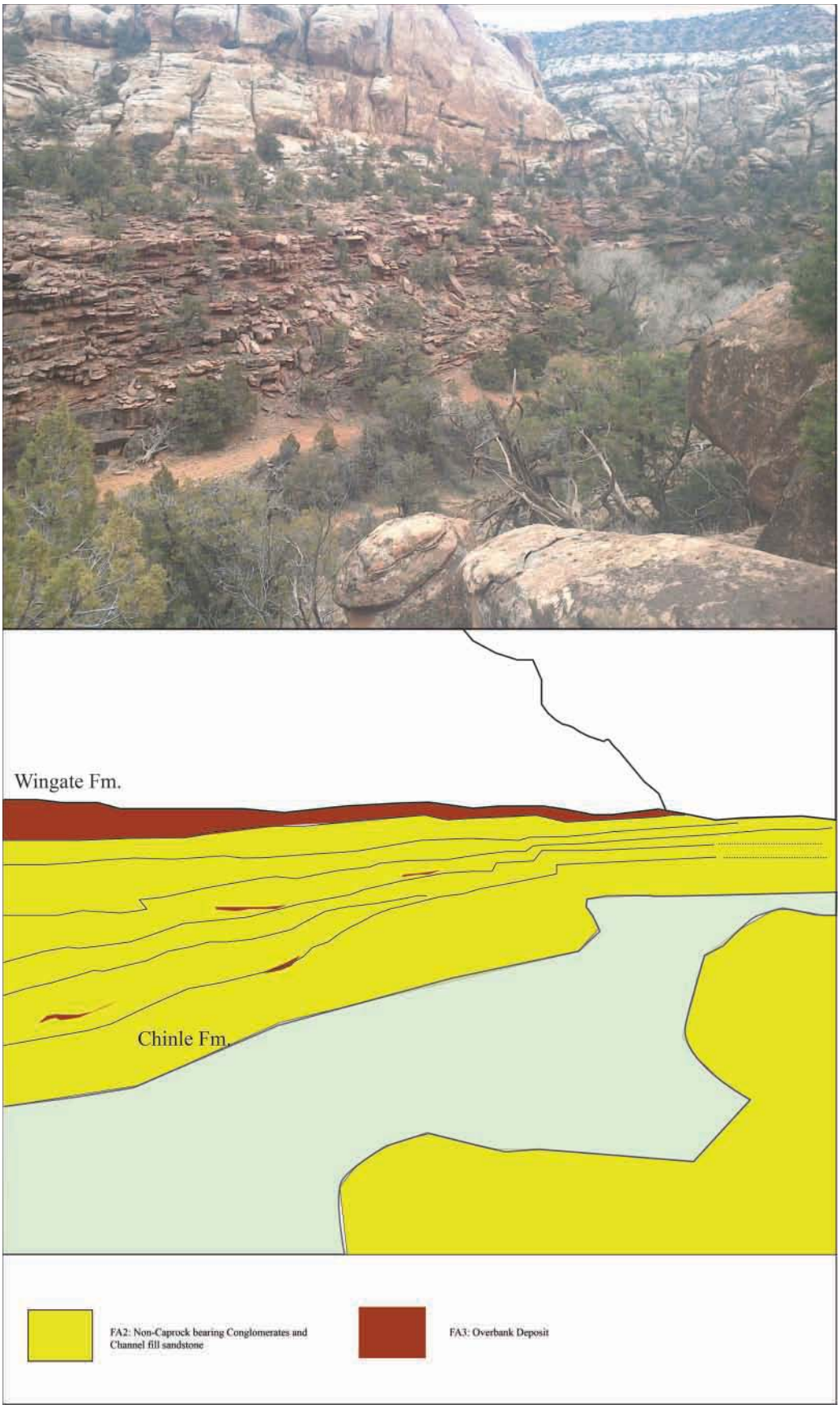
Wingate Fm.
Chinle Fm.
FA2: Non-Caprock bearing Conglomerates and Channel fill sandstone
FA3: Overbank Deposit

Figure 6: Stratigraphic Distribution of Facies Associations of Summit Canyon. Summit Canyon, 10 Km from GVSW, the FA changes to a majority of unconfined channels containing non-caprock bearing sandstones.

2.1 Lithofacies

2.1.1 Poorly Lithified Siltstones (Fh, Fl, Fc)

This facies forms brick red slopes, outcrops are poor and few sedimentary structures are visible because they break down so easily. The siltstones also contain illitic mud (Stewart, 1972) and very fine-grained sand (Figure 7). Units can be from 0.1 meters to greater than 15 meters thick and extend in outcrop over 50 meters. In good exposure, the siltstones are laminated. This unit is present in several facies associations including overbank deposits, paleosols, and lacustrine ponds (See section 2.2 Facies Associations).

2.1.2 Climbing rippled cross-stratified sandstone (Scr)

This facies within channel complexes and silty climbing rippled sandstones also occur in overbank deposits (Figure 7). Grain size is upper to lower fine-grained sand and petrographic analysis (see below) reveals sandstones to be subarkose. The subarkose framework grains consist of quartz, chert, feldspar, mica, and the cements are carbonate. Units are 0.1-1.5 meters thick and laterally continuous in outcrop (+15 meters) before being covered by slope detritus. This facies is common in both the overbank and non-caprock bearing sandstone channel fill facies associations. In channel fills the climbing rippled units crop out as purplish red intervals.

2.1.3 Ripple cross-stratified sandstone (Sr)

This facies forms tan or red ledges on outcrop. Units are thin, tabular beds, typically found below siltstones (Fh, Fl, Fc), and contain well-sorted, upper fine to lower-medium-grained sandstone (Figure 7). The petrographic analysis reveals these are subarkose and contain framework grains of quartz, chert, feldspar, and mica. Thicknesses of units are variable within outcrop but ranges from 0.2-2.0 meters and are visible on outcrop for over 10 meters laterally

before becoming covered by detritus or laterally changing into (St or Sp). This facies is found in both caprock and non-caprock bearing conglomerate and sandstone channel fills.

2.1.4 Trough cross-stratified sandstone (St)

Bedding appears in robust ledge forming units, tan to red in color. Units are thick, tabular beds, typically found above conglomerates and below rippled sandstones (Figure 7). St form within channel complexes and occur in conjuction with Sr, Sp, or G. The grain size of St ranges from upper fine to lower medium and are subarkose to litharenites. The framework grains consist of quartz, chert, feldspar, mica, carbonate, clay, and minor volcanic grains. The thickness of bedding can be from 0.1-2.5 meters and extends over 5 meters in outcrop. This facies is found within both caprock and non-caprock bearing conglomerate and sandstone channel fill.

2.1.5 Planar-tabular cross-stratified sandstone (Sp)

Bedding appears as tan to red, robust ledges. Units are thick, tabular beds, typically found above conglomerates and below rippled sandstones or siltstone units (Figure 7). The grain size of Sp ranges from upper fine to lower medium-grained and form subarkose to litharenites. Petrography reveals that the facies contains framework grains of quartz, chert, feldspar, mica, carbonate, and clay. The thickness of bedding ranges from 0.2 to 2.5 meters. Planar - tabular cross bedding is often associated with rippled sandstones and trough cross bedding. These channels occur within both caprock and non-caprock bearing conglomerate and sandstone channel fills.

2.1.6. Massive sandstone (Sm)

One of the less common facies, Sm appears as ledges on outcrop (Figure 7). They are associated with fluvial channels and can be found associated with planar-tabular stratified (Sp) and trough cross-stratified (St) facies above and below (Figure 7). They form as laterally continuous tabular sheets 0.3-3.0 meters thick. The grain size consists of very fine to lower

medium-grained sandstone and is subarkosic in composition. Petrography indicates framework grains are composed of quartz, chert, feldspar, mica, and clay.

2.1.7. Unsorted Conglomerate (Gmm)

These consist of light brown to brownish gray resistant ledge formers (Figure 7). The unit outcrops as lenses and is only found in sections close to the diapir (Figure 4). Clasts are angular to subangular black gray and brown and consist primarily of dolomite derived from the adjacent diapir. The average clast diameters range from 20 cm in sections adjacent to the diapir, to an average of 2.5 mm in sections 0.3 km from the diapir.

2.1.8. Chert bearing conglomerate (Gt, Gp)

Chert bearing conglomerates have over 10% chert pebbles. This facies is not as abundant as caprock and rip-up bearing conglomerates but is documented in Box Canyon. Gt form with an erosional contact below, the base of a ledge fines into planar (Sp) or trough (St) cross-bedded sandstones (Figure 7). They form in the base of channels, lenticular in shape, 0.5-2 meters in thickness. Matrix is silt to granules with clasts ranging from pebble to cobble size.

2.1.9 Caprock bearing conglomerate (Gt, Gp)

Caprock bearing conglomerates are more abundant than the chert (Gt, GP) or unsorted conglomerates (Gmm), they occur in close proximity to the GVSW (less than 10 meters from the contact) and disappear 0.7 km distance perpendicular to the diapir in Bridge Canyon (Figure 7). Along strike the conglomerates are visible just above the lower Chinle contact and are seen all along strike of the diapir. The composition of the caprock, as visible in thin sections, can be either dolomite or calcite depending on locations. The clasts are sub-rounded to rounded and semi-spherical. The thickness of caprock conglomerates can vary from 0.1 m to 1.5 m, forming with an erosional base. Above the base, the conglomeratic ledges form lenses in the base of channels that fine upward into planar (Sp) or trough (St) cross-bedded sandstones.

2.1.10 Rip-up clast conglomerate (Gt, Gp)

Rip-up clast conglomerates contain mud rip-up clasts and reworked clasts, such as sandstone concretions and rare bivalve fossils (Figure 7). Rip-up clast conglomerates are

characterized by bright red to green mud rip-up clasts. Forming an erosional base with reworked clasts from mud- and silt- dominated units below. Rip-up clast conglomerates fine upward into planar (Sp) or trough (St) cross-bedded sandstones. Rip-up clast conglomerates are relatively rare in comparison to the caprock bearing conglomerates (Gt, Gp) but are found along the transect of Box Canyon, parallel to the strike of the diapir, and at the contact with the overlying Wingate Formation.

2.1.11. Mudstone (Fm)

Mudstones are poorly exposed red slope formers (Figure 7). They are hard to distinguish from the more abundant siltstones and have gradational contacts. Studies (Hazel, 1994) recognize similar mudstones in the region that are composed of quartz and clay minerals (illic or smectitic). A typical unit is 0.1-10 meters thick and appears in lenses. Mudstones occur in several facies associations such as paleosols, pond/marshes, and lacustrine.

Table 1: Lithofacies table with corresponding codes, grain size, abundance, and geometry.

Lithofacies

Lithofacies Code	Lithofacies	Interpretation	Grain/clast size	Abundance/Distribution	Geometry
Fh,Fl,Fc	Siltstone	Overbank deposit	Dominantly silt	Common throughout	Laterally continuous (up to 30 meters thick)
Scr	Climbing ripple cross-stratified sandstone	Fluvial channel fill, overbank deposit	upper very fine to lower medium-grained sand	Common throughout	Laterally continous
Sr	Ripple cross-stratified sandstone	Fluvial channel fill	upper fine to lower medium-grained sand	Common throughout	Laterally continuous
St	Trough cross-stratified sandstone	Fluvial channel fill	upper fine to lower medium-grained sand	Common throughout	Laterally continuous
Sp	Planar-tabular stratified sandstone	Fluvial channel fill	upper fine to lower medium-grained sand	Common throughout	Laterally continuous
Sm	Massive sandstone	Fluvial channel fill	very fine-lower medium grained sand	Less common but found throughout	Laterally continuous
Gmm	Unsorted angular clast conglomerate	Debris Flow	clasts: granule-boulder matrix: silt to upper medium grained sand	Found locally along strike of diapir (up to 15 meters thick)	Laterally discontinuous, lenticular
Gt, Gp	Chert bearing conglomerate	Channel bedload, bar forms	clasts: granule-cobble matrix: silt to upper medium-grained sand	Typically only found at bases of channels	Laterally discontinuous (2-5 meters wide)
Gt, Gp	Caprock clast conglomerate	Channel bedload, bar forms	clasts: granule-cobble matrix: silt to upper medium-grained sand	Common throughout (found at bases of channels and components of heterolithic channel fills)	Laterally discontinous (typically up to 2-5 meters wide)
Gt, Gp	Rip-up Clast Conglomerate	Channel bedload, bar forms	clasts: granule-cobble matrix: silt to upper medium-grained sand	Typically only found at bases of channels	Laterally discontinuous (2-5 meters wide)
Fm	Mudstone	Overbank deposit, paleosol	Dominantly mud	Common throughout	Laterally continuous (up to 15 meters thick)

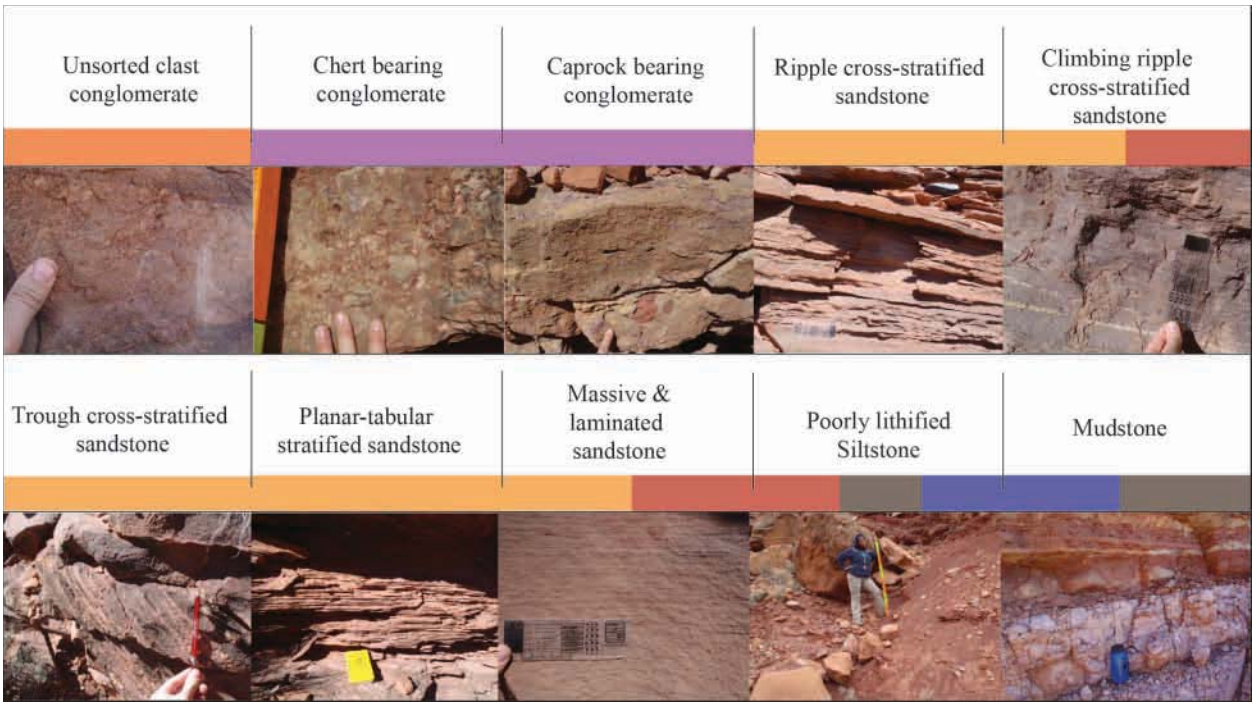

Figure 7: Lithofacies photographs on outcrop. Color bars above images indicate which FA the lithofacies are apart of. Orange is Disorganized Conglomerate (FA8), Purple and Yellow apply to both Caprock and Non-Caprock bearing conglomerates and sandstone (FA1-2&7), Red is Overbank Deposits (FA3), and blue and grey represent wetlands, lacustrine and paleosols (FA 4-6). Facies Association 7, Heterolithic Channel Fill can be represent by a combination of all lithofacies. Rip-up clast conglomerate not shown.

2.2 Facies Associations

Eight facies associations were defined from the lithofacies groupings, bedding geometry and sedimentary structures. 1) Caprock-bearing stratified conglomerate and sandstone channel fill (FA1), 2) Noncaprock-bearing stratified conglomerate and sandstone channel fill (FA2), 3) Overbank deposits (FA3), 4) Paleosols (FA4), 5) Ponds/marshes (FA5), 6) Lacustrine deposits (FA6), 7.) Heterolithic channel fill (FA 7) and, 8.) Disorganized conglomerate (FA8). A description of each facies association is in Table 2.

2.2.1. Facies Association 1: Caprock-bearing stratified conglomerate and sandstone channel fill

2.2.1.1 – Description – FA1 consists of channel forms filled with sandstone and conglomerates (Figure 8 and Table 2). Sandstones and conglomerates range in color from tan to reddish purple. Clast composition of conglomerates is predominately composed of carbonate caprock, limestone, and dolomite, eroded from the diapir. Caprock clasts are subrounded to rounded, and oblong to spherical and well to moderately-sorted. Conglomerates are matrix supported and in some instances imbricated. The matrix is composed of semi-rounded, well-sorted sandstones. The composition of the sandstone is lithic arkose to feldspathic litharenite.

The beds form medium to thick ledge forming outcrops of single, laterally stacked, or vertically and laterally stacked channels (Figure 4 and 5). FA1 channels fine upward into FA3 (overbank deposits), or are overlain by another FA1 channel fill. A typical vertical channel fill in this facies association contains an erosional contact at the base, caprock bearing conglomerate (30% of ledge), fining upward into trough cross-stratified sandstones (St) or planar tabular cross-stratified sandstones (Sp) (50% of ledge), and then ripple-laminated or climbing-rippled sandstone (Sr) (20% of ledge).

The distribution of facies within this association changes with distance from the diapir. Conglomeratic lenses disappear 0.7 km away from the diapir and ripple cross-stratified sandstones (Sr) thicken away from the diapir. Near GVSW shoulder, ribbon geometry, channels with low width to depth ratios, are more common (McFarland, 2016). Farther from the GVSM, channels are laterally stacked with high width-to-depth ratios and, in some units, vertically stacked with sandstones composing continuous ledge forming units separating the red silty intervals. Paleocurrent directions indicate a predominant south to southeast flow (see Appendix 1).

FA1 channel geometries vary, depending on gradient and proximity to the GVSW. Individual channels are approximately 0.5 – 1.0 m thick and extend roughly 20.0 m outcrop before becoming covered by slope material or plunging below the surface. Different channel types (*i.e.* sheets versus ribbon sands) are visible in cross-section (Figures 4 and 5) with different geometries created from changing gradients and types of deposition.

2.2.1.2 Interpretation – The caprock-bearing channel fill is interpreted as forming in a high-energy environment transporting the large clasts that form the basal lags of channels. High width-to-depth ratios indicate broad braided streams with intermittent, probably seasonal flow (Parrish and Good, 1987). The caprock clasts incorporated within the channels indicate a nearby source and were eroded or shed off the exposed diapir. These contrasts with carbonate clast comglomerates of Dubiel et al. (1991), which contained clasts eroded from lacustrine nodules. For the caprock to be incorporated into the channels, incision of the GVSW by channels would have to have occurred. The materials would have been transported as cones of debris and deposited as mass wasting events, that were subsequently reworked and incorporated into channels.

The lithofacies Sp and St indicate a decrease in energy, reflecting episodic flow. High width-to-depth channel geometry also indicates episodic or seasonal flow of channels.

This facies association is similar to Matthews et al. (2007)'s fluvial channel-fill sandstone in its geometry, erosive base and lithologic characteristics. However Matthews et al. (2007)'s channels are floored with mud clast lags, which would better represent FA2's non-caprock bearing conglomerates (see below). Gypsum Valley paleocurrent measurments are similar to those found by Matthews et al. (2007) following a south-southeast direction. Shock (2012) documented carbonate caprock incorporated into fluvial channels of the Cutler and Moenkopi

formations. Shock (2012) interpreted that the dolostone clasts were not from depositional carbonates associated with Lower Cutler beds but from erosion of the rotated caprock bedding.

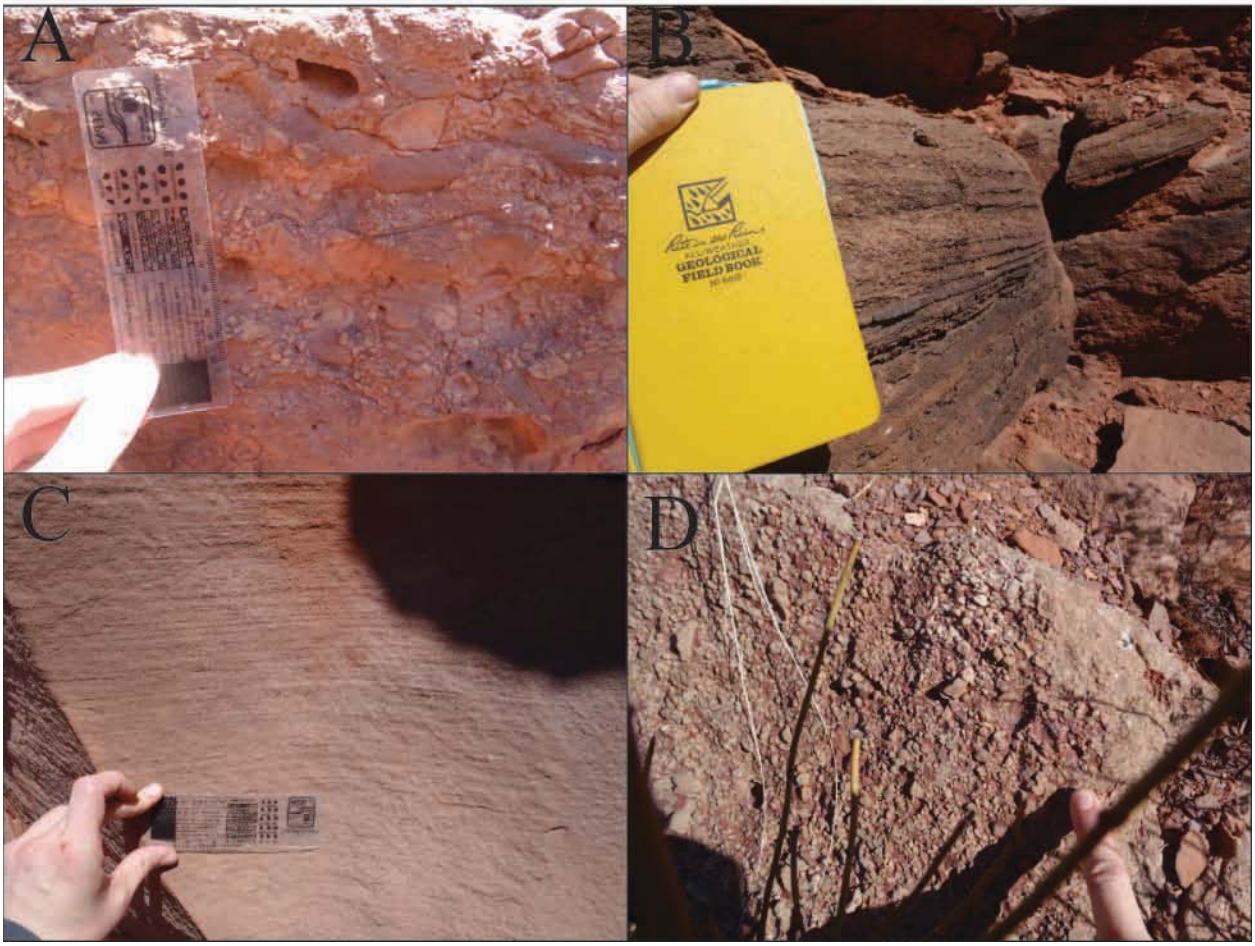

Figure 8: Facies Association 1. A-D are field photos of sedimentary structures associated with FA1. A.) Caprock clasts within a sandstone matrix. B.) View of bedding, C.) Ripple laminations seen in channels, and D.) Overhead view of caprock pebbles from a weathered surface.

2.2.2.) Facies Association 2 - noncaprock bearing stratified conglomerate and sandstone channel fill

2.2.2.1 Observation –FA2 consists of channel bedforms filled with sandstone and conglomerate (Figure 9 and Table 2). Sandstones and conglomerates range in color from tan to reddish brown. Clast composition of conglomerates is predominately composed of rounded chert, mud rip-up

clasts, sandstone concretions and rare septerian carbonate nodules. Non-caprock clasts are angular to rounded, and oblong to spherical in shape tending to be moderately sorted. Conglomerates are matrix supported and in some instances appear imbricated. The matrix is composed of semi rounded well-sorted sandstone. The composition of the sandstone is lithic arkose to feldspathic litharenite.

Medium- to thick-bedded sandstones and conglomerates form thick ledges in outcrops of the laterally and vertically stacked channels (Figure 4 and 9). A typical channel fill consists of an erosional contact at the base, conglomerate clasts composed of chert fragments, and mud rip-up clast (20% of ledge), fining-upward into trough crossbedded sandstones (St) or planar tabular crossbedded sandstones (Sp) (40% of ledge), and then ripple cross laminated or climbing rippled sandstone (Sr) (40% of ledge). In rare instances massive sandstone beds can be found. FA2 are rare in the Gypsum Valley location but conglomerates are incorporated in normally graded bedding and trough cross-stratified sandstones.

2.2.2.2 Interpretation – The non-caprock bearing channel fill is interpreted as being a high-energy environment from the large clasts that form the basal lags of channels. The sand-dominated Sp and St indicate a decrease in energy. High width-to-depth ratios indicate broad braided streams with intermittent, seasonal flow and flooding. The clast types indicate that both proximal and distal sources (chert and volcanic fragments interpreted as being shed off the Uncomphage Highlands) whereas the nodule and concretion clasts would have been eroded locally from FA3, FA4 or FA5, by the migrating cutbank erosion nto overbank and older channel fills (Miall, 1996). Martz et al. (2014) indicated that in Lisbon Valley the extrabasinal clasts may have arrived syndepositionally or were reworked from the underlying Cutler Group.

This FA2 is similar to Matthews et al. (2007)'s fluvial channel-fill sandstone for geometry, erosive base, and lithologic characteristics; Matthews et al. (2007)'s channels are lined with mud-clast lags, which would better represent FA2's non-caprock bearing conglomerates. Martz et al. (2014) interpreted red ledge beds with conglomerates composed of fine-grained sandstone and minor extrabasinal sourced conglomerates as being a braided fluvial system based on sedimentary structures and absence of lateral accretion sets. Dubiel et al. (1991) interpreted the upper Chinle as a dryer environment; fine- to medium-grained sandstones dominated large unconfined channels with few structures except large lateral accretion sets.

Figure 9: Facies Association 2. Outcrop photos from non-caprock bearing conglomerates and sandstone. A.) Thinly bedded rippled sandstone, B.) Massive sandstone above a trough cross-stratified sandstone, C.) Finger is pointing to a mud rip-up clast in a sandy matrix. D.) 1.5 meter stick is at the contact between two channels, E.) Concretions were eroded and re-deposited into the basal lag of a channel, F.) Hand is right below chert pebbles in a sand and mud-filled matrix. Meter stick is 1.5 meters high.

2.2.3.) Facies Association 3: Overbank deposits

2.2.3.1 Description - Overbank deposits are red, purple, green, and grey in color with some mottling (Figure 10 and Table 2). Lithologies are siltstone, mudstone, claystone, silty-sandstone and very fine-grained sandstone. The silty-sandstones are poorly lithified and crop out as poorly exposed slope formers. The few beds in this facies that provide outcrop exposure exhibit red silty fine and very fine-grained sandstones with horizontal laminations and climbing ripples (poorly lithified siltstone (Fh, Fl, Fc), climbing rippled cross-stratified sandstone (Sr)).

FA3 bedding is tabular and laterally and vertically extensive. Individual beds are cm-scale, the units are ~16 meters in thickness and extend several hundred meters. Individual sandstone units are 2-5 meters thick and laterally grade into siltstones. Overbank deposits form contemporaneously with FA4 paleosols, FA5 ponding deposits, and FA6 lacustrine deposit. But, FA3 separates FA1 and FA2 channel sandstones and conglomerates, and is also eroded into by FA2 channels.

2.2.3.2 Interpretation – The FA3 is dominated by fine-grained sediments, indicating a low energy environment and suspension settling. Sandstone deposition would have occurred as splays or flood event deposit (Matthews et al., 2007). The widespread distribution of overbank deposits are linked with ephemeral streams and washover zones where the river overtopped the banks. As these overbank deposits became wider spread, stable areas became rooted and paleosol formation occurs. Also, areas that were periodically inundated became swamp or lake-like over time.

This FA3 is similar to Matthews et al. (2007)'s fluvial overbank and channel-fill mudstones. Matthew et al.'s FA is similar in lithology, clay-siltstones, and ripple-cross laminated sandstones. However, Matthews et al. (2007)'s includes channel-fill mudstones occurring as inclined beds, this is separated in this study as heterolithic channel fill. Similar mudstones have been documented at diapirs in the northern Paradox Basin (Matthews et al.,

2007). Matthews et al. (2007) interpreted that the laterally extensive nature of these beds indicates splays or sheets associated with flooding events and noted that root traces and mud cracks indicate subaerial exposure. In Lisbon Valley to the northeast of GV, Martz et al (2014) interprets the slope forming siltstones and muddy sandstones of the upper Kane Springs beds of the Chinle Formation as overbank deposits based on grain size and associated sedimentary structures.

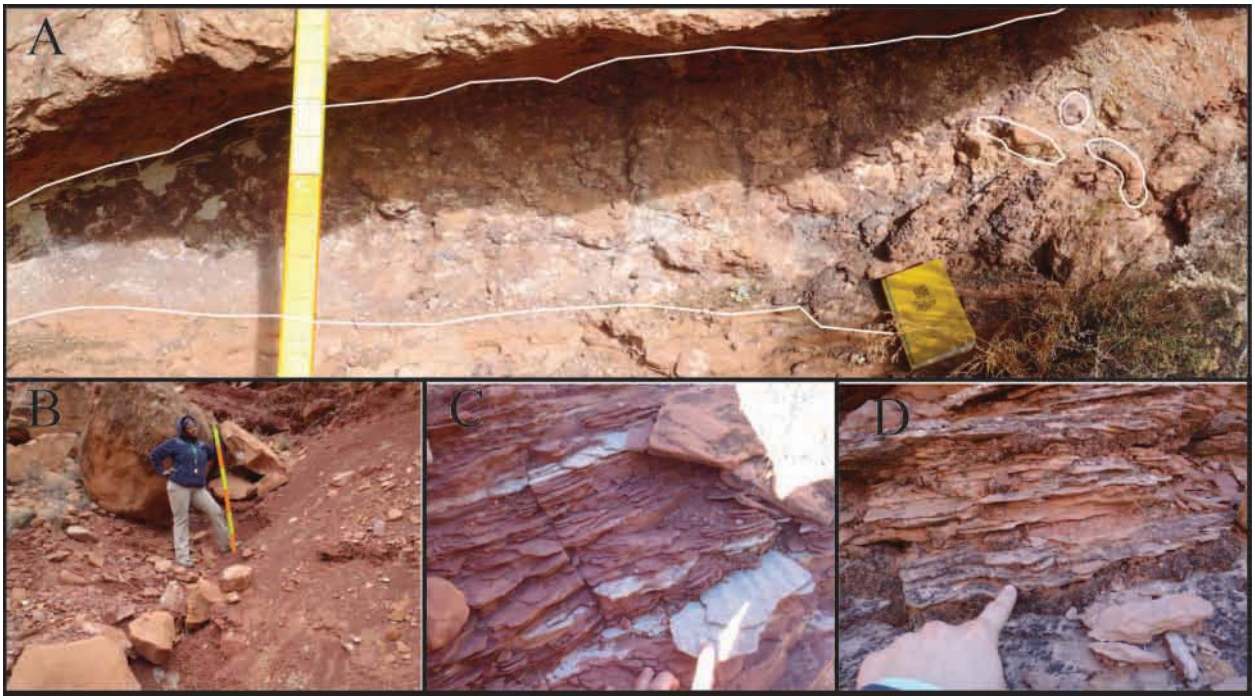

Figure 10: Facies Association 3. Sedimentary structures within the Overbank Facies Association, A.) Mottled bedding including highlighted crayfish burrow, B.) slope forming within the overbank, Jacob Staff is 1.5 meters, C.) rippled stratification within a silty sandstone, D.) rippled stratification within a sandstone.

2.2.4.) Facies Association 4 - Paleosols -

2.2.4.1 Description – Paleosols are pink, red, green and grey clay/siltstones with very fine-grained sandstones and form beds 0.5 – 5.0 meters thick (Figure 11 and Table 2). Bedding is tabular and horizontally bedded and horizons measured 5-20 meters wide. Sedimentary

structures characterizing the paleosols are the root casts, discoloration halos/mottling, sand-filled mud cracks, root traces, concretions, and trace fossils. The lower units of the Chinle form silty mud-rich localized blocky peds, with few reduced root haloes, beds grade into overbank deposits. In the uppermost unit of the Chinle Formation, trace fossils identified as beetle traces (*Scoyenia*) and insect larva burrows (*Fuersichnus*) (Hasiotis, 2002) occur in very fine-grained sandstone. The next bed above forms clay rich horizons with prismatic ped morphology, and contains vertical and horizontally curved cracks, bedding is over 20 meters wide on outcrop. Above the prismatic ped bed casts of root traces are preserved in very fine-grained sandstones.

2.2.4.2 – Interpretation - Root traces and pedogenic fabrics indicate probable vertisol development with mounded curved fractures (Figure 11 and Table 2). The shape of the peds, blocky or prismatic, indicates maturity of paleosols and various amounts of development. Prochnow et al. (2006) defines prismatic peds being characteristic of vertisols. The clay rich horizons, 0.5 meters in thickness, contain extensive lateral root horizons and lesser-burrowed surfaces that indicate a moisture rich environment. The burrow types present indicate the presence of fresh water composing the water table (Hasiotis, 2002). Mud cracks indicate subaerial exposure, whereas mottling of some horizons indicates fluctuating water table.

FA4 is similar to Matthews et al. (2007)'s paleosols, however their paleosols are 10-200 cm thick and contain ferric concretions, sandstones and gravels, where the GV paleosols are finer grained and contain carbonate concretions. The two FA's are similar by containing root traces, discoloration haloes, and mottling. Martz et al. (2014) interpreted paleosols in the Church Rock Member of the Chinle Formation to have occurred within the overbank deposits. Other paleosols with mottling, desiccation, and burrows can be classified as aridisols or calcisols (Dubiel and Hasiotis (2011). Dubiel et al (1991), interpreted pedogenic development of the Moss Back and

Petrified Forest members of the Chinle Formation as vertisols which form in tropical settings with episodic precipitation. Dubiel et al. (1991) documented in the Church Rock Member of the Chinle Formation meniscate back-filled trace fossils and desiccated mudstones filled with sandstone from the overlying Wingate Formation. At the top of section 3.1 and 3.2, in Bridge Canyon, are paleosols with basal rooted horizons grading into calcic vertisols with slickenlines, rare bioturbation occurs. This paleosol is not interpreted as a mudflat or lacustrine unit unlike Dubiel et al. (1991) who interpreted the Chinle Formation in northwestern Colorado as having floodplains with "Petrocalcic" horizons. Dubiel and Hasiotis (2011) documented paleosols within different members of the Chinle Formation. Their paleosol suite consists of oxisols, alfisols, vertisols, and aridisols. Oxisols are characterized by white to purple mottles. Alfisols are 1-7.5 meters thick and contain *Scoyenia gracilis*. Reported vertisols have a thickness range of 5-25 ft (1.5-7.5 m), slickenlines, and nodules. Aridisols form 1-1.5 m meter thick beds, blocky to prismatic peds, and rhizoliths. Oxisols indicate a fluctuating water table and a wetter climate (Dubiel and Hasiotis, 2011). Vertisols indicate seasonal wetting and drying cycles. Aridisols or calcisols also indicate a drier climate (Dubiel and Hasiotis, 2011). If these paleosols are taken as an indicator for paleoclimate, then over time the Chinle Formation was deposited in dryer climate (Parrish and Good, 1987). Dubiel and Hasiotis (2011) also indicated that the wettest time of the Chinle Formation was related to months of rainfall and distance to the equator, and then overtime the Colorado plateau began to drift northward.

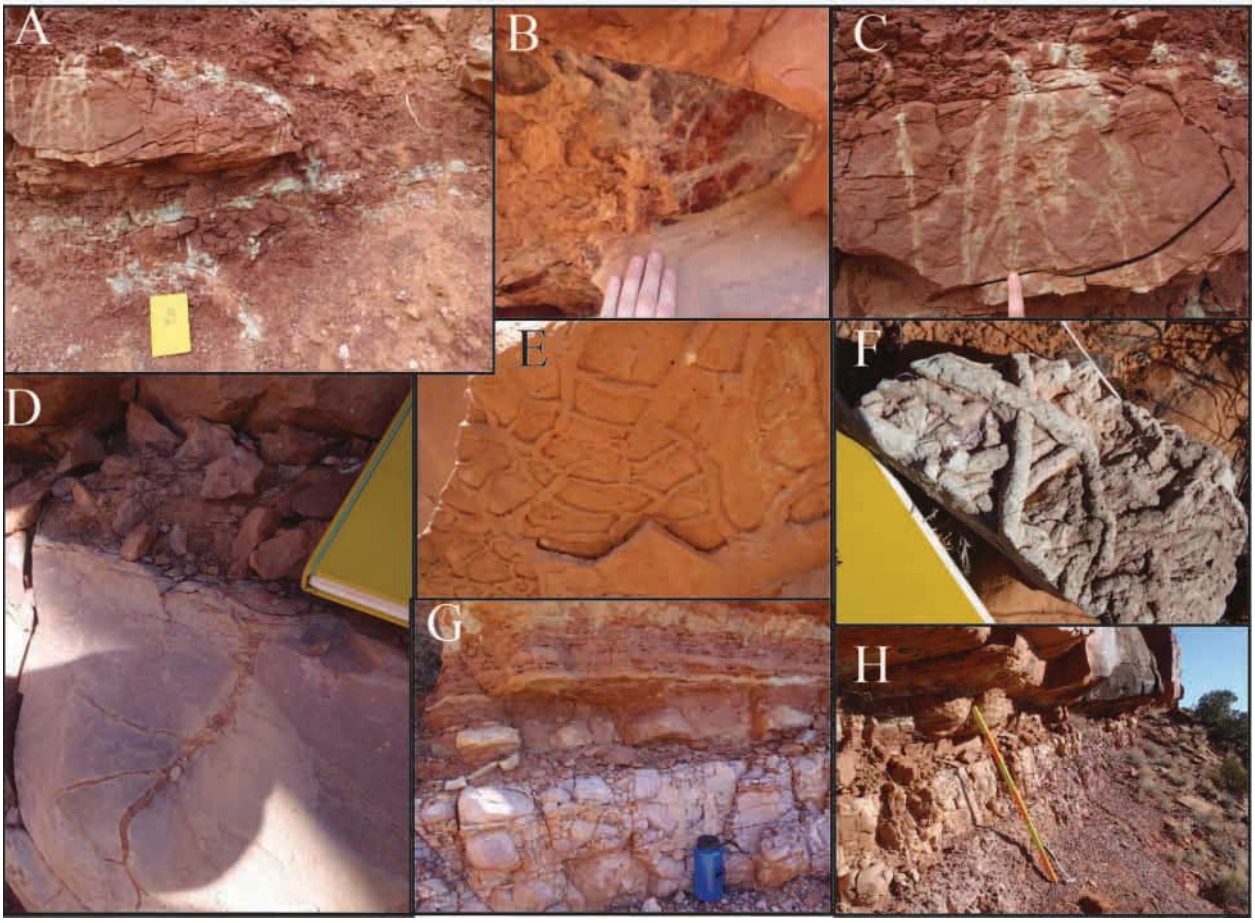

Figure 11: Facies Association 4, outcrop photograph of paleosol features in the Chinle Formation. A.) Occuring within the more unconsolidated sediments, paleosols have many characteristics. A.) A reduced horizon above the field notebook and a prominent ledge with root haloes, that penetrate downward. B.) Underside of a bed, roots fan out laterally, C.) Root traces from photo A magnified, D.) Curved cracks within a clay-rich horizon. E.) Underside of bed, mudcracks are filled with sandstone from unit above. F.) Insect traces, G.) Zoomed out image where D is the lower one third, E is the contact above, H.) Shows lateral extent of G.

2.2.5.) Facies Association 5 – Marsh and ponds

2.2.5.1 Description – FA5 has been documented along the GVSW in the Box Canyon transect. Red to brown, poorly lithified mudstone, siltstones, and sandstones contain abundant septerian nodules, sandstone concretions, petrified wood fragments, carbon films of plant remains, thin–shelled unionid bivalve fossils (*Triasmanicola,* Parish and Good, 1987), and rare crayfish burrows (*Camborygma*) 6 to 12 cm in width (Figure 12 and Table 2; Hasiotis, 2002). The

fossils, concretions and nodules form in a matrix of massive siltstone with minor sandstone. Fabric is rarely preserved; mottling and bioturbation disrupt original lithologic structures or primary sedimentary structures.

These features form in lenses with gradational lateral margins, ~1 meter thick and ~20-50 meters wide, within the overbank deposits but topographically, are unique to basins forming on the buried part of the shoulder. McFarland (2016) has documented along strike thickness variation of > 30 m of along the diapir margin (See figure 12). However, FA5 is rare or absent on the GVSW (McFarland, 2016). It is unclear whether differential rise of the diapir, or salt dissolution created these local basins.

2.2.5.2 Interpretation – The unionid bivalves have generally been interpreted as a taphonomically transported assemblage in crevasse-splay deposits, occurring from high-discharge flood events with fragmentation or disarticulation of shells. Lacustrine bivalves have been documented in the Petrified Forest Member equivalent in southwestern Colorado and were generally intact and associated with other biota such as freshwater gastropods (Parrish and Good, 1987). The bivalves were most likely supplied to the ponds or marshes from the crevasse-splay deposits and most closely resembles the bivalves documented along the GVSW because of the disarticulation of shells, small location size and shell size similarity. Inundation by flood events is also evident from different petrified wood samples (i.e. branches and stumps) which would have been deposited during the seasonal flooding events. The high concentration of septarian nodules and concretions indicate high water table (Dubiel et al., 1991). Simple vertical crayfish burrows and mottling of fabric indicates a fluctuation in water table depth (Hasiotis, 2002). Sandstone concretions have been incorporated into the basal lag of channels. For this to happen, concretions

needed to form at shallow depths, early, and then later be eroded. The abundance of carbonized leaf and tree imprint indicates a suitable habitat for plants (Dubiel, 1987) but high concentration of hematitic cement and lack of coal or black shales indicates partially oxygenated waters. These ponds are the product of localized basin subsidence and probably fed by seasonal flooding of crevasse splays from channels. Matthews et al. 2007's moderately to completely bioturbated sandstones and mudstones has similarities in the mottling but in GV there is no intense bioturbation from crayfish burrows,. But Mathews et al. (2007) interprets this FA as being a low sedimentation, marginal-lacustrine to flood-plain environment. Dubiel et al. (1991) also recorded marshes in the Petrified Forest and Mossback members of the Chinle Formation. They contained isolated carbonate nodules and 1 cm-diameter trace fossils, with external ropey texture. Dubiel et al. (1991) attributes the carbonate nodules to the formation of calcic paleosols, the unionid bivalves deposition from perennial flooding events, and that the ropey trace fossils as resembling *Scoyenia gracilis*, an arthropod associated with shallow water table environments. Fresh water marshes in the Green Moniter Butte Member (a member not present in GV) contain detrital organic matter and carbonized plant fossils. Dubiel et al (1991) also attributes the carbonate nodules of the Petrified Forest Member to flood plain paleosol formation. The Petrified Forest Member is interpreted to contain isolated marsh mudstones, similar to those in GV. Dubiel et al. (1991)'s ferns and carbonized remains indicate a near surface water table rapid sedimentation that prevented decay.

Figure 12: Facies Association 5, outcrop photographs of pond/marsh features in the Chinle Formation. A.) Mottling of siltstone, where exposed primary fabric could not be determined. B.) Sandstone concretion that weathered from surrounding siltstone. C.) Pen runs parallel to carbon film of a petrified wood log. D.) Smaller branches are preserved as carbon film on a silty-sandstone surface.

2.2.6.) Facies Association 6 - Lacustrine deposits

2.2.6.1 Description – The lacustrine deposits are isolated but visible as thin laterally extensive intervals (Figure 13; 10 meters thick and +15 meters across). FA6 are found in the Box Canyon area (Figures 2, 5, and 13). FA6 is differentiated from FA5 because being dominated by mudstones and siltstones but have few visible sedimentary structures and lack plant material and roots. The main sedimentary structures are horizonally laminated siltstones and mudstones but overprinting by mottling and bioturbation has disrupted fabric in places. Contacts are

gradational with the overbank deposits (FA3) both vertically and horizontally but generally exhibit reduced muds around edges.

2.2.6.2 Interpretation – The fine-grained nature of the sediment size indicates suspension deposition. The lacustrine deposits are thought to be low productivity or lesser signs of life, possibly the result of large scale, episodic flooding events forming perennial lakes (Dubiel et al. 1991; Matthews et al, 2007). The absence of sedimentary structures could indicate that productivity was high for episodic periods of time. The lack of plant material preserved in this FA could indicate the presence of oxic conditions in which the plant material would not be preserved (Dubiel et al. 1991). The reduced horizons within the muds could indicate an interaction between groundwater and rising salinity of lacustrine waters (Dubiel and Hasiotis, 2011).

Matthews et al. (2007) describes a lacustrine mudstone FA that is significantly thicker than the GV lacustrine mudstones (up to 50 meters). Matthew et al.'s FA is gradational into overbank mudstones and lacks association with channel-fill sandstones. Matthews et al. (2007) and Hasiotis (2002) interpret the lack of root traces but mottled bedding as indicating suspension deposition in shallow perennial lakes. Several of the Chinle Formations members have been documented to include marginal lacustrine and lacustrine facies including Petrified Forest, Owl Rock, and Churchrock. Dubiel et al. (1991) reports red to reddish brown lacustrine mudstone facies from the Church Rock Member that are characterized by thin to medium-grained sandstone, siltstones and mudstones. Bedding in the Rock Point Member contains horizontal laminations and extensive bioturbation that disrupted the fabric (Dubiel, 1987). Dubiel and Hasiotis (2011) interpreted the deposition of the Owl Rock Member to have alternated between lacustrine and marsh settings. Flooding was ephemeral in nature as noted by mudcracks,

indicating periodic wetting and drying cycles, this is not fully evident along the Box Canyon transect because the fabric in the mudstones and siltstones has been obscured (Dubiel et al., 1991). The red color of the siltstone/mudstones indicates that the lacustrine mudflats were ephemeral and subaerially exposed (Dubiel et al., 1991).

The gradational contact with overbank and marsh facies suggests that the lacustrine facies would represent the areas of greatest subsidence. Deposition and preservation of lacustrine facies is related to local increased rate of subsidence (Dubiel, 1987). Dubiel and Hasiotis (2011) indicate a possible mechanism for lacustrine deposits occurred from damming and flooding of drainages coupled with a high groundwater table and aggradation of channels. The monsoonal/seasonal precipitation would have caused flooding and replenished topographic lows.

Figure 13: Facies Association 6. Lacustrine Facies Association characterized by laterally extensive mudflats with few sedimentary structures preserved. Each unit on the Jacob Staff is 10 cm. A.) Climbing rippled bedding below massive mud unit, white box is 1.5 meters. B.) Massive bedding with reduced horizons, and C.) Inset of reduced and oxidized mudstones.

2.2.7.) Facies Association 7 - Heterolithic Channel Fill

2.2.7.1 Description – Isolated FA7 outcrops in close proximity to the CVSW as documented in McFarland (2016). Sandstones and conglomerates are tan to brown in color; the siltstones and claystones are red in color (Figure 14 and Table 2). Lithofacies include and upward-finning

from Gt and Gp, stratified sandstone, St, Sp, and Sh, to mudstones/siltstones Fl, Fc. Conglomerate clasts are subangular to subrounded carbonates and centimeter scale mud rip-ups. The conglomerate facies form beds ~0.5 meters in thickness. Sandstones are upper fine- to lower medium-grained and bedding is 0.1-0.6 meters in thickness. Confined channels 3 to 7 m thick display sigmoidal-shaped, alternating layers of basal conglomeratic lags, sandstones, and silty shales (Figure 14). Sandstone beds are centimeter to meter thick and form lenses that thicken upward. The silty shales are centimeter to meter in thickness and form alternating lenses with the sandstones but thicken at the bottom of the lens. The sandstones are sometimes layered with clay drapes, 1-10 cm in thickness, and the overlying mudstones sometimes contain mudcracks.

2.2.7.2 Interpretation – FA7 represents a preserved point bar in a muddy meandering stream with fluctuating seasonal changes in flow (Miall, 1996). The presence of lateral accretion sets and fining-upward bundles indicate a meandering stream system (Hazel, 1994; Miall 1996). Changes in lithology and grain size indicate cyclic changes in stream energy. Clay drapes and mudcracks represent flooding of bar forms followed by exposure. The cutbank sediments becomes cannibalized breaking down into individual grains and is incorporated into the suspended load, and then is eventually deposited in the river system (Miall, 1996). The appearance of caprock clasts indicates that either exposure of the GVSW occurred during deposition or cannabalization of the disorganized conglomerates supplied this material to the channels.

Many ephemeral meandering streams are partially confined, suspended, mixed load deposits (Hazel, 1994; Miall, 1996). Hazel (1994) documented a heterolithinc facies association, describing them as containing well developed lateral accretion sets, fining-upward bundles, and

preserved cutbanks. Dubiel (1987) and Matthews et al. (2007) documented similar channels within the Chinle Formation and interpreted the deposits as partly confined suspended and mixed-load meandering-stream deposits.

Figure 14: Facies Association 7. Outline of heterolithic bedform channel sets, channel located in Bridge Canyon, Jacob staff at lower left is 1.5, overall scale of bedforms is 2-5 meters in thickness and extends 10 meters in outcrop. Note the sigmoidal shape of beds (White) and erosional contact (Red) truncating the lower channel from the upper channel. Photos courtesy of Josh McFarland.

2.2.8.) Facies Association 8 - Disorganized conglomerate –

2.2.8.1 – Description –FA8 forms brown, tan or purple lenticular cliffs and ledges 2-15 meters thick and extend no more than 10 m in outcrop (Figure 15 and Table 2). FA8 are found exclusively in GV, on the contact between the Chinle Formation and underlying caprock and is restricted to within 200 meters of the GVSW (McFarland, 2016). Sedimentary structures are not visible except for the poorly sorted and massive nature. Within these units, clasts are multi-hued ranging from white, tan, brown, purple, to red. Clasts are angular to subrounded and sizes range from pebble to boulder. Clast composition is sandstone, mudstone, limestone, and dolomite.

FA8 is clast supported and the matrix is poorly sorted of fine to coarse-grained sandstone (Gmm).

2.2.8.2 Interpretation –FA8 are found exclusively in the interval closest to the inboard (proximal) edge of the salt shoulder (McFarland, 2016). Disorganized conglomerate's clast composition, poor sorting and lack of sedimentary structures are interpreted to represent deposition adjacent to the diapir by debris flows derived from a topographically high diapir. The proximity of deposits to the GVSW, isolated nature of the lenses, and the caprock, mudstone and composition of clasts necessitates a localized source. In the Triassic Moenkopi Formation in Castle Valley, Lawton and Buck (2006) described matrix-supported conglomerates containing dolostone clasts as debris flows derived from the topographic highs of the diapir in the Chinle Formation. Debris flows form as part of halokinetic sequences that consists of reworking older deformed strata and the non-evaporite part of the diapir (Giles and Rowan, 2012).

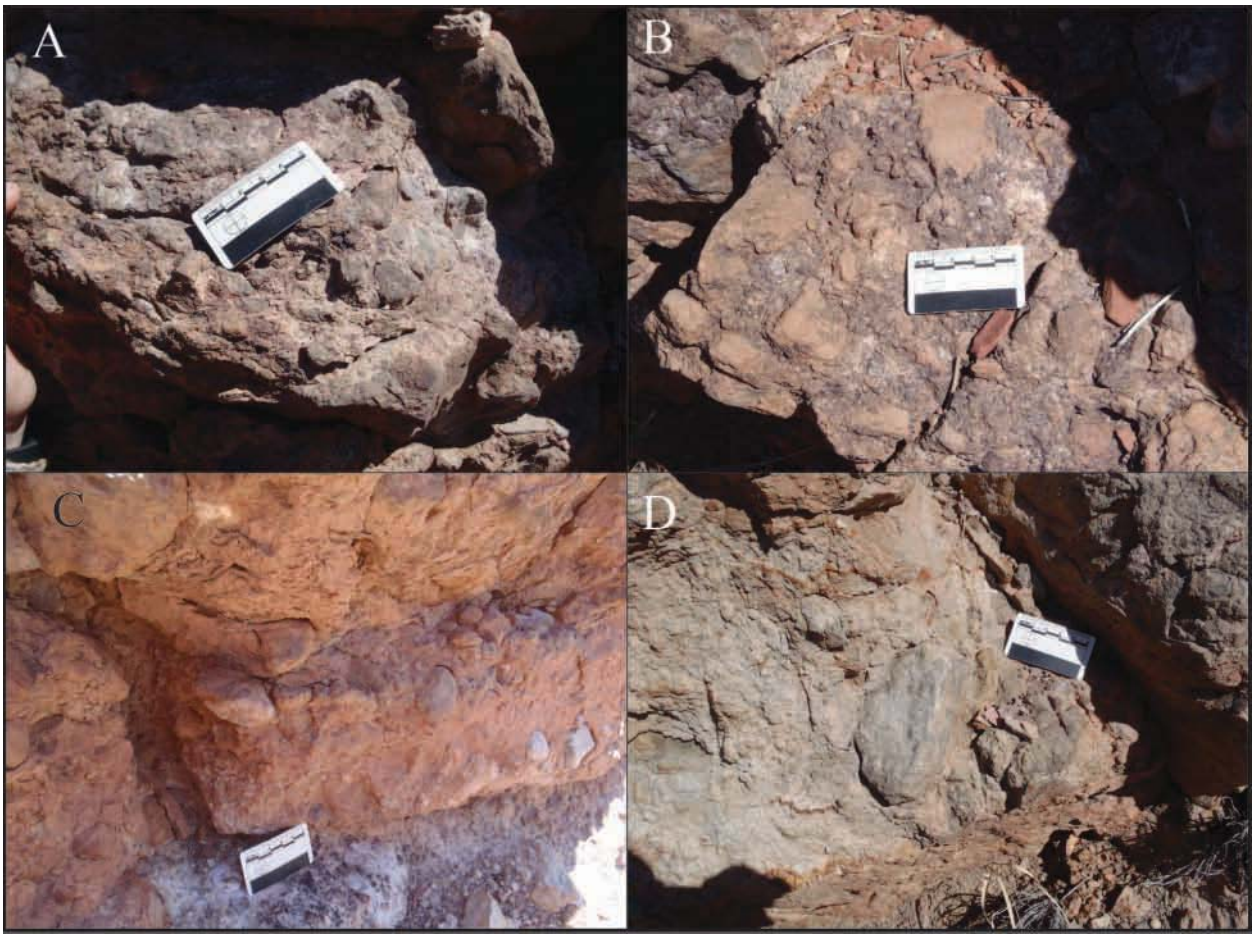

Figure 15: Facies Association 8, photographs display different angular angular caprock clasts of disorganized conglomerates. Scale indicates 5 cm. A.) Cm sized caprock clasts in a sandy matrix, B.) Clasts range from 1 to 10+ cm in a mud rich matrix, C.) No vertical grading is visible as large clasts appear at various intervals, D.) scale is positioned above a clast 5.5 cm wide and to the right of a clast 10 cm long, in a sandy matrix.

Table 2: Facies Associations with corresponding Miall facies.

Facies Associations with Corresponding Color Code

Code	Facies Associations	Color	Grain size	Lithology	Contacts	Bedding Thickness	Geometry and Distribution	Sedimentary Structures	Fossils/ Concretions	Miall Facies
FA1	Caprock bearing Stratified Conglomerate and Sandstone Channel Fill	Light tan, grey, red or brown	Matrix lower fine sand, Clasts go from sand to cobble	Carbonate Caprock Clasts, mud rip ups, quartz and feldspar sand,	Lower erosional contact	10 cm – 5 m	Thin to medium bedding, 1-5 m wide, multi storied channels, conglomerates are truncated by sandstones on either side, interbedded or grades with channel sandstones	Normal grading, T X-beds, Some horizontal bedding	Occasional petrified wood	Gm, Gt
FA2	Noncaprock bearing Stratified Conglomerate and Sandstone Channel Fill	Tan, light – dark red, grey	Fine to medium sand	Sub Arkosic	Lower erosional contact	10 cm – 10m	Single to Multi-story channels, single channels can reach up to 75-100 meters along strike	Lateral Accretions, T X-beds, Ripple and horizontal laminations	Occasional petrified wood and carbon film	Ss, Gr, Gt, St
FA3	Overbank	Brick red, green or grey	Mud to fine sand	Quartz, Clay minerals	Gradational	10 cm – 10+m	Laterally continuous, Tabular bedding	Climbing Rippled, Dessication cracks	Root casts, mottling Burrows,	Fl, Fm, Scr
FA4	Paleosols	Light red - red	Clay to very fine sand	Quartz, Clay Minerals	Gradational	~12 m	Laterally continuous, associated with overbank deposits, developes in top of beds	Blocky looking peds	Rare ryzoliths, root mottleing	P, Fr
FA5	Marsh/Pond	Dark red	Clay to fine sand	Quartz, Kspar, Clay minerals	Gradational	~1m	Isolated lenses	Laminated sandstones	Concretions, Septerian Nodules, Bivalves	Fh, Fl
FA6	Lacustrine	Dark red, green	Clay to fine sand	Quartz, Kspar, Clay minerals	Gradational	~10 m	Isolated lenses	———	Bioturbation	Fh, Fl
FA7	Heterolithic Channel Fill	Dark red, tan, grey	Matrix lower fine sand, Clasts go from sand to cobble	Carbonate Caprock Clasts, mud rip ups, quartz and feldspar sand,	Lower erosional contact	~7-10 m	Sigmoidal bedding, isolated, occuring near salt contact	Normal grading, T X-beds, Some horizontal bedding, some clay drapes	———	Ss, Gr, Gt, St Fl, Fm, Scr
FA8	Unsorted Conglomerate	Light grey, tan, green, red	Coarse sand to boulders	Carbonate Caprock, Quartz, Chert	Lower erosional contact	2.5 m+	Isolated, occuring near salt contact	no internal bedding	n/a	Gmm

2.3 Differences in Facies Association by Locality

Each location of study provides insight into the complexity of salt-sediment interactions. The facies associations indicate distinct environmental differences related to diapiric rise and basin subsidence. From a large-scale perspective, Chinle Formation sediments coarsen away from the GV diapir and less facies associations are also present with distance (Table 3). Near the diapir, the conglomeratic lenses of FA1 disappear after 0.7 km of the diapir and ripple cross-stratified sandstones (Sr and FA2) correspondingly thicken. The stratigraphic section in Summit Canyon, is interpreted to represent the upper ~50 m of the far end of Bridge Canyon, sharing both unconfined fluvial systems and an absence of FA1.

Table 3: Facies Association Percentages by Stratigraphic Section. Each stratigraphic section and facies association percentages for Bridge Canyon, Box Canyon and Summit Canyon. The green percentages indicate the dominant facies association per section. Sections are visible in figure 36 a&b, 37 a&b.

Bridge Canyon						
Stratigraphic Section	3.3	S4	S2	S3	S1	
Distance from Diapir (km)	0.48	0.68	0.83	0.20	0.55	
Covered	2.96%	2.78%	6.64%	15.15%	13.33%	
FA1 Caprock Bearing	10.37%	9.72%	18.85%	0.00%	0.00%	
FA2 Non-Caprock Bearing	62.96%	7.64%	9.05%	35.61%	80.00%	
FA3 Overbank	23.70%	72.92%	58.22%	41.67%	4.67%	
FA4 Paleosol	0.00%	6.94%	7.24%	7.58%	2.00%	
FA6/7 (Marsh/Pond Lacustrine	0.00%	0.00%	0.00%	0.00%	0.00%	
Box Canyon Transect						
Stratigraphic Section	3.5	3.6	3.7	3.4	R2	R1
Distance from Diapir (km)	0.00	0.01	0.01	0.02	0.25	0.26
Covered	8.35%	0.00%	0.00%	21.23%	0.00%	0.00%
FA1 Caprock Bearing	6.11%	19.67%	13.19%	26.10%	34.16%	20.73%
FA2 Non-Caprock Bearing	60.08%	3.28%	6.25%	15.72%	34.16%	45.73%
FA3 Overbank	14.26%	67.21%	65.28%	33.81%	29.82%	30.49%
FA4 Paleosol	0.00%	0.00%	0.00%	0.00%	0.00%	0.00%
FA6/7 (Marsh/Pond Lacustrine	0.00%	9.84%	15.28%	3.14%	1.85%	0.00%
Summit Canyon						
Stratigraphic Section	3.8					
Distance from Diapir (km)	12.00					
Covered	14.66%					
FA2 Non-Caprock Bearing	46.55%					
FA3 Overbank	38.79%					

Percentages of different lithologies were estimated from measured stratigraphic sections. Facies were grouped into the dominant Facies Associations: FA1-6 and covered interval, and the percentages calculated (Table 3).

Of the three study locations, Summit Canyon, 12 km from the diapir, is dominated by ~50 meters of coarse to medium-grained sandstone of FA2 and minor fine-grained sandstone and siltstone of FA3. No caprock conglomerates were identified, indicating that the material either breaks down before it can travel that far, or there is a depositional barrier to the source carbonate material.

Summit Canyon is characterized by broad FA2 channels, composed of medium to coarse-grained sand, could be traced >50 meter along the canyon wall. Lithofacies of light red to tan, well-sorted trough cross-bedded sandstone (St), massive sand (Sm) and siltstone (Fm, Fh) were documented. Thin FA3, overbank deposits crop out over in the section, at the top of the section was the thickest interval of FA3 at 20 meters.

In the Bridge Canyon study location, ~1 km away from the GVSW, stratigraphic section S1, records the uppermost strata of the Chinle Formation (Strata dips away from the diapir into the Dry Creek Minibasin). In Bridge Canyon, the furthest section (S1), also the thinnest (30 meters, other stratigraphic sections range from 66-170 meters), was 80% sandstone. Although a poor representation of total stratigraphy, the facies documented indicate a facies change at the top of the Chinle Formation ~1 km from the GVSW. The dominant facies association was FA2, consisting of lower medium-grained sandstones with rare FA3 documented. No FA1 conglomerates were found. Stratigraphic section (S1) bedding was thin to medium, where beds thickened upward, contacts between beds were rarely scoured and predominantly sharp.

Lithofacies documented Sr, Sh, rare St, and Fl. These lithofacies and facies associations indicate an unconfined braided stream with few preserved flood plain deposits.

In the area of Bridge Canyon (S2 and S3), 0.5-0.7 meters from the diapir, and is the extent of FA1 caprock conglomerate beds. Sections closer to the diapir illustrate that siltstones becomes the dominant lithology, in the fullest sections measured (58% in S2 and 48% S3). Conglomerate percentages increase towards the diapir (18.8% in S2 and 0% S3). Stratigraphic sections measured varied greatly in thickness from 166 meters in S2 and 66 meters in S3. Facies associations include FA1 caprock bearing conglomerates and sandstones, FA2 non-caprock bearing conglomerates and sandstones, FA3 overbank deposits, and FA4 Paleosols. Lithofacies of these associations include Sm, Sr, Sl, conglomerates, Scr, and siltstones. Bedding is medium to thick and scoured contacts occur between channels.

In Bridge Canyon 0-0.3 km from the GV in the area of the GVSV (stratigraphic sections 3.3 and S4) (Figure 4, 36a), stratigraphic thicknesses differ greatly, 67 meters in 3.3 and 144 meters in S4. McFarland (2016) documented the facies distribution and channel geometry in detail. The closest sections illustrate, which is thinner because it is on top of the GVSV, and becomes sandstone dominated (for stratigraphic section 3.3 FA1 composes 10.4% and FA2 composes 63%). This probably occurs as the salt wall sheds diapiric material that remains proximal to the source while coarser sediment from the Chinle rivers was deposited in depocenters in the minibasins far from the onlap of the GVSW.

Three-dimensional exposure of intraformational unconformities formed when rotated growth strata eroded on the flank of the diapir indicating that the Upper Triassic Chinle Formation deformed syndepositionally as the salt diapir rose. Permian and Triassic angular unconformities have been attributed to salt tectonics in the past but have not been placed in a

halokinetic sequence framework until recently (Matthews et al., 2007; Dubiel et al., 2009). Additionally, breaching of the diapir occurred when Chinle fluvial systems penetrated the diapir, forming unique and restricted conglomerates derived from the eroding caprock. As strata deformed and tilted because of halokinesis, sedimentation, subsidence, and deposition continued (Kluth and DuChene, 2008).

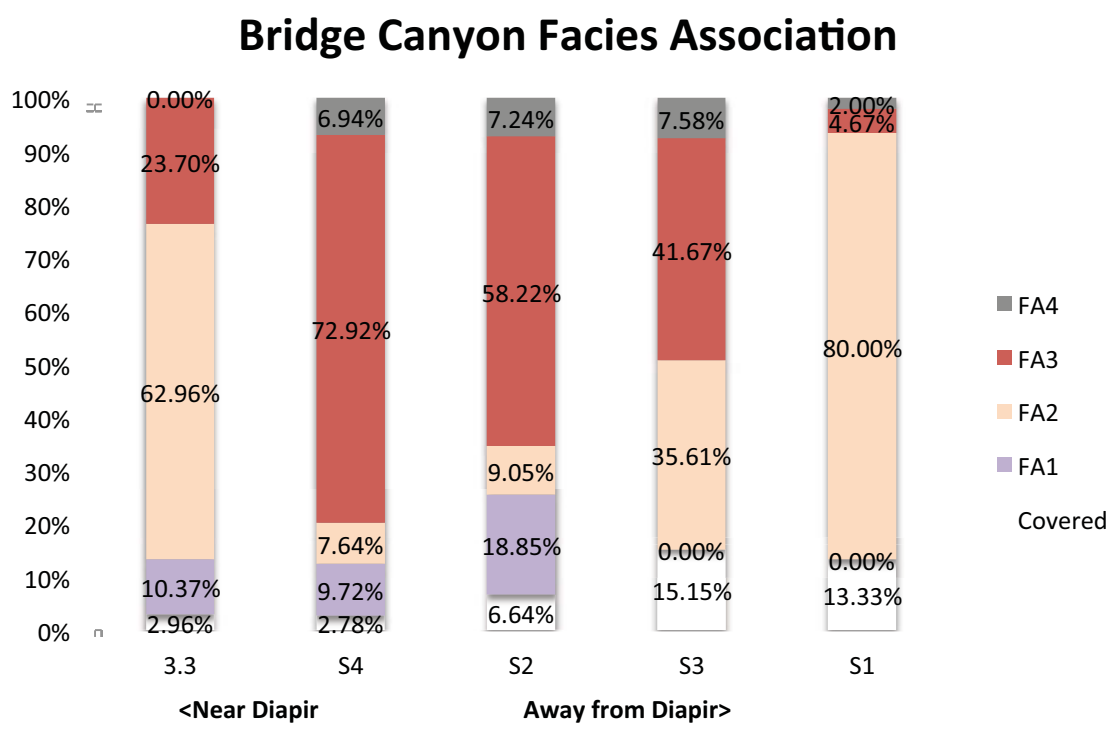

Chart 1: Graphic representation of facies association as seen in Table 3 for Bridge Canyon. Section 3.3 is most proximal section to diapir and section S1 is the most distal section to the diapir. Section locations visible in figure 36a&b and Appendix 2.

Along the GVSWcontact the Box Canyon transect strata displays the greatest variations in facies associations (Table 3, Chart 2). Proximity to the topographic highs and lows altered bedding geometries, depositional environments, and facies distributions. The Box Canyon traverse provided an along strike view of the undulating surface topography. The forming topographic lows provided adequate accommodation space for development of pond or

lacustrine facies. Along strike of the diapir, over 3 km, the dominant lithology evolved from siltstones to sandstones. Siltstones were greater than 50% where the GVSW had formed a depression. Sandstones dominated and conglomerates appeared closer to the topographic highs, where sections were also thinner.

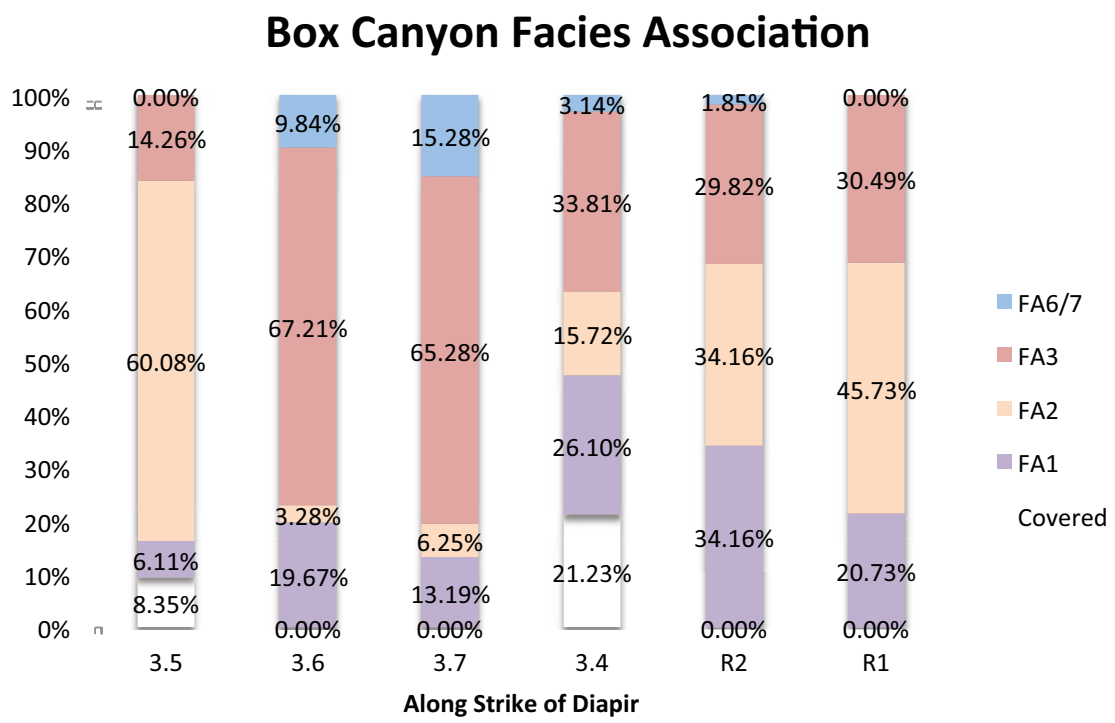

Chart 2: Graphic representation of facies association as seen in Table 3 for Box Canyon. Section 3.5 is section furthest to the North and R1 is closer to Bridge Canyon. Section locations visible in figure 37a&b and Appendix 2.

Chapter Three: Petrographic Facies and Diagenesis

Samples were selected to reflect the variety of different lithologies as well as to represent different distances form the GVSW. Of the 58 thin sections analyzed petrographically, 25 were from FA1, 16 from FA2, 8 from FA3, 6 from FA4, 2 from FA8 and 1 from FA5. Thirty-four samples came from sandstones, 16 from conglomerates and 8 from mud/siltstones. Samples were divided into petrographic facies based on detrital mineralogy, cement, and pore fabric. Cement, dissolution, and compaction relationships were used to reconstruct the paragenetic history.

On outcrop several different diagenetic overprints are obvious as color variations in the Chinle strata (Figure 4). The zone nearest the salt wall, "collar" of the shoulder of McFarland (2016) is faulted and the color is reduced from red to yellow. The usually obvious stratal differences between facies and formations are obscured by diagenesis in this area, and are often difficult to separate Chinle from the overlying Wingate Sandstone. Nine samples were collected from sections 3.3 and S4 within this zone (Figures 15 and 16). Farther from the GVSW, sandstones are colored red, and brown red, whereas siltstones are colored orange-red. Ten samples were collected from the area nearest the salt wall from this area, the "lateral" of McFarland (2016)(Figures 16, 28). The greatest number of lithofacies changes occurs in this interval. At the Summit Canyon outcrop, 12 km from the GVSW, sandstones are light red in outcrop. Seven samples were collected from this unit, all from FA2 (Figures 16, 28). Summit canyon samples are distinct from other areas sampled because of their coarser grain size and more rounded clasts.

Of 58 thin sections 23 sandstone samples were point counted to estimate lithology, cement types and porosity. Three hundred points were counted on each thin section. Clastic grains formed 47-82% of the samples (Figure 15). Grain composition varied from 53-87% quartz, 10-25% feldspar, and 1-35% lithics. Plotted on a ternary diagram of Folk (1974), samples can be classified as lithic arkose or feldspathic litharenites.

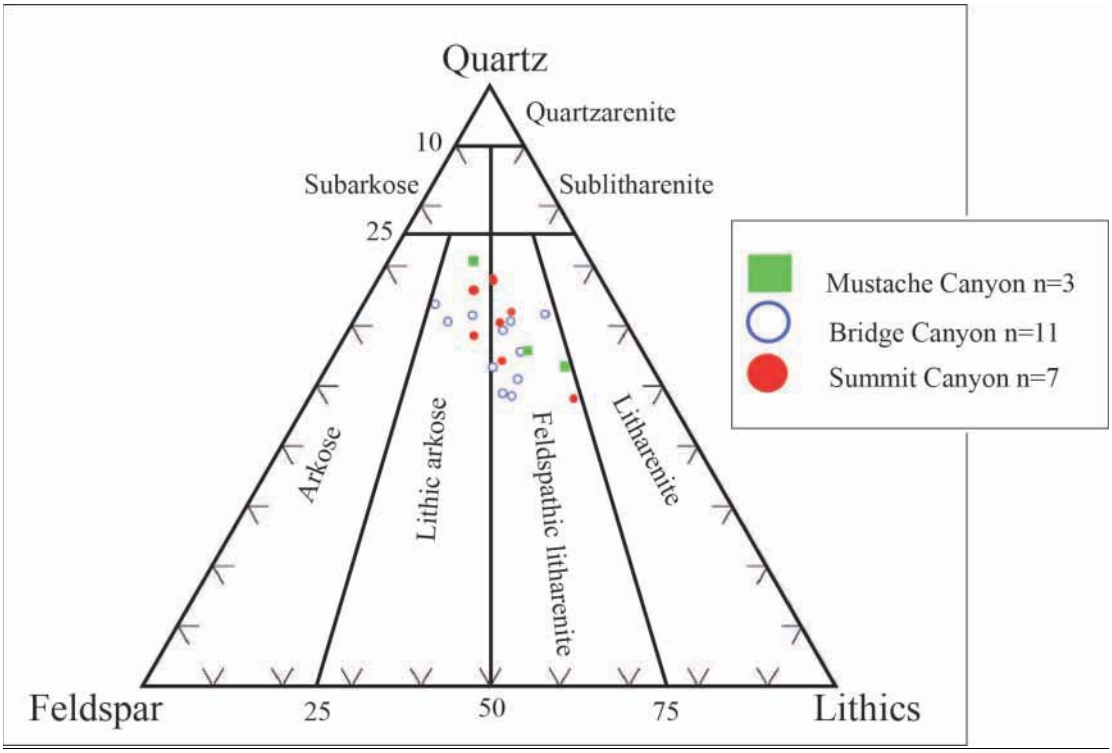

Figure 16: Ternary sandstone composition diagram after Folk (1980) for Mustache Canyon, Bridge Canyon, and Summit Canyon. Samples from the three locations were compared to determine compositional differences.

Figure 17: Locations of thin sections and thin section labels, excluding Summit Canyon.

3.1 Petrofacies Association (PFA)

Six petrofacies were identified from the 58 thin sections. These were differentiated based on percentages of cement, porosity, and grain composition.

3.1.1 PFA1: PFA1 was identified in samples BMS1, LS3, and S4S3. These samples were from reddish gray sandstones and were from FA2. All three samples were obtained in sections S1&2 (Figure 36a&b), 1 km from the diapir wall in the Bridge Canyon area in HS-3, the upper unit, right below the Wingate contact. PFA1 samples (Figures 18, 19, and 20) display less compaction than other samples; grains contain abundant quartz overgrowths and a small amount of secondary porosity. Grains form 60-76% of this facies. Monocrystaline quartz varies in abundance from 48 to 61%. Feldspar varies from 22 to 25%. Lithic clasts are dominated by micas and amphiboles, which form 13-24% of the samples. Grains are not deeply embayed but do appear to touch, forming a mosaic fabric, indicating that, while less than in other units, these samples were compacted. Cements compose 10 to 30% of these samples and include 10-23% calcite (both pore-filling and lining) and 29-80% dolomite (pore lining). Secondary porosity makes up 0 to 1.8 % of the samples. The secondary porosity evolved from the dissolution of early calcite cement.

PFA1 is characterized by early quartz overgrowths and can be differentiated from the other diagenetic facies based on lack of porosity, high percent of dolomite cement and detrital grain composition. Early quartz overgrowths prevented overcompaction of grains as seen by sutured contacts then a late stage dissolution event caused secondary porosity (Figure 19). As seen in Figure 18, the images indicate early quartz overgrowth cement occurring before compaction and irregular pores and dissolution fabric on some grains show late stage secondary porosity.

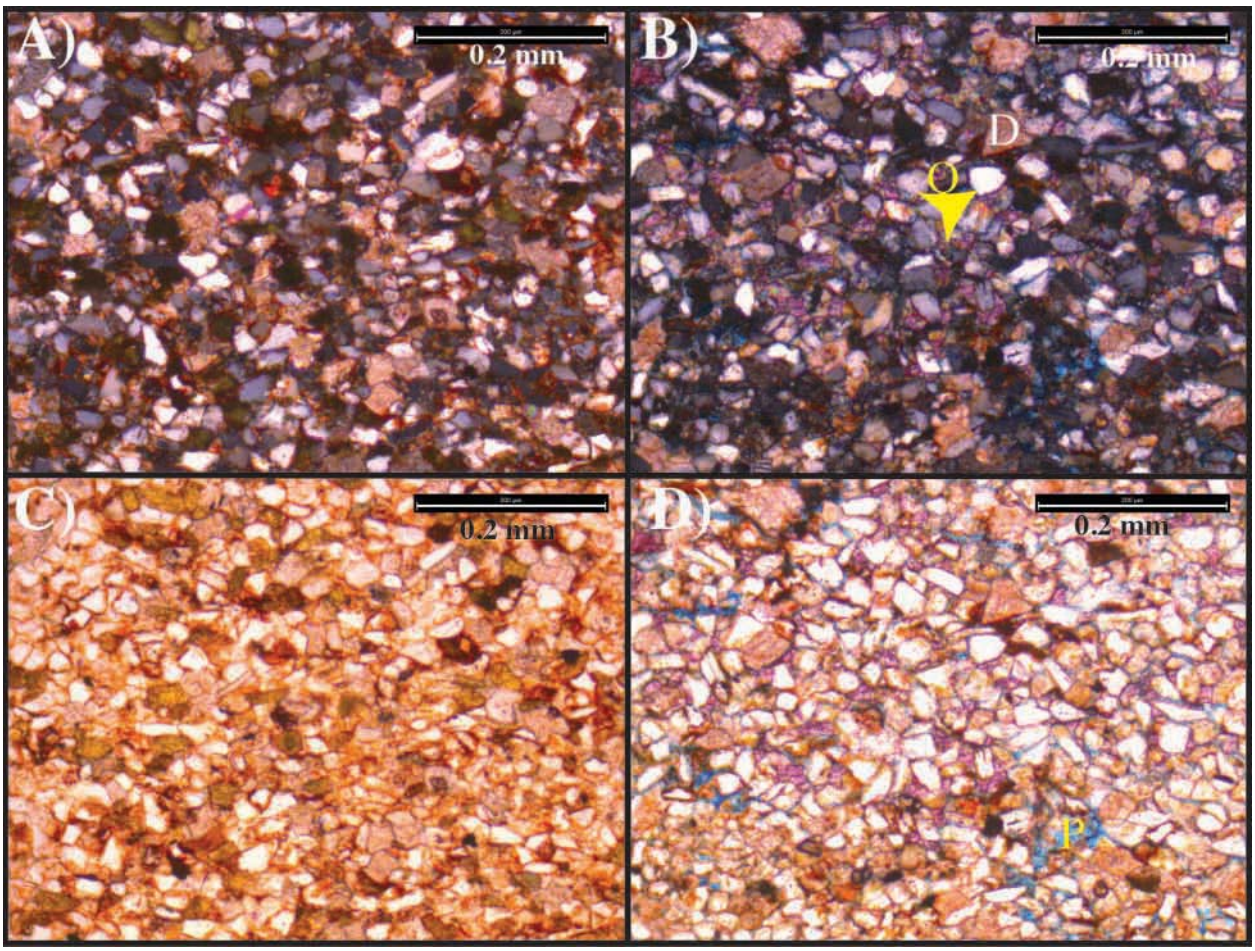

Figure 18: PFA1 thin section BMS1 from Bridge Canyon Section S1. From Unit 1, FA2, Stained for Potassium Feldspar on the left (A&C) and Calcite and porosity on the right (B&D). (A&B) are photographed under cross-polars and (C&D) are under plane light. The pink indicates calcite grains, dolomitic cements form as rhombic crystals (D) between grains. Secondary porosity appears in pods or isolated areas (P). Quartz overgrowths are identified with (Q). Scale is 0.2 mm in all photomicrographs.

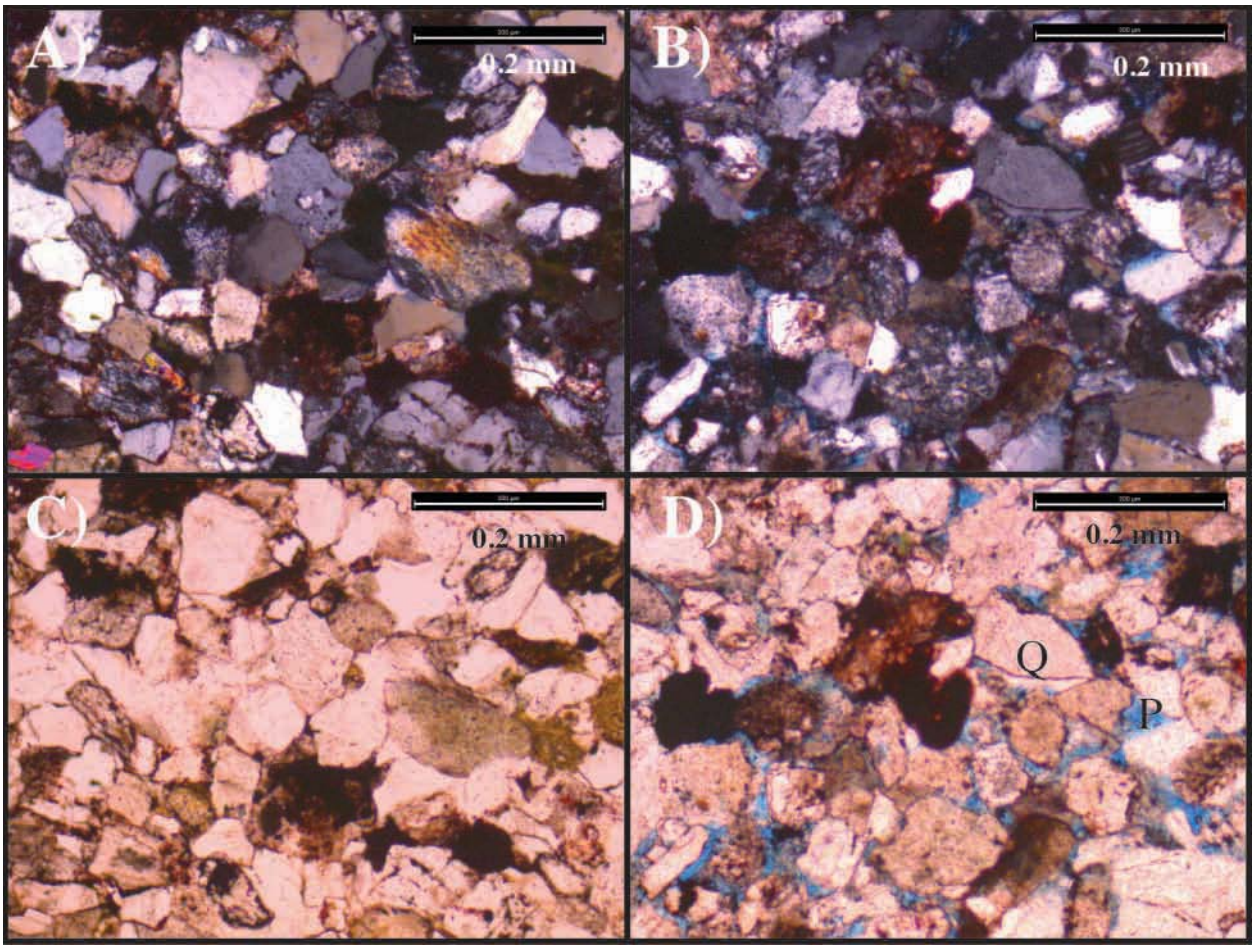

Figure 19: PFA1, thin section LS3 from Bridge Canyon. Stained for Potassium Feldspar on the left (A&C) and Calcite and porosity on the right (B&D). (A&B) are photographed under cross-polars and (C&D) are under plane light. The images indicate early quartz overgrowth cement (Q) occurring before compaction and irregular pores (P) and dissolution fabric on some grains late stage secondary porosity. Sandstone is coarser than previous two samples. Scale is 0.2 mm.

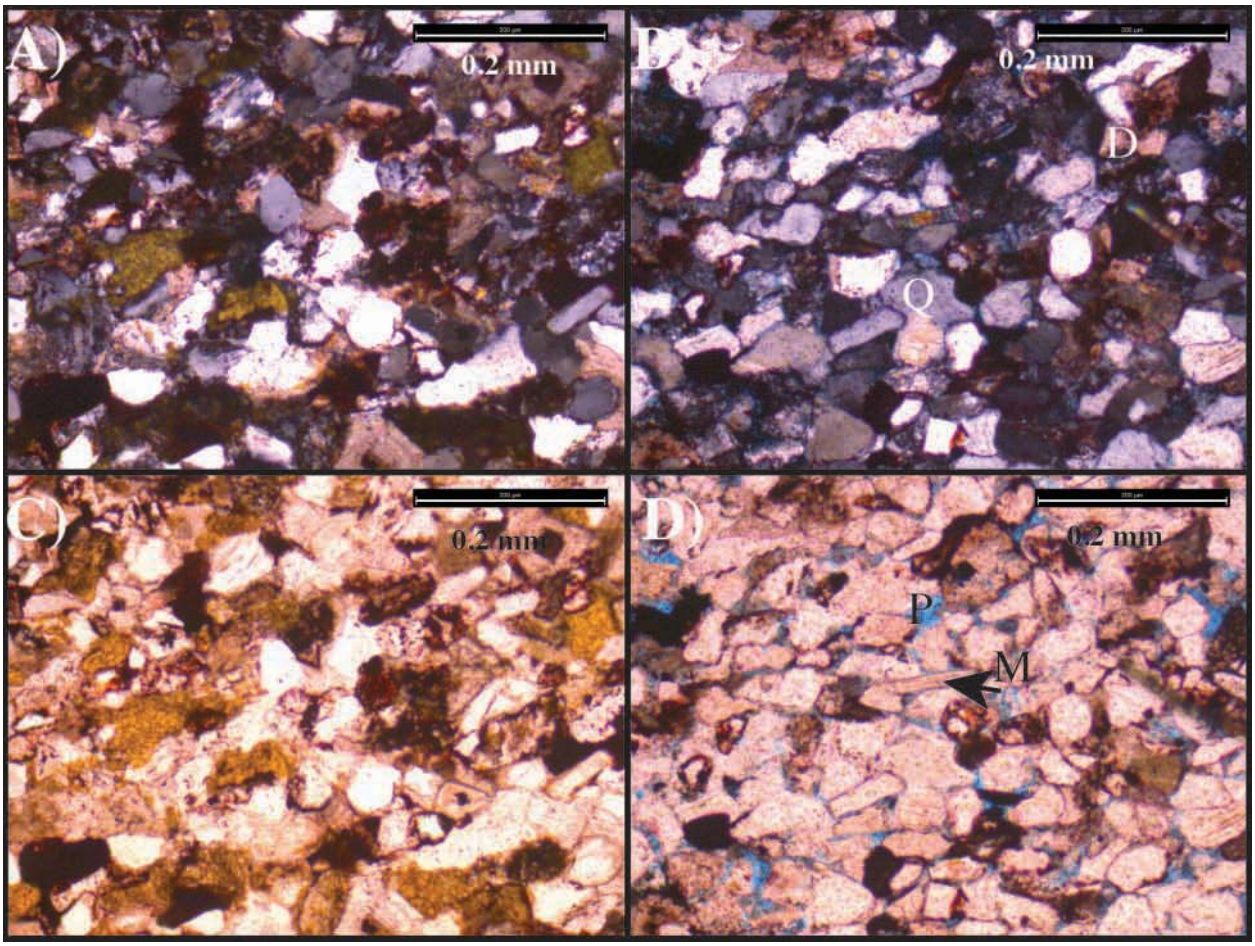

Figure 20: PFA1, sample S4S3 from Bridge Canyon. Location shown in Figure 16. Stained for Potassium Feldspar on the left (A&C) and Calcite and porosity on the right (B&D). (A&B) are photographed under cross-polars and (C&D) are under plane light. Detrital grains indicate a slightly higher potassium feldspar content compared to Figure 18 above. Early quartz overgrowths prevented overcompaction of grains as seen by sutured contacts then a late stage dissolution event caused secondary porosity (P). M and arrow points to uncompact muscovite grain. Scale is 0.2 mm.

3.1.2 PFA 2: PFA2 was identified in samples S5S5, and #8. These samples were from red sandstones of FA1. Samples were collected from unit 2 in sections S3 (Figure 28). Samples identified with just a #number were collected by Josh McFarland and are proximal to the salt wall and faulted strata.

Detrital grains compose 69-77% of sample; clasts include quartz, potassium feldspar, dolostone lithic grains (derived from the adjacent diapir) and clays (Figure 20). Grains appear to

be in contact with each other and have slight embayment (Figure 21). In this petrofacies, clay rims are visible, and significant compaction had occurred before cementation. The detrital minerals are 51-64% quartz and a higher lithic content of 18-28%. Cements compose 22-30% of samples and of that 22-30% cement dolomite is greater than calcite (50%) for dolomite and for calcite (0-15%). Porosity is very limited, forming 0.92-1.8% of samples.

This petrofacies can be distinguished from PFA 1, because it exhibits little to no porosity. Though it has early quartz overgrowths it shows higher degrees of compaction. Quartz grains (Figure 21, arrows, R) appear to have a jagged edge. This is reflected in the smaller percentage of early cement and porosity (Figure 21), which indicates less early cementation and resultant greater compaction.

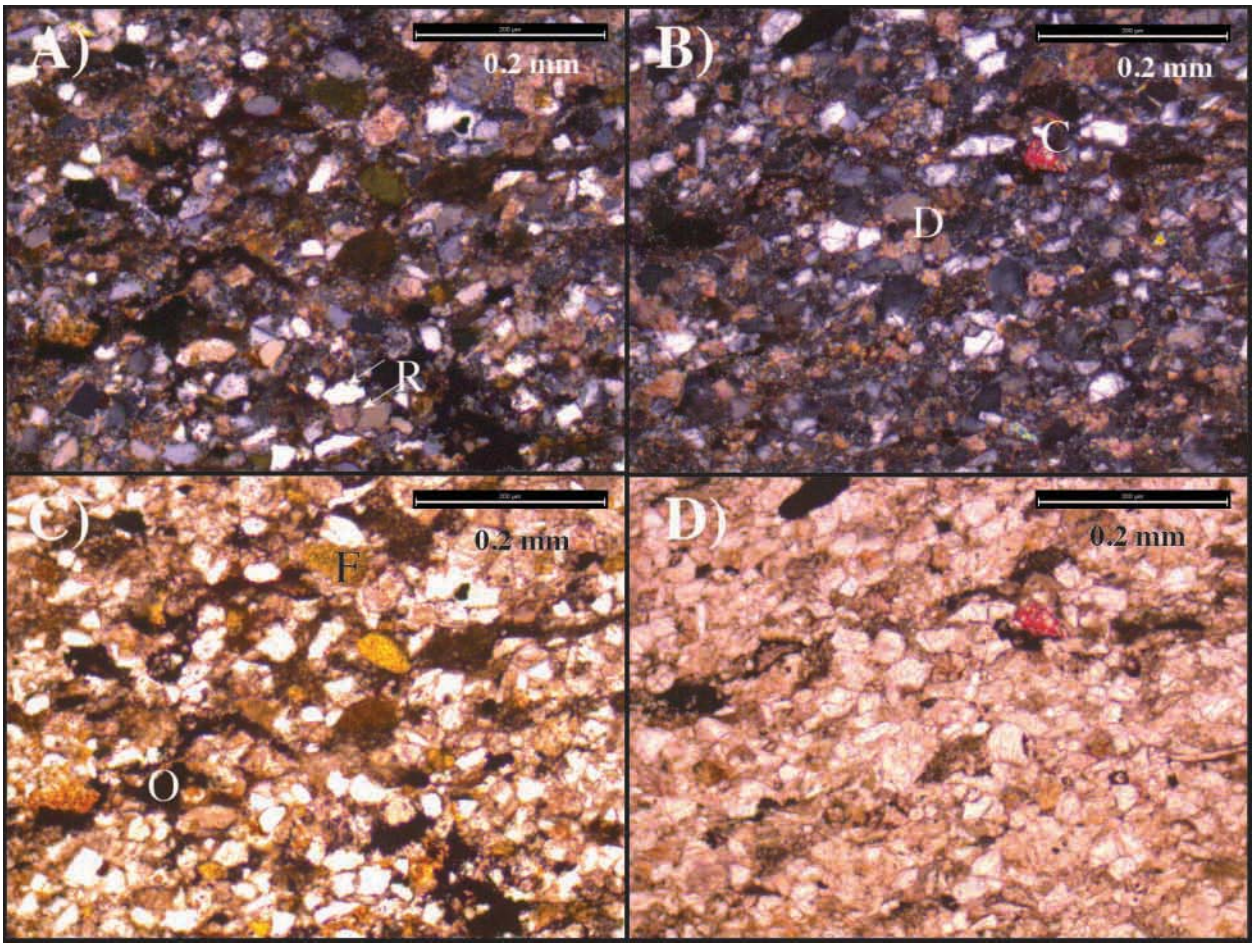

Figure 21: Sample S5S5 from close proximity to the diapir in Bridge Canyon. Stained for Potassium Feldspar on the left (A&C) and Calcite and porosity on the right (B&D). (A&B) are photographed under cross-polars and (C&D) are under plane light. Detrital composition consists of quartz grains (Q), potassium feldspar (F), dolomite grains (D), and clays (O). This location exhibits little to no porosity but does show signs of early quartz overgrowths and compaction; quartz grains (arrows, R) appear to have a jagged edge. Scale is 0.2 mm.

3.1.3 PFA3: PFA3 was identified in samples GVEH5, S3S2, and GVEH6. These samples were from yellow-tan sandstones. Sample GVEH5 is found in the uppermost Chinle Formation, in WHS-3 (see Chapter 4) in an area highly impacted by faults and fluid flow, on the collar of the GVSW shoulder. The samples from petrofacies 3 were collected are less than 0.3 km from the diapir wall, some were collected in strata that overtopped the salt wall. Detrital grains compose a much smaller percentage of this petrofacies (55-70% of sample). Grains include quartz,

potassium feldspar, dolostone lithic grains (derived from the adjacent diapir), and clays. PFA-3 samples exhibit no porosity, early compaction, quartz overgrowths forming euhedral crystals and dolomite cement (Figure 22). Although grains are compacted a clay rim appears between grains (Figure 21).

PFA3 can be distinguished from the other petrofacies based on grain percentages, lack of porosity and embayment of grains. Figure 22 has undergone greater compaction than the other samples as seen by the embayed grains (D) and the number of grains with quartz overgrowths (Q). C indicates clays (arrows) between grains.

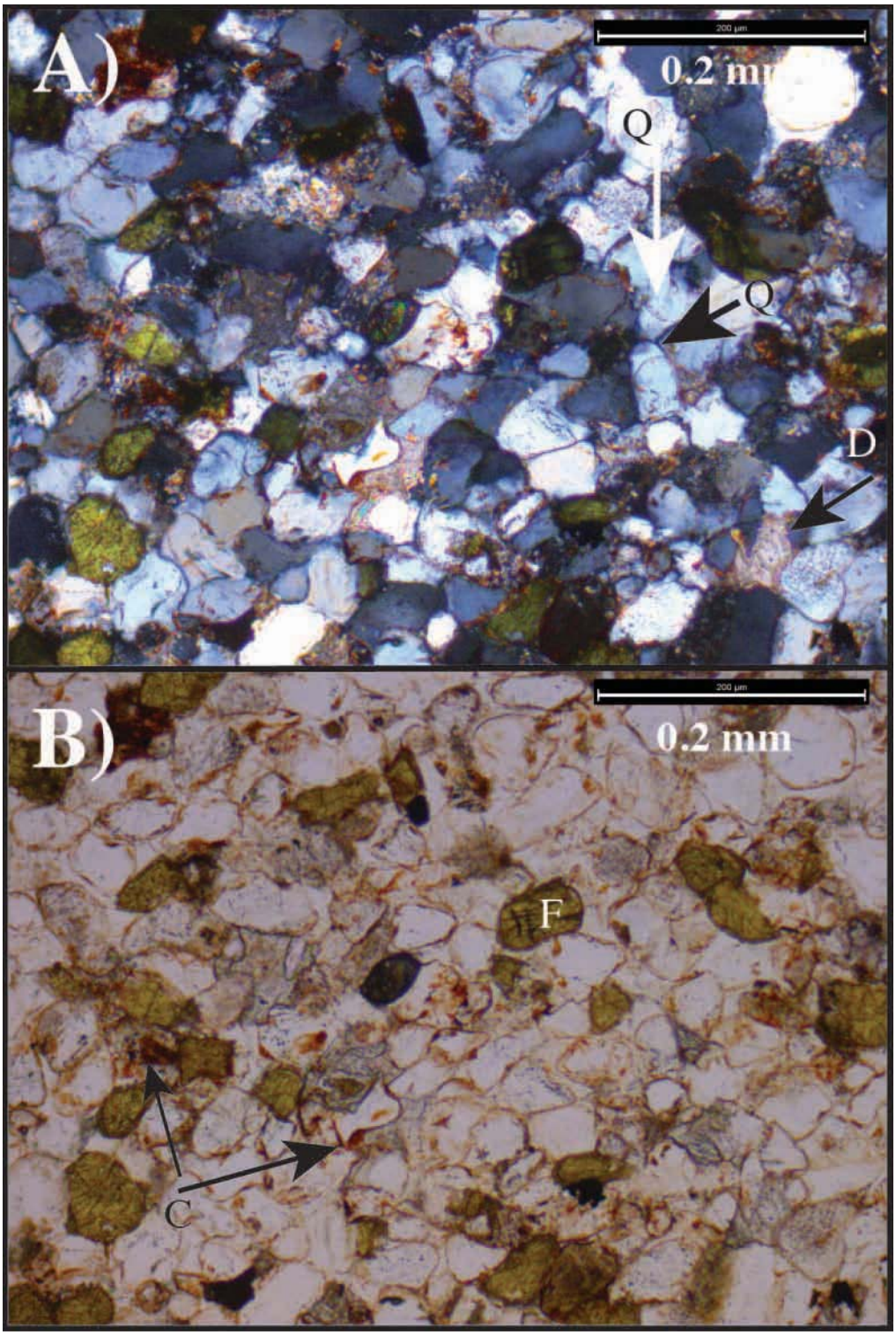

Figure 22: Sample GVEH5 is from Chinle Strata that overlapped the SW in Bridge Canyon. Sample GVEH5 as seen in figure 17, 28, from PFA3. (A) photographed under cross-polars and (B) under plane light. The location of this sample occurs in the upper unit of the Chinle Formation (See Chapter 4) but has undergone greater compaction than the other samples as seen

by the embayed grains (D) and the number of grains with quartz overgrowths (Q). C indicates clays (arrows) between grains and F indicates feldspar grains. Scale is 0.2 mm.

3.1.4 PFA4: PFA4 was identified in samples 3.5.4, 3.9.4 and 3.10.1. These samples were from red sandstones. Samples were collected from units 3 and 4 in sections 3.5, 3.9 and 3.10 (Figures 23, 23b, 28). These samples were taken with close proximity to the diapir (<100 m) and were collected in an area called "Mustache Canyon" and from the Box Canyon transect. PFA4 samples contain interstitial secondary porosity, with clay rims between early compacted grains (Figures 23-23b). The distinguishing characteristic of these samples is the presence of calcite replacing dolomite. In thin section calcite replaces the outer edges of cloudy pore filling dolomite cements (Figure 23). Samples point counted exhibit an average of 66% grains, 2-10% porosity, and 15-30% cement. Grain percentage is similar to other petrofacies. The porosity averages the second highest and is most variable in this petrofacies. The cement is one of the higher percentages compared to other petrofacies.

The combination cement and porosity and the occurrence of mud/clay in the sample, this gives them a "dirty" appearance but does not limit porosity. The occurrence of "patches" of calcite and dolomite cement surrounded by secondary porosity between grains indicates that at some earlier diagenetic stage was less porous and has a greater amount of dolomitic cement, but overtime fluids have dissolved this dolomite cement and there has been a minor amount of calcite replacement. There is also potential mechanical fracturing.

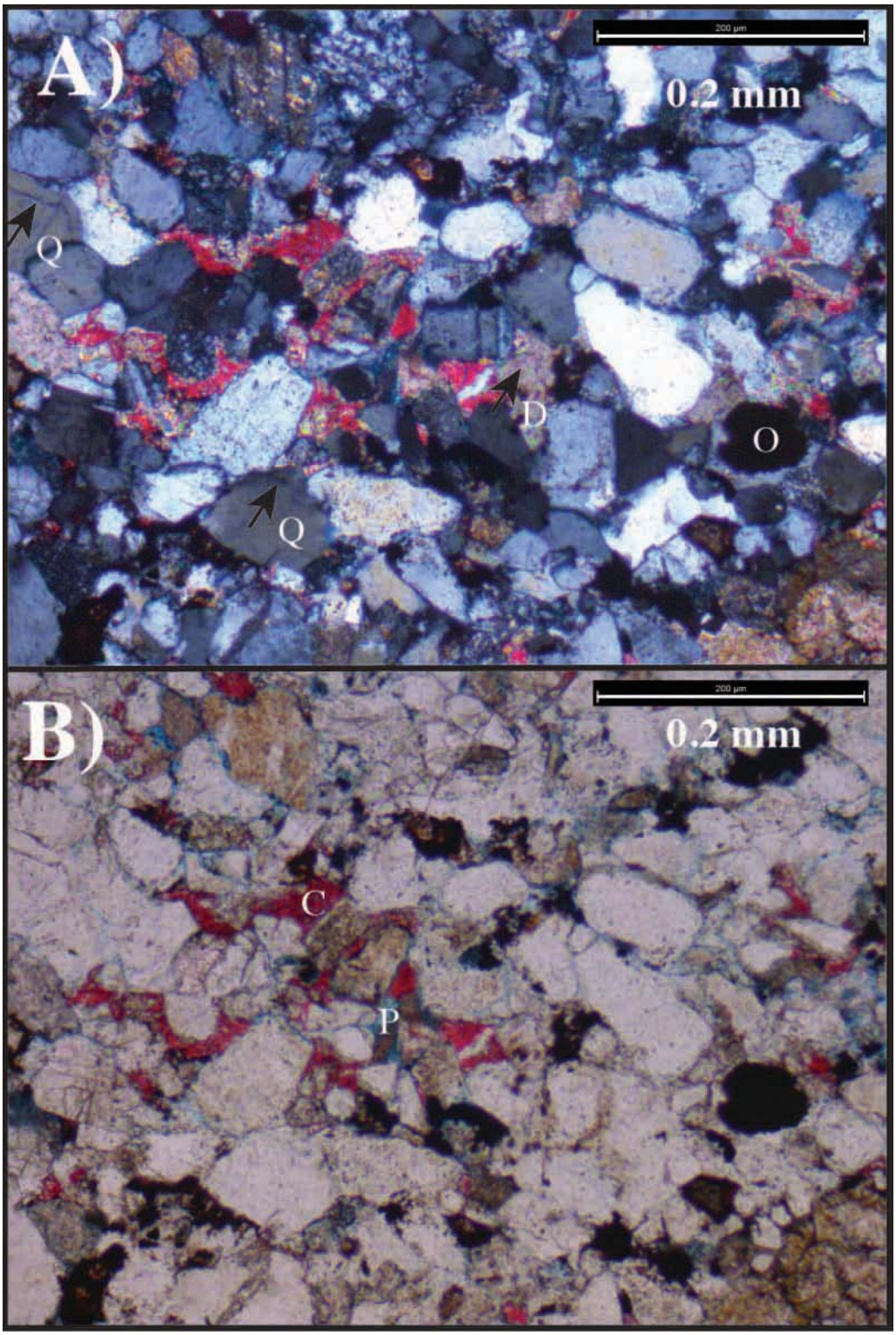

Figure 23: Sample 3.9.4 from Mustache Canyon as seen in figure 17, 28. Scale is 0.2 mm. Quart Overgrowths are seen between quart grains (Q and arrow). Dissolution is seen from secondary porosity (P) preserved by blue dyed epoxy. O indicates rounded opaque grains. Calcite (C) and Dolomite (D) indicate remnant grains.

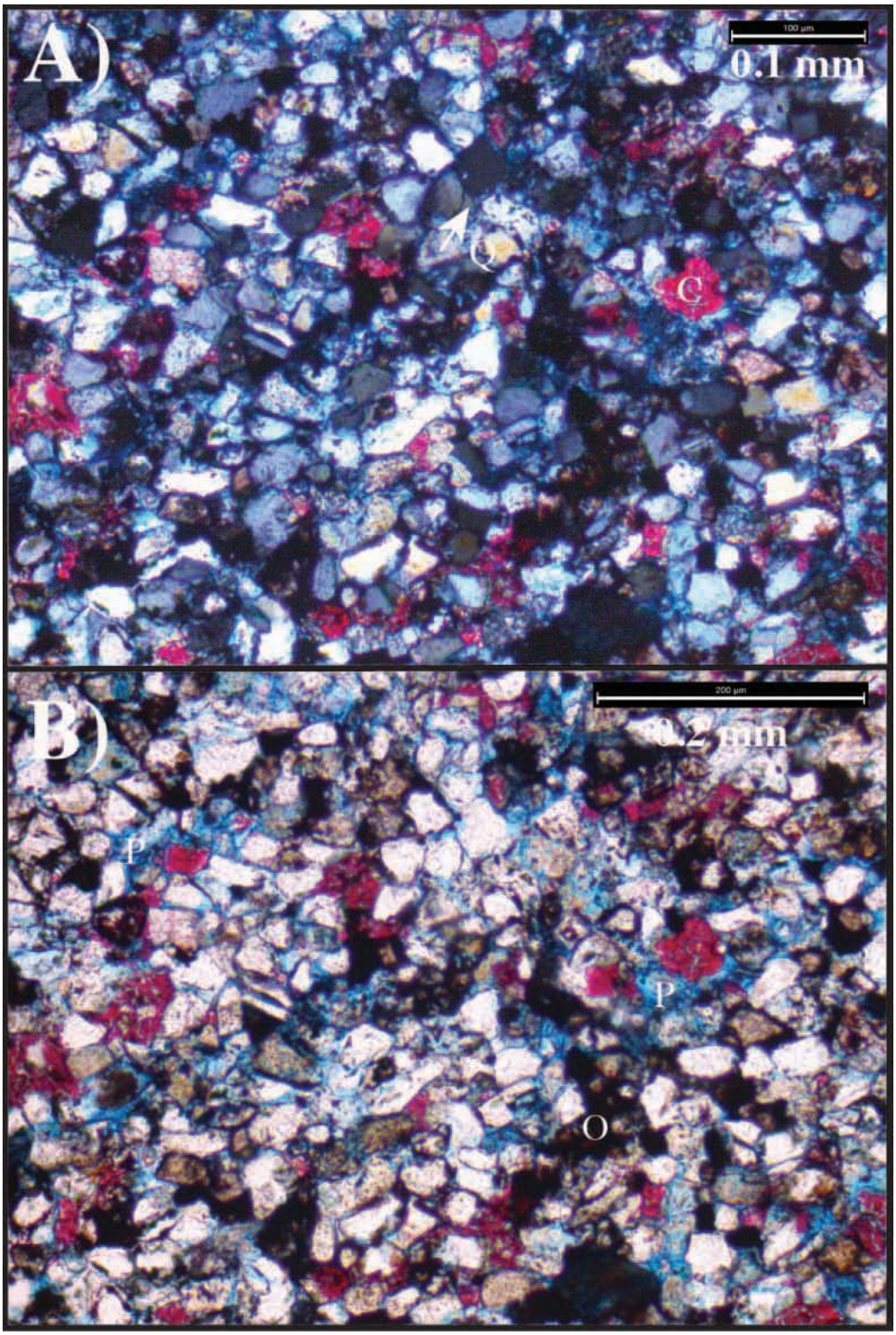

Figure 23.b: Sample 3.10.1 from Mustache Canyon as seen in figure 17, 28. Scale is 0.2 mm. Quart Overgrowths are seen between quart grains (Q and arrow). Dissolution is seen from secondary porosity (P) preserved by blue dyed epoxy. O indicates rounded opaque grains. Calcite (C) and Dolomite (D) indicate remnant grains.

3.1.5 PFA5: PFA5 was identified in samples 3.8.7, 3.8.5, and 3.8.2. These samples were from red coarse-grained sandstone. Samples were collected from units 2, 5, and 7 in section 3.8 of summit canyon (Figure 6), roughly 10-12 km from the edge of the gypsum valley salt wall margin. This petrofacies is different from the other petrofacies because of the high secondary porosity, coarseness, and rounding of detrital grains. These samples are highly compacted but contain late stage dissolution, late stage dolomite and calcite cement (Figures 24, 24.b &25). Detrital grains form 67-78% of samples, and total cements form 7-18%. Porosity within the Summit Canyon samples range between 12-20%, all is secondary porosity resulting from dissolution and fractures. PFA5 have the highest porosity in any of the samples of the study areas. Detrital grains are composed of quartz percentages of 66%, feldspars roughly 18%, and lithics 16%.

Overall grain size in all samples is upper medium- to coarse-grained sand and grains appear well rounded before compaction occurred. Detrital grains consist of quartz, potassium feldspar, and rare micas (Figure 24). Quartz overgrowths occurred before compaction. Compaction is evident by visible embayed grains and a dissolution event has occurred to form secondary porosity (Figure 24). Dolomitic cements are present as well as calcite cements that appear to replace some of the dolomite cements (Figure 25).

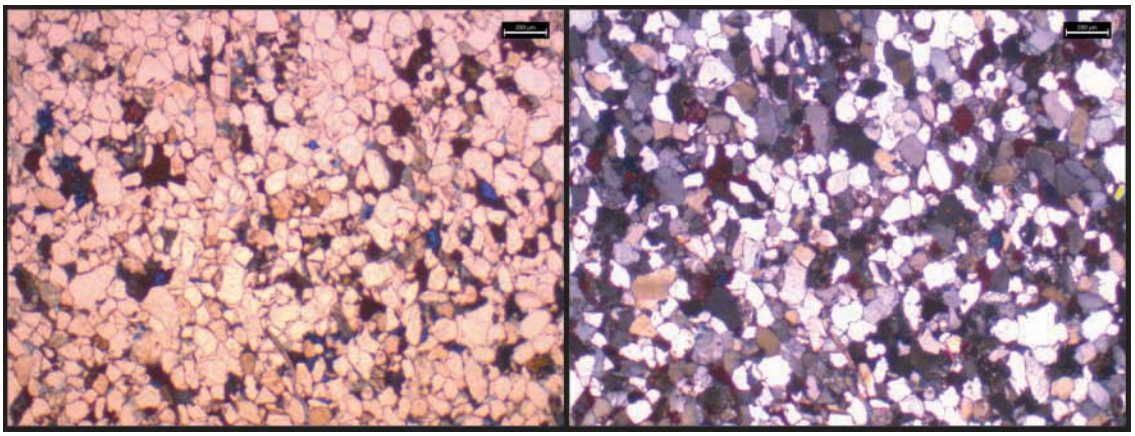

Figure 24: Sample 3.8.7 from Summit Canyon. Scale is 0.2 mm. Samples were stained for calcium carbonate and impregnated with blue epoxy. Detrital grains consist of upper medium to coarse quartz, potassium feldspar and rare micas. This location has undergone compaction as seen by visible embayed grains and a dissolution event has occurred to form secondary porosity.

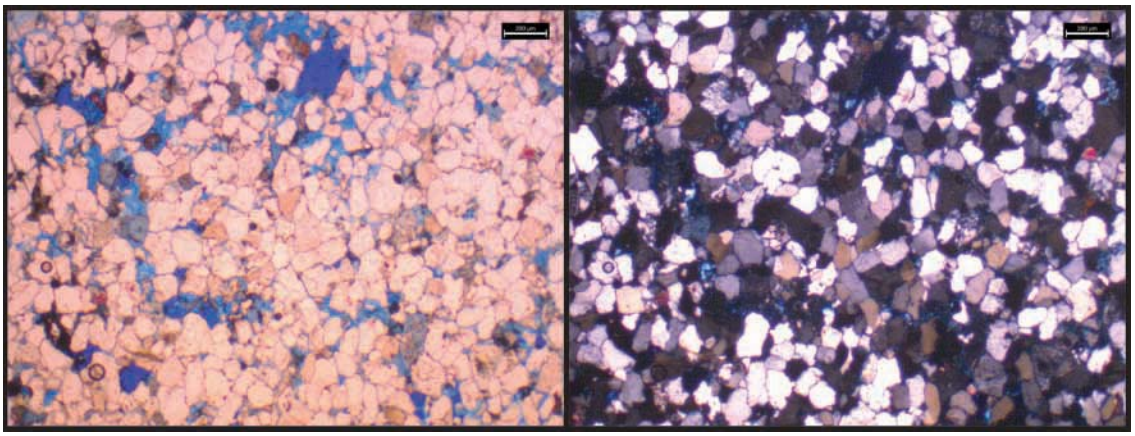

Figure 24.b: Sample 3.8.5 from Summit Canyon. Scale is 0.2 mm. Samples were stained for calcium carbonate and impregnated with blue epoxy. Detrital grains consist quartz, potassium feldspar and rare micas. Late stage secondary porosity is more prevalent in this sample than the sample above.

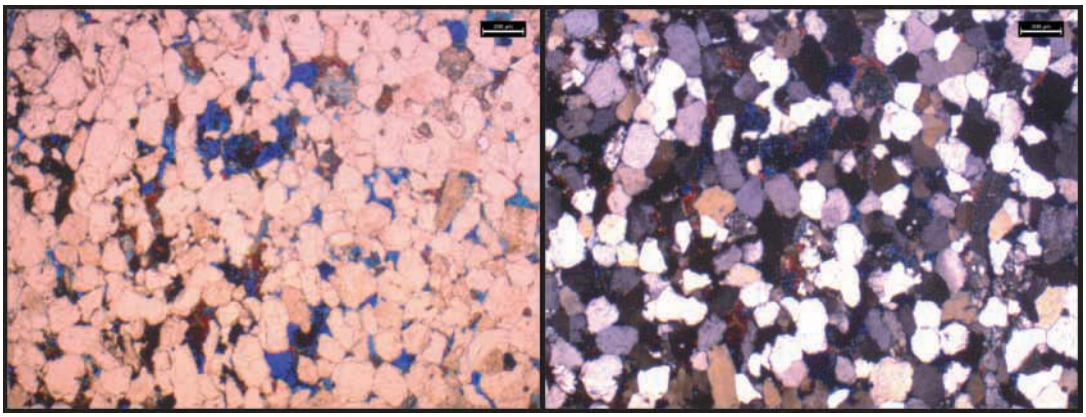

Figure 25: Sample 3.8.2 from Summit Canyon. Scale is 0.2 mm. Samples were stained for calcium carbonate and impregnated with blue epoxy. Detrital grains consist of upper medium to coarse quartz, potassium feldspar and rare micas. Late stage secondary porosity is more prevalent in this sample than the sample above. Dolomitic cements have been found and well as carbonate cements that appear to replace some of the dolomite cements. Quartz overgrowths appear to have occurred before compaction.

3.1.6 PFA 6 – Conglomerates: For simplicity, conglomerates will be grouped together as a single petrofacies and in the next section examined for diagenetic history (Figures 27, 30, 31). PFA6 samples were collected abutting the diapir and similar conglomerates are found to extend 0.5- 0.7 km from the diapir. Conglomerates are found in all stratigraphic intervals.

Samples were composed of 20-50% grains, 1-14% porosity, and 40-70% cements. Carbonate conglomerate clasts (grains) make up 70-80% of the clasts in samples. PF-6 carbonate clasts exhibit numerous carbonate fabrics from micrite (dolomite or calcite) to coarsely crystalline (dolomite or calcite). Conglomerate sample-displaying signs of dedolomitization, carbonate fabrics are mixed, containing micritic dolomite, pore filling calcite cement and detrital quartz grains,

Detrital grains, in the matrix, consist of 21-30% of grains (Figures 27, 30, 31) and are composed of mud chips, fine-medium quartz and feldspar sand. Of the 21-30% detrital clasts, quartz grains in the matrix comprise 50-70%, 7-17% feldspars and 8-50% lithics or muds.

Porosity is entirely secondary porosity and is from replacement or fractures in the conglomerates (Figures 30, 33). Porosity was lost from the high cement content. Cements compose 40-70% of samples of these samples, with the most abundant being dolomite, only one sample was highly calcitized at 84% (Figures 27, 30) (of the 40-70% cement). Small areas of patchy calcite can be found between grains but most cements conain rhombic dolomite cubes (Figures 26, 31).

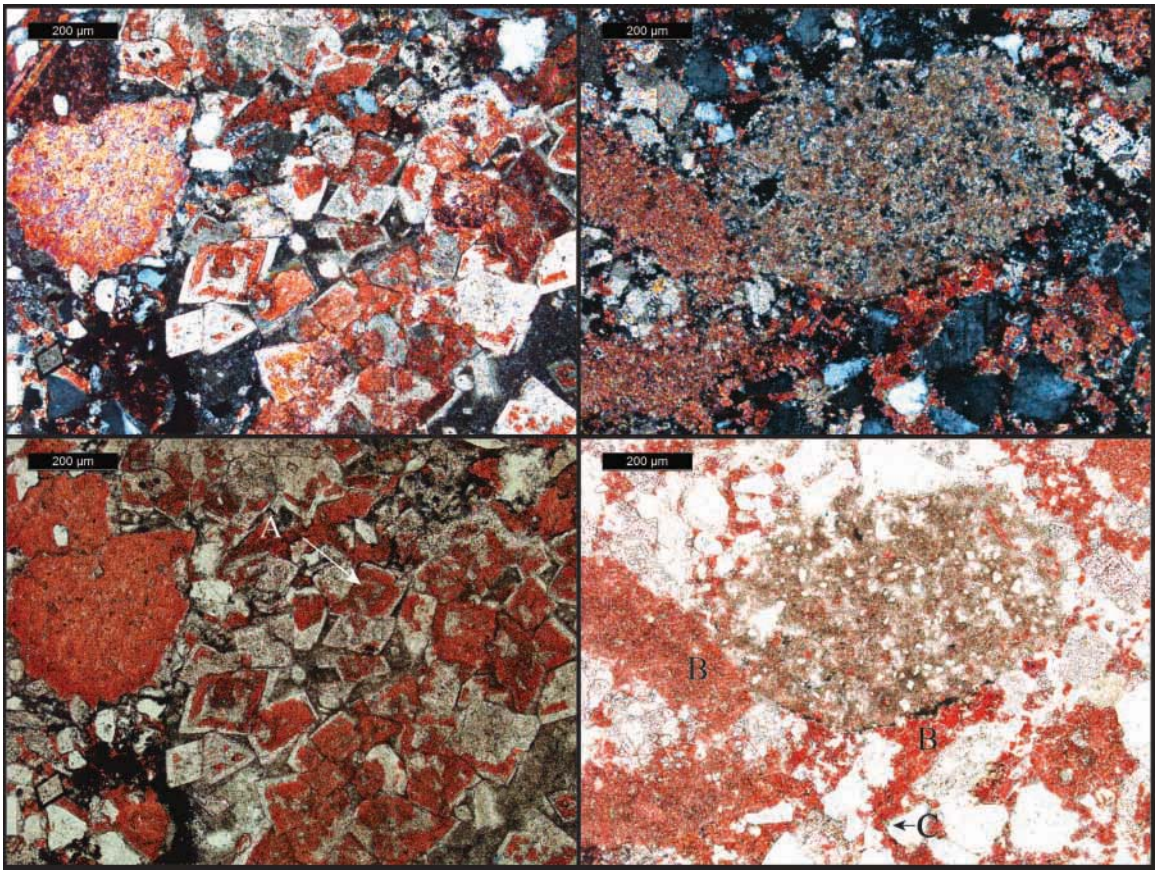

Figure 26: Conglomerate sample-displaying signs of dedolomitization (left images) of calcite replacing parts of the rhombic dolomite crystals. Carbonate fabrics are mixed, containing micritic dolomite, pore filling calcite cement (B) and detrital quartz grains (C). Scale is 0.2 mm.

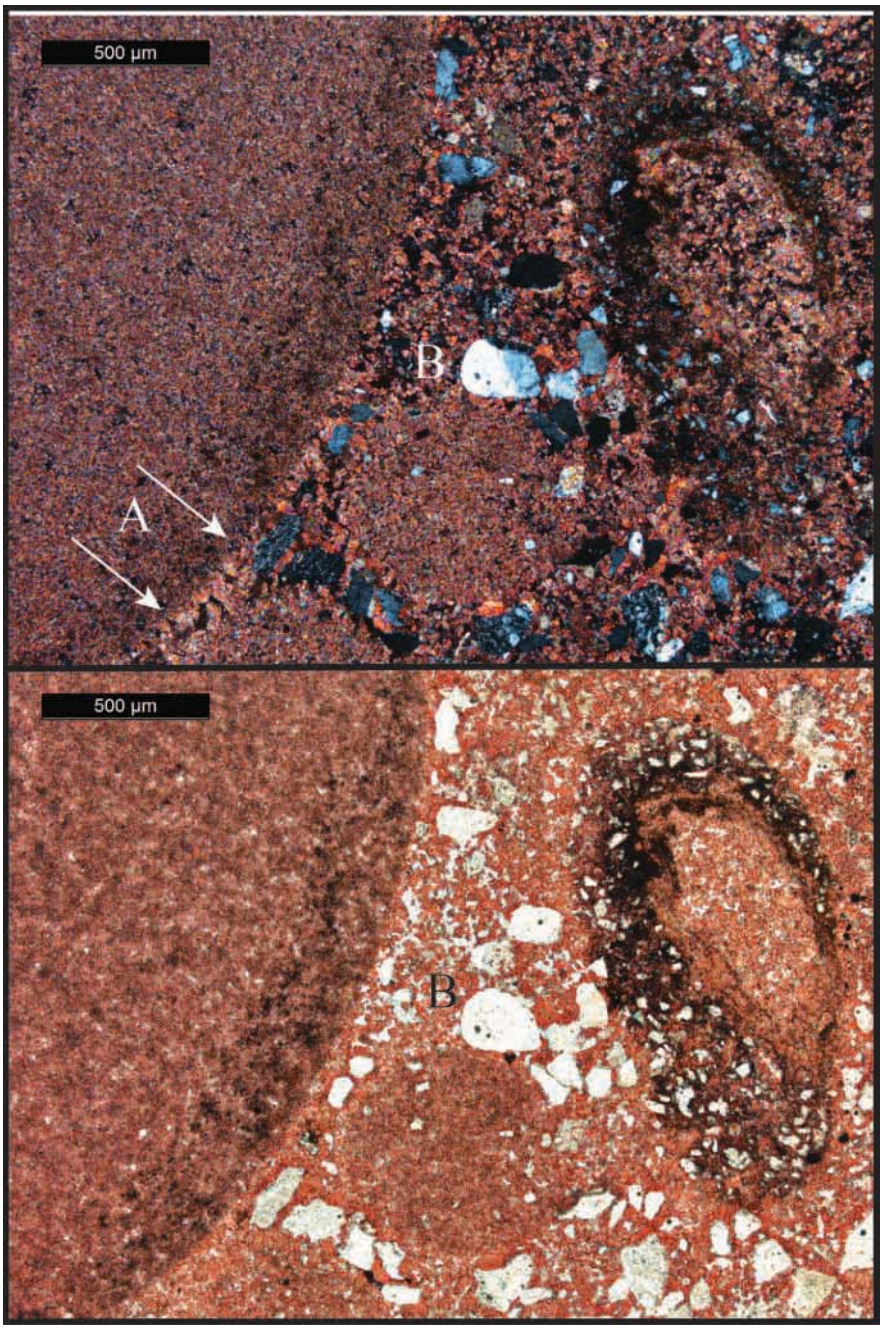

Figure 27: Calcite rich conglomerate sample. A conglomerate sample with different textures. The outline of micritic grains contain a sparry isopacous cement (A), B is a void filling calcite cement that encases detrital quartz grains. Also note micritization around the edges of carbonate grains. Scale is 0.5 mm.

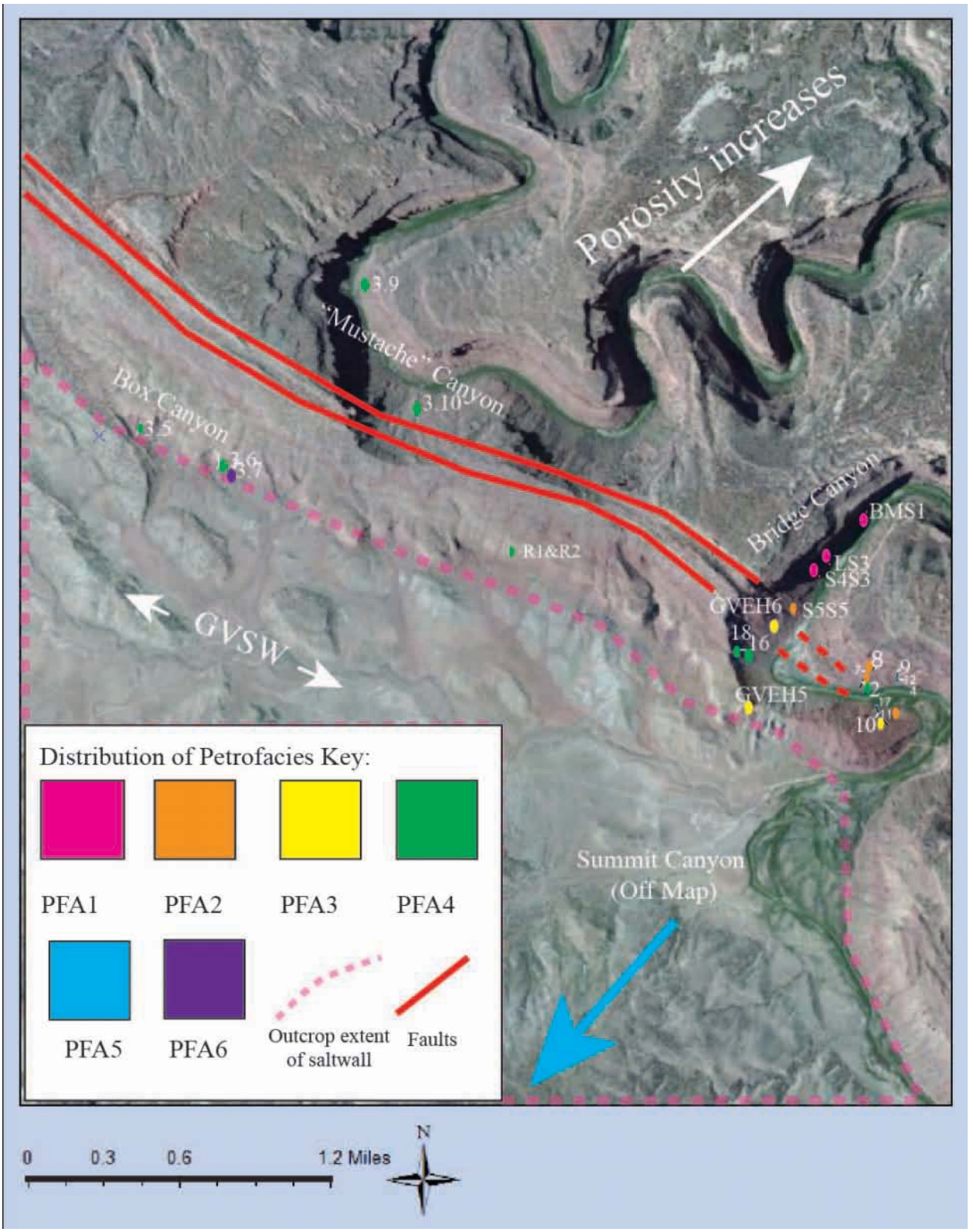

Figure 28: Map displaying locations of Petrofacies. PFA-1 occurs farther down the bridge canyon in a rather mixed region, PFA-2,3 &4 occur within faulted zone that parallels the saltwall, but PFA-4 has a greater diversity of cement and porosity (3.9-3.10), PFA-5 occurs

outside of GVSW in Summit Canyon and shows an increase in porosity but does contain cement percentages of 8-17% and are mixed dolomite and calcite cements. PFA-6 contained comglomerate samples that were overwhelming calcite rich, these samples high in calcite cement occur as "Pods" along the diapir.

3.2 Petrofacies Interpretation

Overall the Chinle samples in the study area reflect a combination of influences, a more distant igneous or metamorphic source mixing with sediment derived from the diapir. Detrital sources of the Chinle Formation have been proposed to be related to tectonics, bordering the Chinle Formation's depositional basin (Hazel 1994; Stewart et al. 1972). Precambrian igneous and metamorphic clasts and grains come from the south, volcanics and recycled Paleozoic sediments were sourced from the uplift of the Mogollon Highlands (Figure 29). The Salt Anticline region was affected by sediments being shed from the Uncompahgre Highlands and the western part of the Ancestral Rocky Mountains (ARM) (Figure 29; Stewart et al., 1972; Blakey and Gubitosa, 1982).

Cater (1970) had documented the mean composition of nine samples as 63% quartz, 10% tuff or chert, 2% quartz overgrowths (silica cement), 19% calcite, 4%feldspar, and 1%mica and heavy minerals. Stewart et al. (1972) identified their sandstones as "feldpathic orthoquartzite" having greater than 9% but less than 25% feldspar content with lesser percentages of orthoquartzite and feldspathic tuff. The overall composition of the samples documented in this study ranges from 10-27% potassium feldspar and indicates a plutonic or metamorphic source. Feldspar content varied the least, samples all plot in the same general region of the ternary plot, showing little compositional change throughout the stratigraphy or across the outcrops, samples were plotted as lithic arkose or feldspathic litharenites (Figure 15). Stewart et al. (1972) documented feldspar percentages as 0-60% of grains. Higher percentages were noted in the

Church Rock and the Petrified Forest members. Feldspar mineralogy contained microcline, sanidine, albite, oligoclase, and anorthoclase. Stewart et al. (1972) also noted that albite was easily replaced by calcite in some samples.

Quartz grains exhibit an undulatory extinction and could have been derived from a number of sources (Folk, 1980). Stewart et al. (1972) documented dominantly monomineralic quartz grains with unstrained extinction. However a small number of grains were angular to rounded and some did contain undulatory extinction. Stewart et al (1972) suggested that embayment of quartz grains indicated an extrusive igneous origin. They also indicated that quartz overgrowths were common in the Shinarump Member (although not found in our study area), which is important to note.

Clasts interpreted as being derived from the diapir are found in petrofacies 1, 2, 4, and 6 (Figure 22, 26, 27). These clasts are distinctive in their dolomite and calcite mineral composition. Grains appear as coarse-grained sand to pebbles, they are generally round but not always spherical. The fabric of the carbonate grains ranges from coarse crystalline to micite.

Away from the diapir, PFA5, samples from Summit Canyon contain the greatest porosity of all samples collected. Potentially indicating that samples away from the diapir would have a greater percentage in porosity.

Zonation of petrofacies seems to indicate that although the detrital mineralogy is similar, over the study area, cements were not distributed equally. The presence of post-depositional faults that parallel the edge of the salt wall could have produced fluid rich in ions, dissolved from the salt structure, and precipitated occluding porosity in the sandstones. The addition of cements, compaction, and secondary porosity, provide a blueprint for potential fluid pathways along the salt wall. The overwhelming amount of dolomite and mixed dolomite-calcite cement

indicates that the youngest fluids flowing through the area evolved in equilibrium from predominantly calcitic to dolomitic.

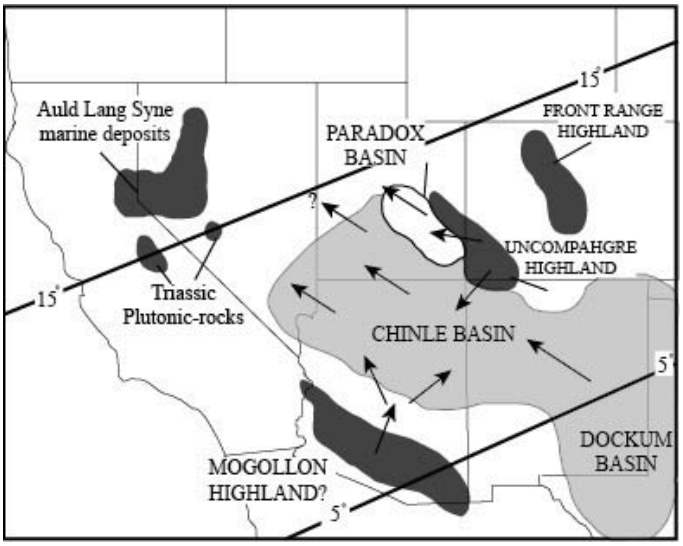

Figure 29: Major sediment sources around the Chinle depositional basin, adapted from Cater (1970).

3.3 Diagenetic Sequences

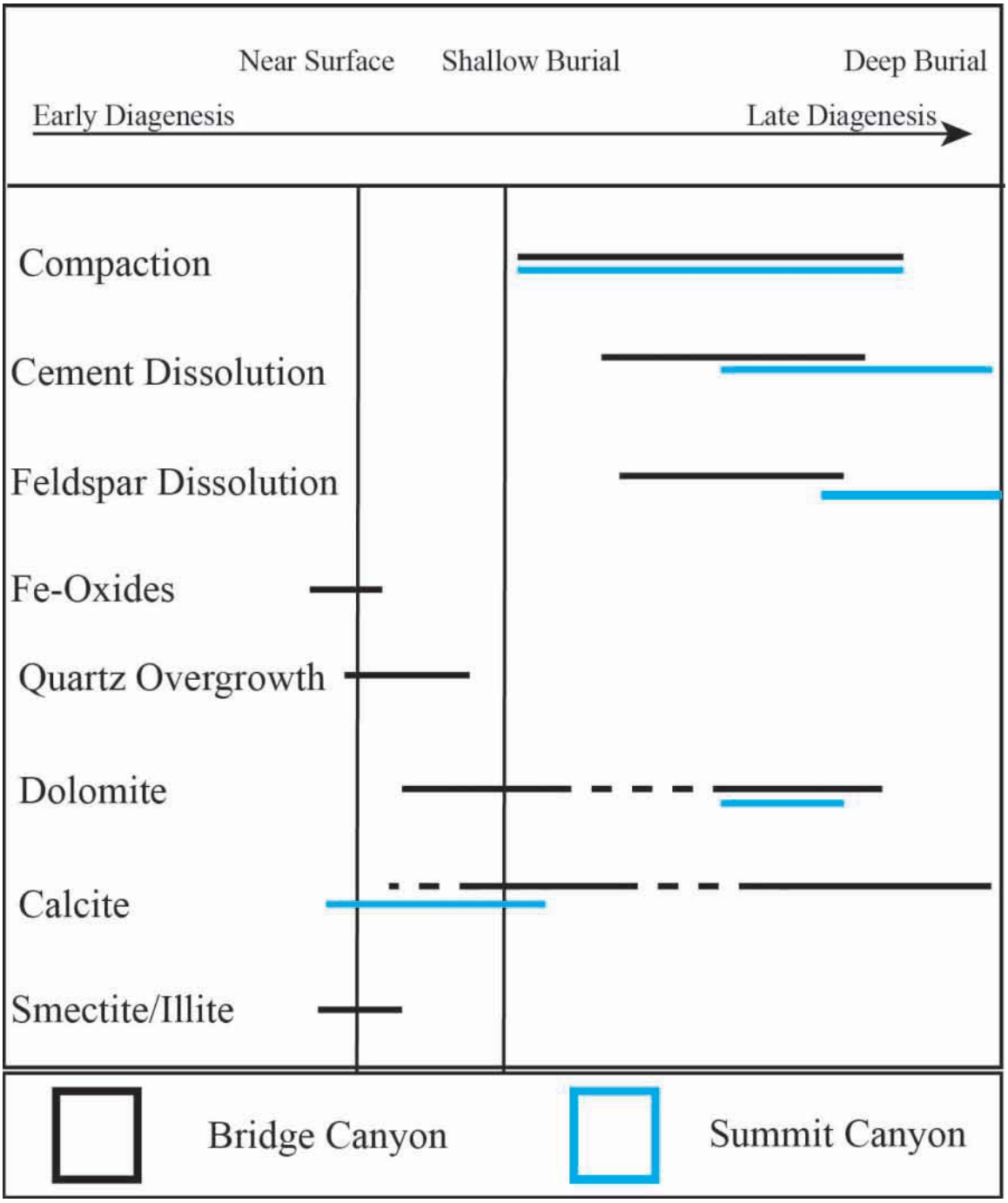

Figure 30: Diagenesis event chart for sandstone samples in Bridge and Summit Canyon.

Authigenic Minerology

The major authigenic cements in the Chinle Formation are hematite, calcite, and dolomite. Hematitic cement composes 0-14% of thin section. Dolomite cement is the most

abundant cement at 2-40% of thin sections (Chart) and is found in neary all thin sections (except figures 27 and 31). There is one phase of dolomitization that postdates the early calcite cement and is replaced by a latter calcite (Figure 22) and there is also a later event that replaces calcite with dolomite (Figure 34). Calcite cement is 0-18% of thin section. Textural features indicate atleast two stages of calcite precipitation (Figures 17, 22, 23).

The earliest cement is a hematitic cement, which form a fine-grained opaque lining to grains in samples LS3, S4S3 and 3.9.4, in petrofacies PFA1 and 4 (Figures 18, 19, 22). Hematitic cement distribution is most variable in sandstone samples but is found in both sandstone and conglomerate samples. Fe cements occurred before quartz overgrowths (Figure 18, below the Q), and are also enclosed by the other early cements where present. Early calcite is not in direct contact with the hematite, suggesting that the iron oxide inhibited the calcite cement.

Quartz overgrowths are seen in sandstone samples and occur at an early stage in the diagenetic history (Figure 18). Early quartz overgrowth cement occurs before compaction and irregular pores, and dissolution fabric on some grains forms late stage secondary porosity. Some samples, such as GVEH5 (Figure 16) have undergone greater compaction than others (Figure 21) as seen by the embayed grains (D) and the number of grains with quartz overgrowths (Q).

Calcite cement has a complicated history; calcite cement is one of oldest cements, potentially precipitating during multiple episodes and has also been dissolved and replaced by dolomite. The second most abundant cement is calcite cement, forming 0-18% of thin section, which forms as either a rim or void filling cement. Calcite cement can form as the dominant void filling cement (Figures 26, 27) or as mosaic void filling cement has been partially dissolved as indicated by the secondary porosity (Figures 22b, 23, 24.b and 25). The occurrence of “patches”

of calcite cement indicates that at some earlier stage there was less porosity, but overtime fluids have dissolved away cement (Figures 22 and 23). Calcite precipitates after clay rims (Figure 23) and also the calcite cement appears to replace an earlier fine-grained dolomite cement (Figure 22).

The youngest and most prevailent cement is dolomite cement. Dolomite cements are found in PFA 1, 2, 4 and 6 and range from 2-40% of the cement in the form of rim or void fills. Rhombic dolomite crystals commonly contain dark or cloudy cores. Dolomite cement displays different appearances and dynamic changes over time (Figures 18. 20, 22, 26). Dark cored rhombic dolomite cements occlude porosity in the sandstones (Figure 18). Fine-grained dolomite rims quartz grains and replaces the earlier remnant calcite (Figure 20. The complex interaction of dolomite and calcite is present as dedolomitization in a conglomerate clast (Figure 26).

Clay rims are also an early diagenetic feature but are limited to PFA 3, 4, and 6 and form dark red to brown layers as observed around carbonate grains and in sandstones (Figures 21, 22, 27). Clay rims are seen between quartz grains or around the outer edge of micrite grains (Figure 21). Figures 22 & 23 show mud/clay in the sample, this gives them a “dirty” appearance but doesn’t limit porosity, occurring between grains, indicating that they were there before compaction.

Secondary porosity varies greatly by location. For example the Bridge Canyon samples exhibited very little porosity whereas the Summit Canyon samples contain a greater percent of porosity and all detrital grains are highly rounded.

Paragenetic Sequence of Sandstones

Samples from Bridge Canyon exhibit a slightly different diagenetic history from samples found in Summit Canyon. The major differences between sandstones are cement types and pore fabrics. The abundance of cement changed by location and petrofacies. The major authigenic cements in the study areas were calcite, dolomite and hematitic cement. Types of cements were either rimming or late-stage void filling.

The paragenetic sequence is as follows: 1.) early iron cementation or clays, 2.) compaction and increase in effective stress causing quartz overgrowths, 3.) calcium carbonate, probably calcite cementation, 4.) localized dissolution of calcite cement or replacement by dolomite, 5.) late calcite calcium carbonate cement and a restricted potential quartz rich cement, and finally 6.) localized dolomitization (Figure 30).

Paragenetic Sequence of Conglomerates

Conglomerate samples are found within 0.7 km of the diapir in sections all sections except except the two sections outside the 0.7 km range, S1 and 3.8 (Figure 16). Conglomerates can be separated based on percent of diapir and nondiapir-derived clasts and cement types. The diapir-derived clasts include calcic micrite, coarse-grained calcite, and some secondary dolomite. The non-diapir derived clasts include mudstones, chert/volcanic grains, and reworked fossils.

Conglomerates rarely exhibit evidence of compaction although adjacent sandstones do. The carbonate clasts tend to cause problems for interpreting the paragenetic history because the detritus shed from the diapir could contain multiple fabrics (i.e. originally micritic or sparry) (Figure 31-34). Because of the changes in fabric the outer rims were first examined for replacement (Figures 31-33). Reduced compaction in conglomerates may be due to the high cement content found in samples, before late stage dissolution (Figure 34).

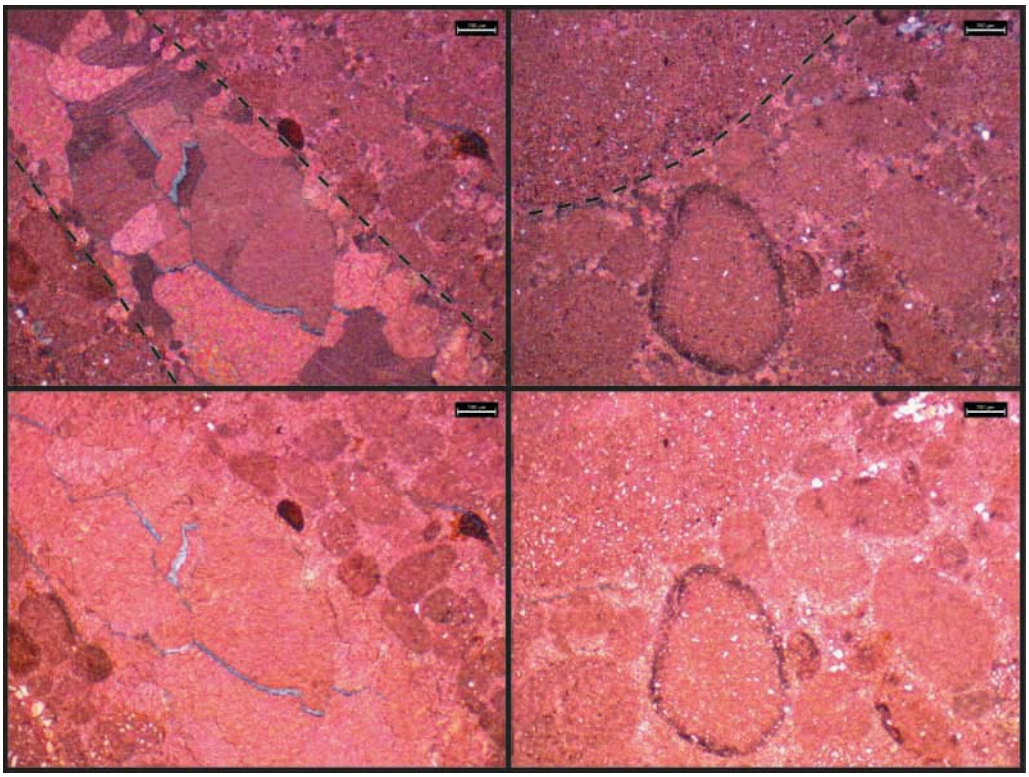

Figure 31: Conglomeratic sample 3.7.4. Left and right images are two images from the same thin section. A calcite rich sample containing a shell fragment (Left) replaced with sparry calcite and rounded carbonate grains. Right image displays rounded carbonate sand grains in calcite cement. Samples were stained for calcium carbonate and impregnated with blue epoxy. Scale is 0.2 mm.

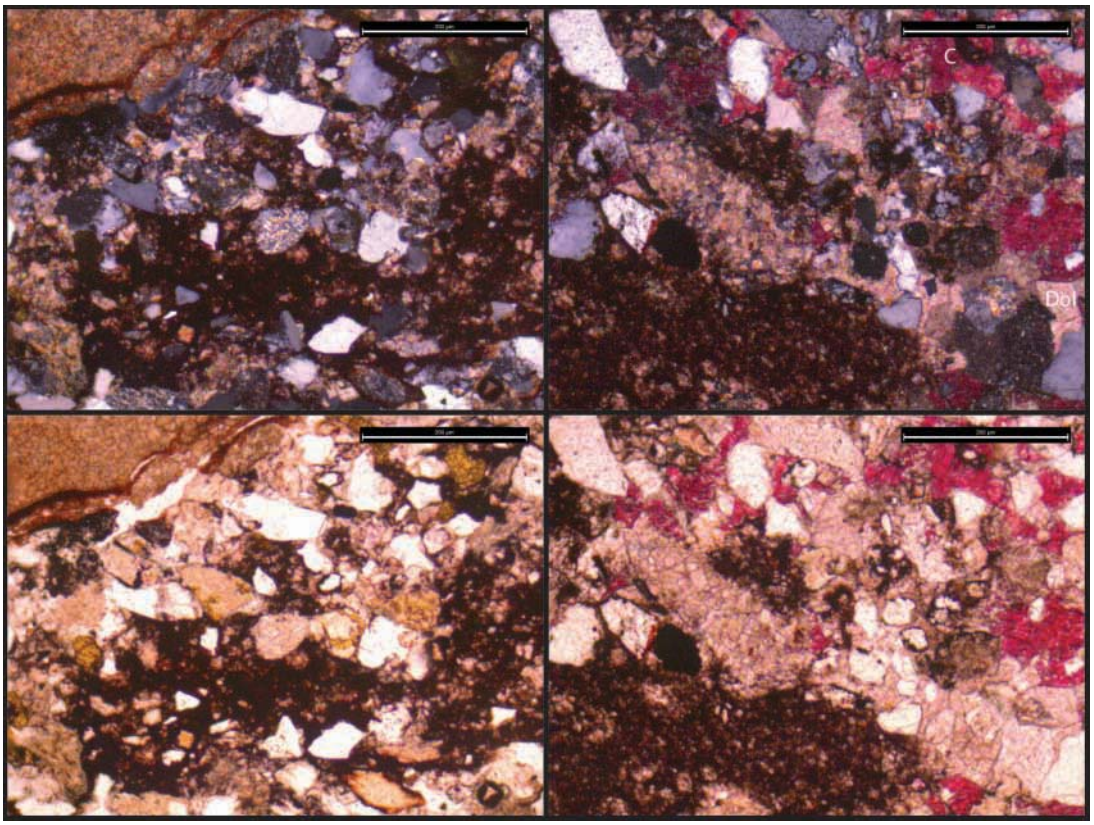

Figure 32: Conglomerate sample GVEH4. Two images from the same thin section. Left images were stained for potassium feldspar. Right images were stained for calcium carbonate and impregnated with blue epoxy. Scale is 0.2 mm. Left images show dark micritic matrix surrounding quartz, feldspar and carbonate grains. Right image shows a mixture of dolomite and calcite grains surrounded by matrix.

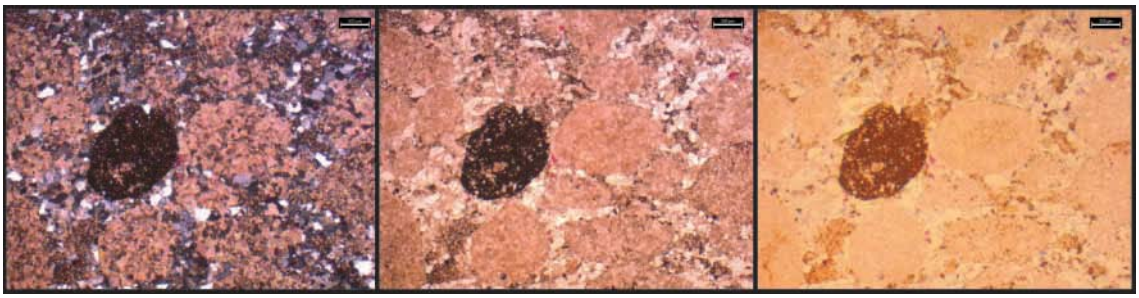

Figure 33: Conglomerate sample 3.3.4. Three images of the same thin section. From left to right, cross-polarized light, plane light, and reflected light. Scale is 0.2 mm. Images display similar rounding of carbonate and clay grains.

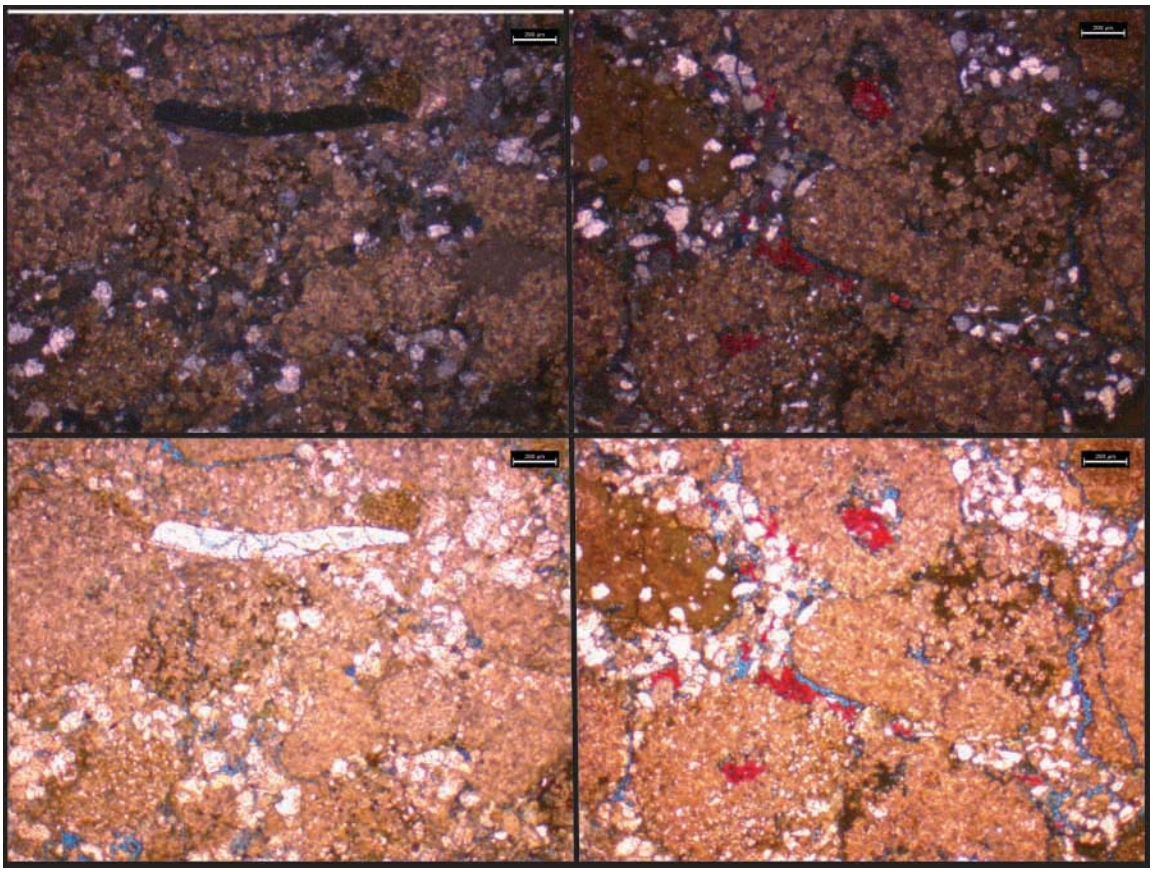

Figure 34: Conglomerate sample 3.3.12. Two images from the same slide showing pervasive dolomitization and secondary porosity and small calcite cores (right image). The left image shows a uniodid shell fragment (top center). Samples were both impregnated with blue dyed epoxy and stained for calcite cement. Scale is 0.2 mm.

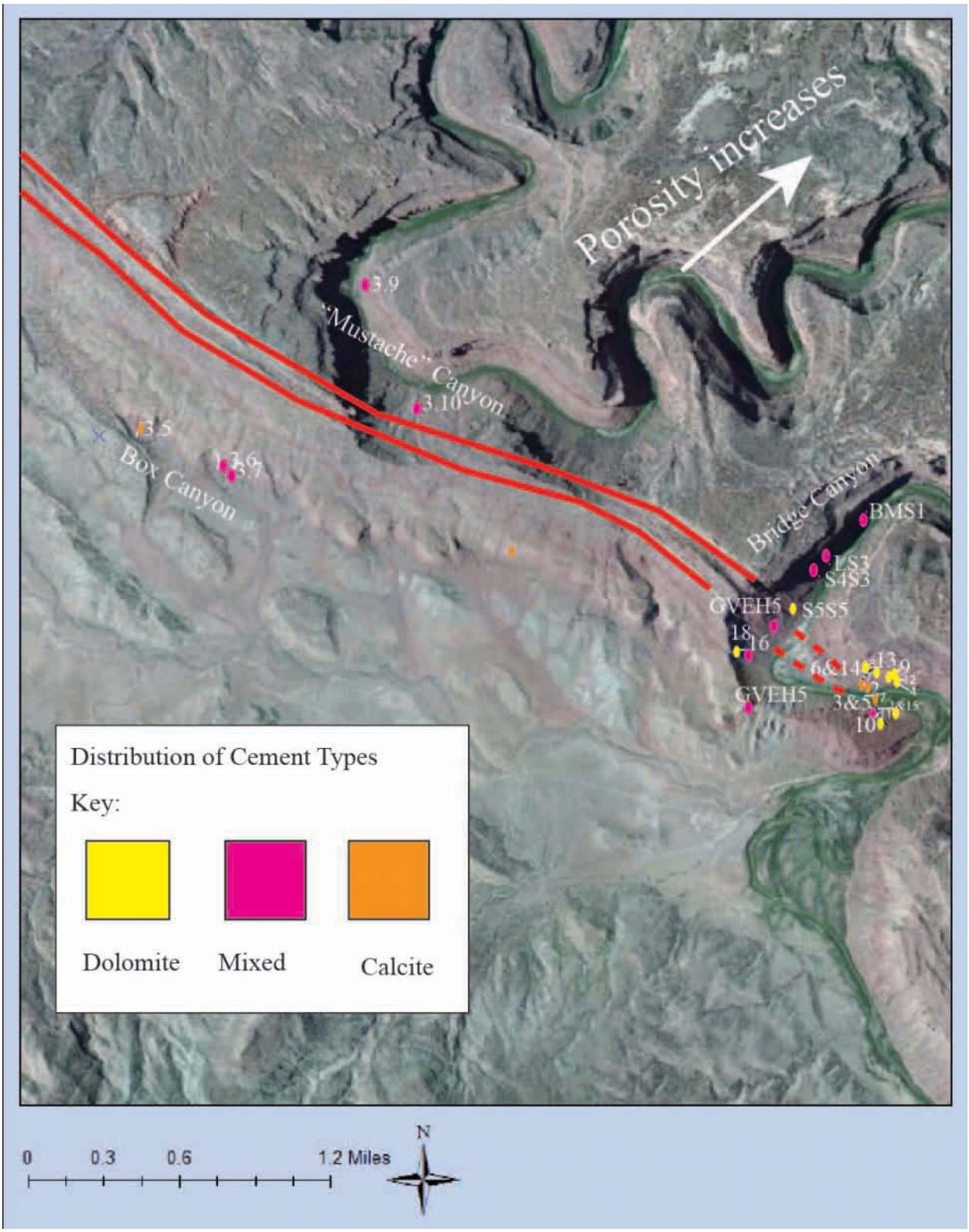

Figure 35: Map displaying summary of cement type. PFA-1 occurs farther down the bridge canyon in a rather mixed region, PFA-2&3 occur within the dolomite region, PFA-4 occurs in

the mixed region (3.9-3.10), PFA-5 occurs outside of GV in Summit Canyon and shows an increase in porosity but does contain cement percentages of 8-17% and are mixed dolomite and calcite cements. PFA-6 contained comglomerate samples that were overwhelming calcite rich, these samples high in calcite cement occur as “Pods” along the diapir. The overwhelming amount of dolomite and mixed cements could indicate that fluids changed from calcite to dolomite dominant.

Chapter Four: Sequence Stratigraphy

Sequence Stratigraphy was utilized in two different ways to separate strata into discrete packages. First, halokinetic sequence stratigraphy was utilized because of the proximity to a salt body as well as the visibility stacking of outcrop packages. Second, a more traditional approach to fluvial sequence stratigraphy was applied. These two approaches serve to compare and contrast the utility and effectiveness of the two approaches adding insights into the controls on the Chinle architecture.

4.1 Halokinetic Sequence Stratigraphy

Two major processes shape fluvial deposition around salt diapirs (Giles and Lawton, 2002). First, if depositional aggradation is greater than salt rise, units will onlap previously tilted beds until the onlapping younger beds begin to erode into older lower strata. Second, if diapiric rise outpaces the rate of deposition, the rising salt tilts strata, and then the tilted beds are eroded. This erosional angular contact – angular unconformity represents a halokinetic sequence boundary (Giles and Lawton, 2002). The halokinetic sequences (HS) are distinguishable being bound by local angular unconformities that converge and onlap the passively rising salt body (Giles and Lawton, 2002; Giles and Rowan, 2012). The arrangement of alluvial strata within a halokinetic sequence starts with an erosional contact at the base (Giles and Lawton, 2002; McFarland, 2016). Conglomerates (organized or disorganized) line the base and fine upward into trough cross-bedded and ripple-laminated sandstones. The sequence then fines upward into silts or mud and then the cycle is repeated.

HS's are only discordant proximal to the salt body, typically a few kilometers (Giles and Lawton, 2002). HS's are organized geometrically into two end-member types; hook and wedge HS's (See Giles and Rowan, 2012) Hook HS's contain narrow zones (50-200m) of deformation with >70° of angularity of beds, associated with mass-wasting deposits, and abrupt facies variations (Giles and Rowan, 2012). Wedge HS's are broader zones (300-1000m) of deformation with low-angle (typically 5-10°) truncation and broader, gradual facies changes (Giles and Rowan, 2012). When HS's are stacked stratigraphically and bound by angular unconformities of greater extent than those of individual HS, the packages are referred to as composite halokinetic sequences (CHS). CHS have been recognized in field exposures and subsurface seismic data sets as having two end-member stratal geometries termed tabular or tapered (Giles and Rowan, 2012).

Contacts between HS's fall under two categories: first the strata can onlap HS, this is usually a result of fine-grained deposition without the ability to erode into the underlying HS. The second occurs from fluvial channels eroding into HS boundaries (McFarland, 2016). In this case, strata are incised by younger channels, which are generally lined with gravel derived from the salt caprock, when available.

4.2 Fluvial Sequence Stratigraphy

The application of traditional sequence stratigraphy, for thick packages of continental strata, is more difficult to use than if it were to be applied to marine strata (Shanley and McCabe, 1994). The interplay between sedimentary processes and accommodation space governs stratigraphic architecture (Shanley and McCabe, 1994). Continental sequence stratigraphy does not follow the same rules or guidelines used for marine sequence stratigraphy in which sea level

changes control accommodation space generation and there are few examples of the transition between marine and terrestrial sequence stratigraphy (Cantuneanu et al., 2011). No marine transition is documented within the Chinle Formation across northern New Mexico and southern Nevada (Stewart et al., 1972; Howell and Blakey, 2013). Shanley and McCabe (1994) recognize the important differences between terrestrial and marine sequences and propose several models. Shanley and McCabe (1994) recognize three systems tracts in alluvial strata from Argentina. First lowstand system tracts (LWST) are dominated by sandy to gravely bedload deposits that coarsen upward. Transgressive systems tracts (TST) contain a mix of bedload and suspension deposition that fine upward overall. Then, highstand systems tract (HST) contain suspension deposits and the occurrence of soil profiles. These systems tracts are useful in areas with limited accommodation space, which is not the case in Gypsum Valley. Posamentier and Allen (1993) suggest that sequence boundaries are related to greater vertical amalgamation of channels related to filling of available rates of accommodation space.

Cantuneanu et al. (2011) proposes a different sequence stratigraphy nomenclature for continental strata. Sequence boundaries (SB) are subaerial unconformities and represent the lowest point before base-level rise. Typically the contact is cut into the underlying facies succession and is identifided by a coarse-grained basinal lag in channels or pedogenic structures in the interfluve areas. Lowstand normal regression (LW) indicates a rise in base-level generated by an increase in accommodation space. Typically identified by channel amalgamation in the form of a “blocky vertical profile”. The maximum regressive surface is between the amalgamated channels of the LW and the overlying floodplain dominated transgressive system tract (TST). In non-marine strata TST are thick packages of floodplain deposits encasing isolated channels. TST can house immature soils and lacustrine or pond deposits. The highstand

normal regression (HSNR) contains laterally interconnected channels. Broadsheet channels and mature soils linked to a decrease in base level rise and a reduction in accommodation rate.

A number of geologists divide sequences into fluvial aggradational cycle sets (FACSETs) which in turn are divided into a smaller unit fluvial aggradational cycles (FACs) (Prochnow et al., 2006; Cleveland et al., 2007). Sequences are defined as a 100-m thick package, laterally continuous over kilometers and are unconformity bound. FACSETs are on the scale of 10's of meters, continuous up to a kilometer, generally the base is a conglomeratic lens that grades upward into a mudstone, and the upper surface is either bound by a paleosol or erosional contact. FACs are 1 to 10 m thick and are not laterally continuous, extending for tens of meters.

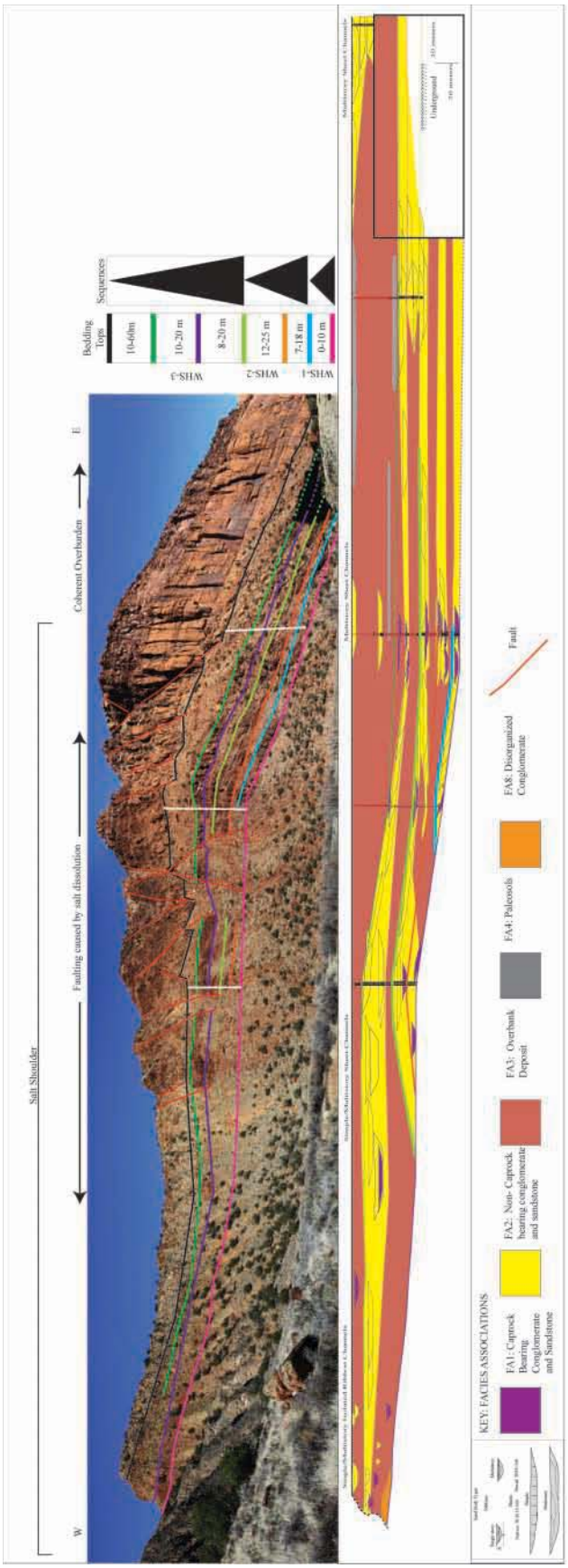

Figure 36a: Bridge Canyon photopan with

annotated HS. (WHS-1 is topped by blue line, WHK-2 is topped by lime green line, and WHS-3 is above).

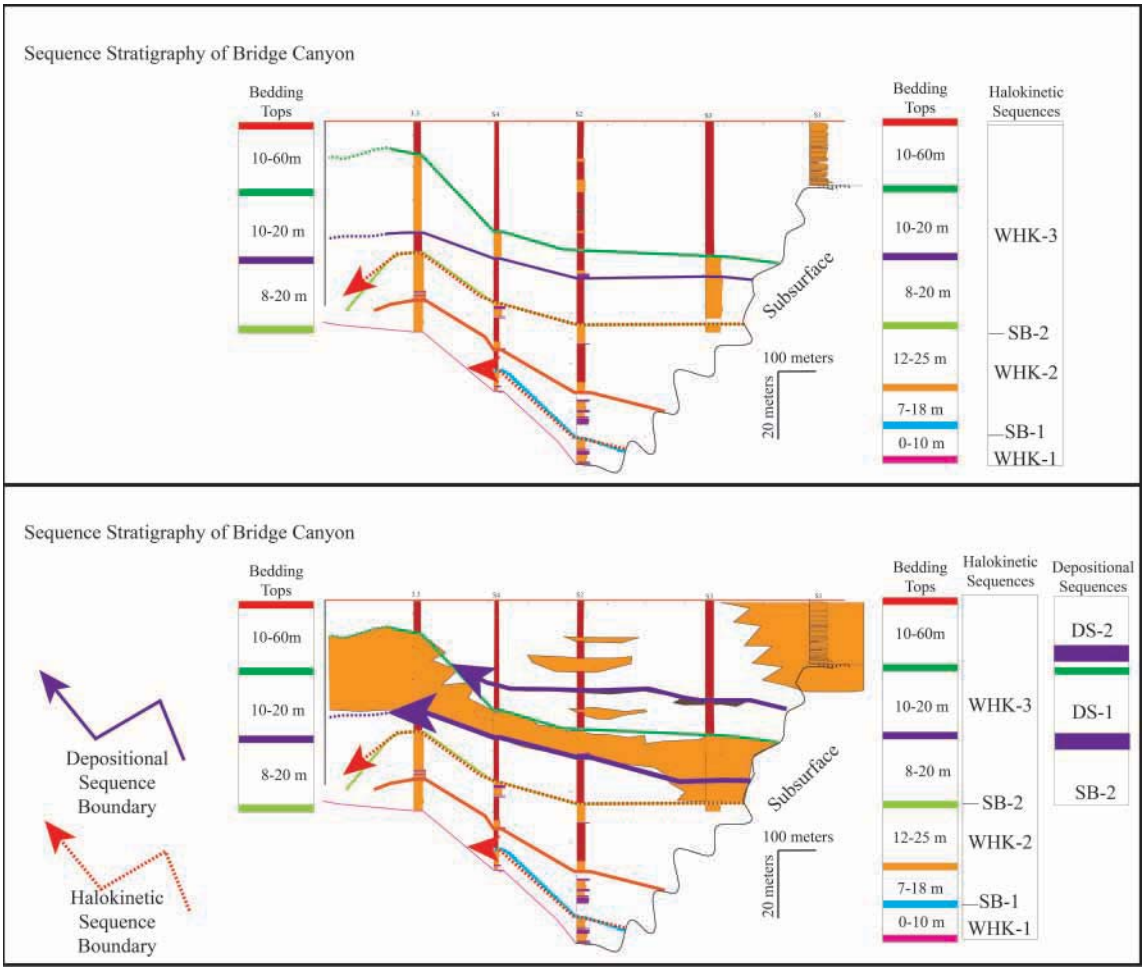

Figure 36b: Illustrated Bridge Canyon stratigraphic sections with annotated HS. WHS-1 is topped by blue line, WHK-2 is topped by lime green line, and WHS-3 is above. The purple depositional sequences are the two potential correlations the sequence boundary for WHS-4 found along strike. At a 1:5 ratio.

4.3 Halokinetic Sequences in the Study Areas

Bridge Canyon

Within the Chinle Formation at GV, the application of Halokinetic Sequences is used to understand the influence of passive diapirism on Chinle Strata. In the Bridge Canyon area of Gypsum Valley McFarland (2016) documented the diapiric derived structure of the "shoulder".

Within the area of the shoulder McFarland (2016) documented three wedge halokinetic sequences, (WHS-1, WHS-2, WHS-3). Each sequence is locally bounded by angular unconformities less than 5º. A sequence thins towards the GVSW and has differing facies based on proximity to the diapir. McFarland (2016) documented thinning of Chinle bedding onto the salt shoulder (160-44 meters). Ledge-forming channel-fill sandstones with local conglomerates form the base of each sequence. Wedges of slope-forming, finer-grained silt-rich sandstones separate the channel sands and pinch out toward the diapir. Figure 36 illustrates the interplay between onlap of silty units onto sequence boundaries and higher energy units erosional truncation.

Each WHS is bound by an unconformity: A 2º angular unconformity separates WHS-1 from the overlying, thicker WHS-2 representing a halokinetic sequence boundary. WHS-2 underlies a 3º angular unconformity with WHS-3. The WHS-3 underlies a regional unconformity with the Late Triassic Wingate Formation (Figure 36).

WHS-1 contains FA1 caprock bearing conglomerates within a broad single story sheet (3-5 meters thick and150 meters wide) (McFarland, 2016). FA3 overbank deposits compose less than 30% of the sequence and no disorganized conglomerates were documented (Figure 36). WHS-1 is only visible in outcrop for a short distance because it dips into the subsurface towards the Dry Creek minibasin (Figure 36).

WHS-2 contains FA1 caprock bearing conglomerate that grade into FA3 overbank deposits as they onlap the salt shoulder (Figure 36). The FA3 overbank strata are in turn onlapped by broad multistory FA1 channel complexes; fewer conglomeratic lenses reach the crest of the shoulder, where there are more sandstone-dominated channels (Figure 36).

WHS-3 is the thickest of the exposed halokinetic sequences. It onlaps the shoulder and extends to the edge of outcrop, where it forms a steep slope overlooking the collapsed salt diapir. Intercalated debris flows suggest that this exposure was near the edge of the rising diapir during the subsequent Chinle deposition (McFarland, 2016). The base of WHS-3 is a thick overbank deposit that is punctuated by small ribbon channels near the diapir (Figure 36). The sequence then coarsens into a broad multistory sandstone-dominated channel complex (Figure 36). Above the sandstone complex, sediments fine into siltstone overbank deposits containing a prominent vertic paleosol before the overbank deposits again see sporadic but sparse single to multistory ribbon sand-dominated channels. WHS-3 amalgamated channels stacking of broad sheets, vertically change to a higher concentration of multi-lateral ribbon channels increasing upward on to the GV shoulder. It is important to note that WHS-3 is the best exposed and shows the greatest variation in facies association. The upper silty unit of WHS-3 is wedge shaped that thins at the diapir and that thickens into the Dry Creek minibasin, with isolated channels evident in section (Figure 36) and the most distal section is a thick section of a thin braided stream system. At the contact for the Wingate and Chinle there are thick, 1-2 meter, isolated conglomerates.

Box Canyon Transect

Bridge Canyon runs perpendicular to the margin of the GVSW, whereas Box Canyon runs roughly parallel to the strike of the GVSW margin (Figure 37). The Box Canyon transect is roughly 3 km long. Box Canyon displays the same patterns of sediment onlap, pinchout, and truncation as Bridge Canyon. However, from the Box Canyon transect four halokinetic sequences are visible in section.

WHS-2 is visbible in sections 3.6 and 3.7 (Figure 37a and 37b), unit one (basal unit) contains a basal conglomerate channel overlain by a siltstone/ mudstone overbank and pond

deposit. Unit one's basal channel, overbank and pond onlaps the topographic high to the south and represents WHS-1.

WHS-3 (Unit 2) is contained between a the uppermost HS-2 and upper HS-3. WHS-3 contains a basal conglomeratic channel fill that fines into broad multistory braided channels as seen in all sections (Figure 37 a and b). Unit 2 is also the only unit that would potentially include disorganized conglomerates.

WHS-3 (Unit 3) formed as an overbank deposit that laterally changes into unconfined channels to the north (section 3.4) and onlaps the topographic high of the shoulder to the south. In sections R1 and R2 the thickness is less than half of the thickness to the north. Sections R1 and R2 display pond/marsh and lacustrine deposits (FA5 and 6) that formed in subsiding local depressions on the shoulder.

Between WHS-3&4 there is a sequence boundary angular unconformity of 3-15 degrees. WHS-4 overlays the third sequence boundary is dominated by laterally extensive braided channels (unit 5) (Figure 37a and 37b) that then fine into overbank deposit (unit 5) FA3. This unit closly resembles the so-called "Black Ledge Member" seen in Bridge Canyon. The Black Ledge forms a discontinuous ledgy outcrop as it onlaps the diapir in Bridge Canyon. This is caused by either, 1) stratigraphic pinch out as the Black Ledge onlaps the diapir or 2) erosion and beveling of the Black Ledge from later episodes of erosion on the boundary between WHS-3&4. At the very top of unit 5, there are rare green and red conglomerates dominated by mud rip-up clasts. These conglomerates occur at the contact with the overlying J-0 unconformity at the base of the Wingate Sandstone. The conglomerates at the top of unit 5 correlate to conglomerates found at the Chinle/Wingate contact of Bridge Canyon.

Cantuneanu et al (2011) identified depositional sequences as the contact is cut into a lower facies succession and is identifided by a coarse-grained basinal lag for channels or pedogenic structures in the interfluve areas. In the study area of Bridge and Box Canyon two possible candidates for depositional sequence boundaries were identified within WHS-3. The first would be the base of the so-called "Black Ledge" (Within WHS-3) and the second would be higher in section (within WHS-3) S2 and S3 where a paleosol extends towards where the "BlackLedge" disappears.

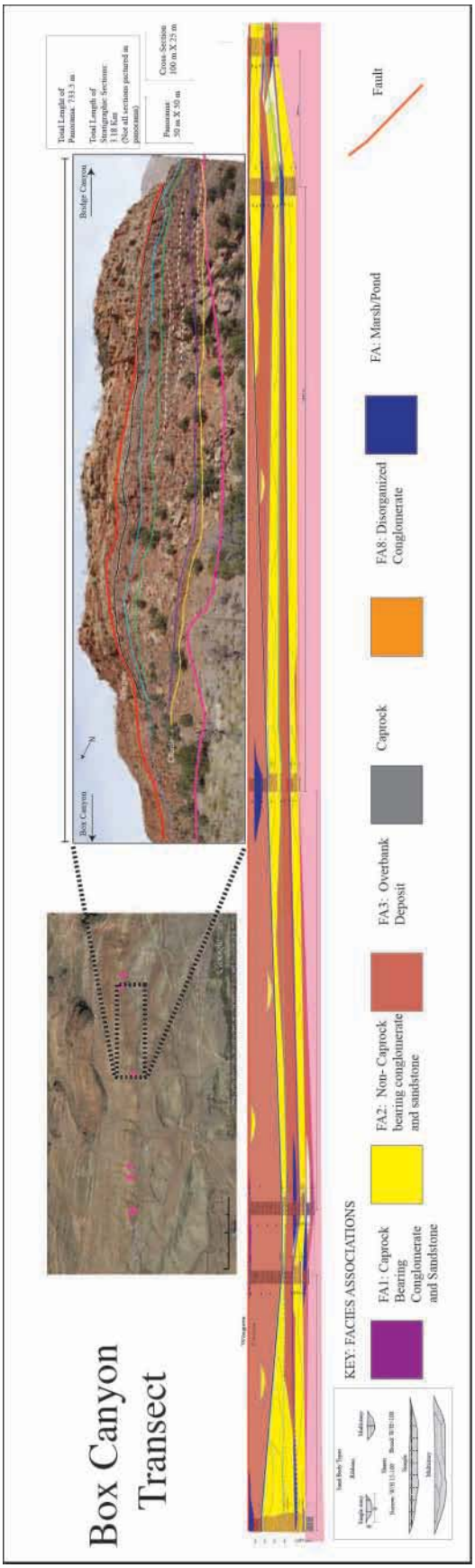
Box Canyon Transect
Total Length of Panorama: 733.5 m
Total Length of Stratigraphic Sections: 1,118 Km
(Not all sections pictured in panorama)
Panorama: 50 m X 50 m
Cross-Section: 100 m X 25 m
Box Canyon
Bridge Canyon
N
Fault
FA: Marsh/Pond
FA8: Disorganized Conglomerate
Caprock
FA3: Overbank Deposit
FA2: Non- Caprock bearing conglomerate and sandstone
FA1: Caprock Bearing Conglomerate and Sandstone
KEY: FACIES ASSOCIATIONS

Figure 37a: The Box Canyon transect with annotated photopanarama and HS. The transect consists of six stratigraphic sections over ~3 km. The basal light pink shade signifies Chinle Caprock. Notice the overall thinning and thickening of channels.

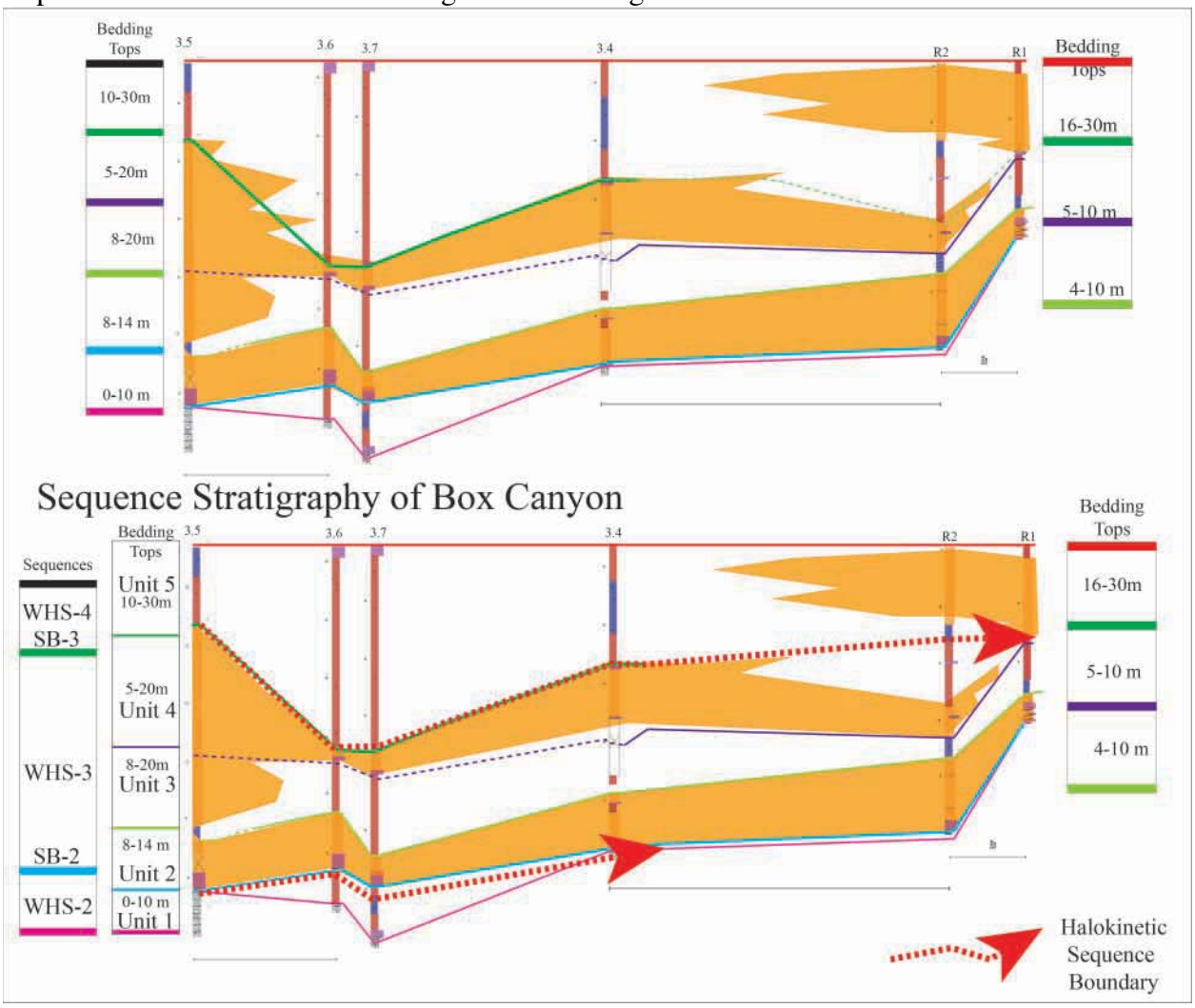

Figure 37b: Illustrated Box Canyon transect sections with annotated HS. The upper diagram shows the major sand bodies and bedding tops. The lower image uses the red arrows to indicate sequence boundaries. At a 1:5 ratio.

Summit Canyon

A section in Summit Canyon was measured and interpreted to understand how the Chinle Formation acted away from the diapir and in close proximity to the Disappointment Minibasin (Figure 2). Overall, because of distance from the diapir, it is impossible to associate the section in Summit Canyon with halokinetic sequence stratigraphy adjact to the GVSW and the overall

stratigraphic patterns. Summit Canyon most closely resembles the distal part of WHS-3 (Figure 2, 6 & 36) and may be a stratigraphic correlative. Five channel packages (4-5m thick and laterally extensive sheets up to 30+ meters) can be grouped as at least part of one sequence. Each channel package contains an erosional base, beds predominantly contain trough cross-stratified sandstones and fine upward from lower coarse to upper medium-grained sand. Above the five channel packages is a thick overbank deposit that contains septerian nodules that is not found in WHS-3 at the edge of Bridge Canyon.

4.4 Chinle Formation Sequence Interpretation

Blakey and Gubitosa (1983, 1984) described two major fining upward sequences within the Chinle Formation with possible smaller cycles relating to salt tectonism. Castle Valley, ~20 km North of Gypsum Valley is interpreted as having two hectometer scale fluvial sequences, consisting of the upper and lower Chinle Formation (Prochnow et al 2006). The lower Chinle is not preserved in Gypsum Valley. Within these two sequences are several smaller scale FACSET's and FAC's (Prochnow et al., 2006).

Within the Chinle Formation in the study area, a number of different channel geometries are visible on outcrop. The lowest units (WHS-1) visibly exhibit single story ribbon sands, with visible lateral accreting sets. The middle of the section (WHS-2 and lower part of WHS-3) consists of single and multistory ribbon sands and sheet sands. Conglomerates line the base of the channels and fine upward to medium and fine-grained sand, then sandy silts. The upper unit consists of a thick package of silty muds, with isolated ribbon channels, individual channels are approximately 0.5 – 3.0 m thick and extend roughly >20.0 m in outcrop. The basinward extent of WHS-3 becomes wide, multistory sheet sands; the opposite of the ribbon channels seen inboard.

A potential interpretation for combining the different schools of thought would be to acknowledge the influence of halokinesis, indicating that HSB-1&2 are fully attributable to salt movement. Then the observations in WHS-3 would include a shift in the axis of passive salt rise, associated with migration of the GVSW margin inboard forming the shoulder.

Channel stacking and pedogenesis have been cited as evidence for low accommodation space, while higher overbank to channel ratios suggest higher accommodation space (Prochnow et al 2006; Cleveland et al, 2007). Upward fining sequences are the result of an increase in accommodation (Shanley and McCabe, 1994; Prochnow et al 2006; Cleveland et al, 2007). WHS-4 would then be hard to discern in Bridge Canyon because of the fine grained nature and high overbank to channel ratios, making angular unconforities difficult to see in outcrop.

Summit Canyon is interpreted to expose bedload dominated channel sands filling in the Disappointment Minibasin. When rate of sediment accumulation outpasses subsidence generation, the associated channel incision develops a erosional unconformity. Limited overbank deposited adjacent to channels may indicate cannibalized or eroded downstream until later in time when suspension deposition was possible.

4.5 Chinle Formation Model Sequence

Fluvial deposition were documented displaying similar mechanisms in the Moab region of Utah (Shock, 2012). In the minibasin, fluvial deposition would onlap salt walls. As a salt structure passively rose erosion of a topographic high would lead to exposure of a salt structure and would lead to continued erosion and drapefold tilt to cause the formation of halokinetic sequences.

From Figure 38 (below the blue boundary), the lowest stratigraphic section (unit 1) overlays the contact with the caprock of the GVSW. In these lower units isolated fluvial channels erode into underlying caprock. Channels onlap the exposed caprock and transition to the NW to an overbank deposit, which separates the channels from the overbank deposits within the same sequence (Figure 38).

The second sequence (between the blue and green line of figure 38) indicates that the sequence began with broad channels onlapping sequence one. This sequence appears differently from different vantage points. In figure 38, the sequence began with an unconfined channel at the base of the sequence but laterally pinches out against the topographic high, the sequence then transitions into an overbank deposit.

The third sequence (between the green and pink boundaries) has unconfined fluvial channels that occur at the contact of the sequence boundary. Then, the sequence fines upward into an overbank deposit that contains isolated single story ribbon channels that onlap the topographic high before being eroded by the overlying unit.

The fourth sequence above the pink sequence boundary starts with a fluvial channel eroding into the sequence boundary below. This channel also appears to onlap the topographic high. The channels then transition to overbank deposits, laterally as you move away from the salt shoulder there is a dramatic facies change from overbank to unconfined sheet flow.

Figure 38: Outcrop highlighting HS. Located southeast of the Box Canyon transect and in close proximity to the salt shoulder of bridge canyon. This outcrop highlights the relationships seen between each sequence.

Then as a model for HS and facies associations this outcrop shows the relationship between accommodation and tectonic uplift. Each sequence begins with channels filling accommodation space and onlapping the topographic high. The facies association transitions from channels to overbank deposits as you near the crest of the topographic high. Each sequence is bound by an angular unconformity of less than five degrees. The ribbon channels that punctuate the overbank deposits in the upper unit are a result of localized tectonic forces.

The Chinle Formation model sequence of events fits the data collected. The model works with currently accepted thoughts on depositional patterns in the Paradox Basin, and further confirms the mode of halokinetic deformation that is currently accepted (See also Appendix 3).

Chapter Five: Discussion

5.1 Discussion

At Gypsum Valley, the influence of salt tectonism makes the application of traditional sequence stratigraphy difficult, while angular unconformities separate halokinetic sequences. Several previous studies have described sequences within the Chinle Formation. Blakey and Gubitosa (1983, 1984) described two major fining upward sequences of the Chinle Formation of the Moab region. Regional studies of the Chinle indicate that Gypsum Valley contains only the upper fining upward sequence (Shawe et al, 1968; Lucas et al, 1997). Within the Chinle Section, in Gypsum Valley, of Southern Colorado four sequences have been proposed. Miall and Arush (2001) proposed a sequence boundary just above the Black Ledge Sandstone within the Church Rock interval. Gypsum Valley exposes this upward most fining upward sequence.

In contrast to the stratigraphic sequence, four HS can be identified. Miall and Arush, (2001) also noted that sequences are easily identifyable near diapirs due to angular unconformities. Halokinetic sequences have been defined on the borders of several of the Paradox Basin diapirs (Foster, 2015; Hazel, 1994; Prochnow et al 2006). In the Bridge Canyon area of Gypsum Valley McFarland (2016) documented the diapiric derived structure of the "shoulder".

This study supports the presence of a fourth halokinetic sequence not documented by McFarland (2016) (Figures 37a&b). The fourth halokinetic sequence was not evident in the shoulder area studied by McFarland (2016) because of subtle dip changes within poorly exposed mudstones. The fourth sequence lies in the same position as a sequence identified by Miall and Arush (2001), immediately overlying the "so called Black Ledge (Figure 37a&b). The Black Ledge disappears within the faulted and generally covered zone in the "collar area" defined by

McFarland (2016). The faulting of the Black Ledge is most likely due to erosion by the overlying unconformity. The 4th sequence boundary is evident on outcrops north and south of Bridge Canyon, where sandstones of HS-4 can be observed lapping onto those of HS-3 (Figures 37a&b, 38).

The halokinetic sequences in the Chinle are interpreted as the wedge halokinetic sequences of Giles and Lawton (2002), in agreement with the interpretation of McFarland (2016). These sequences are similar in geometry and facies to those found in Moenkopi/Chinle Formation of Utah i.e. (Shock, 2012, Matthews et al, 2007). Banham and Mountney (2013) classified broad thin channels that spread out over low accommodation surfaces within the Moenkopi Formation of the Moab region. Diapiric topography and channel pathways were a major component in their discussion of halokinetic controls. High sediment delivery with low subsidence produced braided belts; they similarly talked about overspill (Similar to FA3) deposits onlapping salt topography.

Prochnow et al. (2006) attempted to identify fluvial aggradation cycle (FAC) sets in the Big Bend minibasin in Castle Valley for fluvial sequence stratigraphy using lithofacies and paleosols. However in Gypsum Valley no paleosols were laterally extensive enough to correlate over multiple study areas and so FACSETS could not be utilized in Gypsum Valley.

Previous studies have documented FAC capped by paleosols that may or may not be capped by angular unconformities (Prochnow et al., 2006). Others have documented angular unconformities as a HS boundary (Shock, 2012, Matthews et al, 2007). It is possible that the paleosols exposed in the distal sections of Bridge Canyon (Figure 36a) represents the top of HS-3.

Shock (2012) inferred that caprock was buried episodically during Moenkopi deposition. Diapir derived clasts were only shed during formation of HS boundaries, when the diapir was exposed (Shock, 2012). In contrast the Chinle Formation in this study contains caprock-bearing conglomerates throughout the section implying that the GVSW was exposed atleast episodically throughout deposition of the Chinle halokinetic sequences. GVSW shows facies association changes both near and far away from the diapir with strata near the diapir onlapping the shoulder. Close to the diapir irregularities in channels channel type, overbanks, and caprock debris does not form uniform fining upward sequences. Far from the diapir upward fining sequences display broad multistory channels that fine into silty overbank deposits.

In summary these facies associations are similar to those of Matthews et al. (2007), Dubiel et al (1991), and Martz et al (2014). A unique facies association not documented in the Chinle Formation is the disorganized conglomerates but those were documented by Shock (2012) and Foster (2015). However, more dramatic changes are seen in facies associations away from the diapir.

Two different facies associations are located in the outcrops closest to the diapir in the study area. FA1 and FA2, composing isolated channel fills that contain carbonate clast conglomerates can be observed in Halokinetic Sequences 1 and 2. These two sequences are on the "Lateral" (McFarland, 2016) part of salt shoulder. These same channel fills (FA1), and overbank strata (FA3), along with disorganized conglomerates (FA8), pond deposits (FA5), and lacustrine deposits (FA6) are found in Halokinetic Sequences 3 and 4 in the "collar" part of the salt shoulder as described by McFarland (2016).

The lateral part of the collar consists of a sloping contact between the salt and overlying sediments that formed in the outboard part of the shoulder. During development of the lateral,

the salt was being onlapped by sediment, but was still rising (McFarland, 2016). This resulted in deposition of strata that were rotated by drape folding, and then overstepped further toward the diapir by the next halokinetic sequence as the salt shoulder developed. The lateral was linked to minibasin subsidence as the shoulder developed and was progressively rotated after deposition.

The collar part of the salt diapir is the portion of the shoulder nearest the core of the diapir (McFarland, 2016). Deposits on the collar were rotated into local basins, and upturned against the diapir margin. However, this was combined with subsidence into small local basin on the shoulder. The collar formed a deformed roof on the former diapir that did not rotate into the Dry Creek minibasin. Therefore an anticline developed between the collar and lateral as the outboard/lateral region was rotated, probably through Navajo deposition in the middle Jurassic (McFarland, 2016). The faulting that extends throught Navajo time is observed in the study area formed along this anticline (McFarland, 2016).

The halokinetic sequences developed on the lateral exhibit the same strata, although little of Halokinetic Sequence 1 is exposed (Figure 4, 36a). As the diapir rose and the adjacent basin subsided, Chinle strata was tilted, and beveled off along the diapir margin. Then younger beds were deposited on top of the tilted bedding creating angular unconformities (Figure 4, 36a). Two potential angular unconformities are visible from outcrop indicating periods of erosion or non-deposition (Figure 4, 36a). Chart 3.1 illustrates the changes in Facies Associations in Bridge Canyon, which exposed all four halokinetic sequences against the diapir. The most notable change is at the shoulder where from section 3.3 to S4 there is a dramatic shift from FA1-2 to FA3 (Figure 36 a&b).

Paleocurrent directions (Appendix 1) indicate a predominant south to southeast current direction and are similar to the paleocurrent directions found in the Moab region (Matthews et al.

2007). However this is the opposite of the regional paleocurrent to the north and northwest (Stewart et al., 1972; Shawe et al., 1968). Paleocurrent data indicate that the fluvial systems ran perpendicular to the wall as the rivers cut through the salt wall and eroded the caprock. There is also potential for drainage to form on top of the salt wall. The south to southeast direction is opposite of the regional trends (N-NW) found by Stewart et al (1972), potentially indicating an area of localized subsidence, linked diapiric salt rise, that would redirect the channels opposite to the regional trend. Another possibility is a topographic high to the north would redirect channels, causing them to follow the trend of the salt wall until another pathway was found. Caprock eroded from the salt wall and incorporated into channels would also indicate a flow path along and towards the salt wall.

The distance from diapir was the dominant influence on petrography rather than stratigraphy. Porosity of samples increased farther the diapir as seen in percentages from Summit Canyon. Faults along the edge of the diapir seemed to control a decrease in the porosity. QFL ternary plots show consistent ratios of major constituent grains among all the thin sections (Figure 15), indicating that sand in the study area were derived from the same source. All halokinetic sequences also exhibit the same clast compositions (Figure 15, 28), indicating that the sediment source was the same or similar throughout deposition of the Chinle Formation.

The samples contain 10 to 27% feldspar (Figure 15). This is similar to feldspar percentages documented by Stewart et al (1972) who documented feldspar percentages as 0-60% of grains. However my sample percentages are different from Cater (1970) with feldspar percentages of 4%.

When comparing the petrography of the Chinle Formation in different areas of the Paradox Basin, samples in this study were slightly lower in quartz percentages and higher than

Cater's (1970) mean composition of samples. Cater had documented the mean composition of nine samples as 63% Quartz, 10% tuff or chert, 2% quartz overgrowths and silica cement, 19% calcite, 4% feldspar and 1% mica and heavy minerals. Similarly Stewart et al (1972) identified their sandstones as "feldpathic orthoquartzite", percentage of feldspar ranging from 10-27%, which is more comparable to feldspar percentages documented in Gypsum Valley. Beer (2005) point counted sandstone samples from the Chinle Formation at four locations: San Rafael Swell, White Canyon, Circle Cliffs and Capitol Reef. Samples from stratigrahicaly lower in the Chinle Formation (Shinarump, Mossback, and Lower Petrified Forest) were classified as arkosic, sub arkosic and quartz arenites. Their samples of the Monitor Butte and Temple Mountain (not documented in GV) were less mature and were classified as arkosic, subarkosic arenite and sublitharenites.

Variation in composition could then lead to three possibilities, first that the samples collected by Beer were from a different source area (because of the greater maturity), second that GV samples are younger than those documented by Beer (2005) and continue the trend of samples being less mature and containing a greater number of lithic grains or third, that as the climate became more arid overtime and feldspars were better preserved.

However, an additional important second source throughout Chinle deposition at Gypsum Valley was the diapir itself. The abundant carbonate and shale clasts (Figure 27, 31), some as coarse as 10 cm, are interpreted as being derived from the eroding diapir. The unsorted conglomerate, FA8 beds are interpreted as being eroded from the immediately adjacent diapir. Similarly, conglomerate clasts are composted of carbonate identical to that exposed in the adjacent salt exposed today (Figure 32, 33, 34). Banham and Mountney (2013), Lawton and Buck (2006) also noted the increase in diapir detritus adjacent to the diapir.

The paragenesis of Bridge Canyon indicated a complex history related to fluid migration from the salt shoulder. The paragenetic sequence is as follows: 1.) early iron cementation or clays, 2.) compaction and increase in effective stress causing quartz overgrowths, 3.) calcium carbonate, probably calcite cementation, 4.) localized dissolution of calcite cement or replacement by dolomite, 5.) late calcite calcium carbonate cement and a restricted potential quartz rich cement, and finally 6.) localized dolomitization (Figure 30).

The loss of porosity indicated that near the salt would be poor areas for exploration but salt shoulders do produce in a number of basins throughout the world (McFarland, 2016). The reason for the lack of porosity is related to compaction from a lack of early cementation. Near surface waters could have mixed with brines flowing from the diapir. The loss of porosity then can be attributed to factors not involved in productive basins throughout the world that have not undergone dissolution and collapse.

From Summit Canyon, thin section we can see that early cementation and compaction did also take place at this distance but the cement has since dissolved to form interstitial porosity among the quartz grains. The enhancement of porosity in Summit Canyon is a later event and occurred after compaction.

Chapter Six: Conclusion

1. Eight facies associations (FA) and eleven lithofacies are present within the Chinle Formation exposed at Gypsum Valley. These FA form as the result of a complex interaction between passive diapirism and deposition. Near the diapir, conglomeratic clasts are predominately composed of carbonate caprock eroded from the diapir margin. The conglomeratic lenses disappear within 0.7 km of the diapir. Channels are laterally stacked and, in some units, vertically stacked. Distally from the diapir fluvial systems change from single and multistoried ribbon sands to broad multistory sheet sands. The furthest stratigraphic section came from Summit Canyon (12 km away), fluvial systems appear as broad single story sheet sands that extend 30+ meters laterally. In Bridge Canyon, the furthest section from the diapir, representing the uppermost 30 meters of the Chinle Formation, was dominated by 80% sandstone. Although a poor representation of total thickness, indicates a facies change in the top part of the section ~0.9 km from the salt wall. Approaching the diapir, siltstone becomes the dominant lithology, interspersed with conglomeratic channel fills, overbank and pond deposits. Conglomerate percentages increase towards the diapir from 0% to 18% then decline on the collar to 10%. In the sections closest to the diapir, the dominant lithology alternates between siltstone and sandstone. Siltstone was greater than 50% where the salt shoulder had formed a depression. Sandstone dominated and conglomerates were deposited closer to the topographic highs on the collar of the salt shoulder, where sections are also thinner.
2. Four Halokinetic Sequences were documented along strike of the Gypsum Valley Salt Wall. This includes three previously identified by McFarland (2016) and an additional

sequence observable in the Box Canyon outcrop panel. The correlative sequence boundary is potentially the laterally extensive paleosols in Bridge Canyon found in McFarland (2016)'s WHS-3.

3. Paleocurrent data (Appendix 1) indicates that the fluvial systems ran parallel to the wall as the rivers cut into the salt wall and eroded the caprock. There is also potential for drainage to form on top of the salt wall. The south to southeast direction is opposite of the regional trends (N-NW) found by Stewart et al (1972), indicating an area of localized subsidence, linked diapiric salt rise, that would redirect the channels opposite to the regional trend.
4. Petrofacies associations indicate that sandstones can be grouped by location, indicating that distances from the diapir cause variation in cement history. Porosity within the Summit Canyon (PFA5) samples range between 12-20%, containing the greatest percentages of secondary porosity, resulting from dissolution and fractures. PFA 1-4 all lack substantial porosity and show differing levels of compaction, quartz overgrowths and cements. The greatest diversity in cement types, clays and compaction are in samples near the diapir (PFA3).

5. Petrography of the Chinle Formation indicates a complex paragenetic sequence of events. The paragenesis of Bridge Canyon could possibly be from a complex history related to fluid migration from the salt shoulder. The paragenetic sequence is as follows: 1.) early iron cementation or clays, 2.) compaction and increase in effective stress causing quartz overgrowths, 3.) calcium carbonate, probably calcite cementation, 4.) localized dissolution of calcite cement or replacement by dolomite, 5.) late calcite calcium carbonate cement and a restricted potential quartz rich cement, and finally 6.) localized

dolomitization (Figure 30). Fluid flow changed from calcite to dolomite dominant over time and is related to the dissolved salt wall.

References

Amador, C.M., Schurger, S.G., and Miller, B.L., 2009, Andy's Mesa Unit, San Miguel County, Colorado: RMAG Special Publication, The Paradox Basin revisited – New Developments in Petroleum Systems and Basin Analysis p. 497-518

Baars, D.L., and Doelling, H.H., 1987, Moab salt-intruded anticline, east-central Utah: *in* Geological Society of America Centennial Field Guide: Rocky Mountain Section p. 275-280.

Banham, S.G., and Mountney, N.P., 2013, Climatic versus halokinetic control on sedimentation in a dryland fluvial succession: Sedimentology v.61, p. 570-608.

Beer, J.J., 2005, sequence stratigraphy of fluvial and lacustrine deposits in the lower part of the chinle formation, south central utah, united states: paleoclimatic and tectonic implications [M.S.Thesis] Minneapolis, University of Minnesota, p. 180

Blakey, R.C., and Gubitosa, R., 1983, Late Triassic paleogeography and depositional history of the Chinle Formation, southern Utah and northern Arizona. In M. W. Reynolds and E.E. Dolly, eds., Mesozoic Paleogeography of West Central United States. Rocky Mountain Section, Society of Economic Paleontologists and Mineralogists, Rocky Mountain Paleogeography Symposium 2, p. 57-76.

Blakey, R.C., and Gubitosa, R., 1984, Sandstone body geometry and architecture of the Triassic Chinle Formation, Colorado Plateau: Sedimentary Geology, v. 38, p. 51-86.

Cantuneanu, O., Galloway, W.E., Kendal, G. St. C., Miall, A.D., Posdmontier, H.W., Strasser, A., Tucker, M.E., 2011, Sequence Stratigraphy: Methodology and Nomenclature: Newsletters of Stratigraphy, v. 44, p. 173-245.

Cater, F.W., 1970, Geology of the salt anticline region in Southwestern Colorado: USGS p. 637.

Cleaveland, D.M., Atchley, S.C., and Nordt, L.C., 2007, Continental Sequence Stratigraphy of the Upper Triassic (Norian-Rhaetian) Chinle Strata, Northern New Mexico, U.S.A.: Allocyclic and Autocyclic Origins of Paleosol-Bearing Alluvial Successions: Journal of Sedimentary Research, v. 77, p. 909 – 924.

Cole III, S.L., DuChene, H.R., and Greenberg, N., 2009, Geology of the Double Eagle Unit, Andy's Mesa Field, San Miguel County, Colorado, in W.S. Houston, L.L. Wray, and P.G. Moreland, eds., The Paradox Basin Revisited – New Developmentsin Petroleum Systems and Basin Analysis: RMAG 2009 Special Publication – The Paradox Basin, p. 519-533.

Dubiel, R.F., and Hasiotis, S.T., 2011, Deposystems, paleosols, and climatic variability in a continental system: the Upper Triassic Chinle Formation, Colorado Plateau, U.S.A. In, Davidson, S., and North, C. eds., From River to Rock Record: The Preservation of Fluvial Sediments and their Subsequent Interpretation. SEPM Special Publication No. 97, p. 393-421.

Dubiel, R.F., Huntoon, J.E., Stanesco, J.D., and Condon, S.M., 2009, Cutler Group Alluvial, Eolian and Marine Deposystems: Permian facies relations and climatic variability in the Paradox Basin, in W.S. Houston, L.L. Wray, and P.G. Moreland, eds., The Paradox Basin Revisited – New Developments in Petroleum Systems and Basin Analysis: RMAG 2009 Special Publication – The Paradox Basin, p. 265-308.

Dubiel, R.F., Parrish, J.T., Parrish, J.T., and Good, S.C., 1991, The Pangaean Megamonsoon - Evidence from the Upper Triassic Chinle Formation, Colorado Plateau. Palaios, v.6, p. 347-370

Elston, D.P., and Landis, E.R., 1960, Pre-Cutler unconformities and early growth of the Paradox Valley and Gypsum Valley salt anticline, Colorado, *in* Short papers in the geological science: U.S. Geol. Survey Prof. Paper 400-B, p. B261-B265.

Elston, D.P., Shoemaker, E.M., and Landis, E.R., 1962, Uncompahgre Front and Salt Anticline Region of Paradox Basin, Colorado and Utah: Bulletin of the American Association of Petroleum Geologists v. 46, p.1857-1878.

Folk, R.L., 1974, Petrology of Sedimentary Rocks: Hemphill Publication Company, p. 125.

Foster, A.M., 2015, Depositional Facies And Interpretation Of Salt-Sediment Interaction In The Lower Triassic Moenkopi Formation Adjacent To The Castle Valley Salt Wall, Paradox Basin, Utah [M.S. Thesis] University of Texas at El Paso, p. 105.

Giles, K.A., and Lawton, T.F., 2002, Halokinetic sequence stratigraphy adjacent to the El Papalote diapir, northeastern Mexico: AAPG Bulletin, v. 86, p. 823-840.

Gregg, J. M., and Sibley, D. F., 1984, Epigenetic dolomitization and the origin of xenotopic dolomite texture: Journal of Sedimentary Petrology, v. 53, p. 908-931.

Gregory, H. E., 1917, Geology of the Navajo country: U.S. Geol. Survey Prof. Paper 93, p. 42.

Gregory, H.E. with Moore, R.C., 1917, The Kaiparowits: A Geographic Reconnaissance of Parts of Utah and Arizona, 1931: #188, The San Juan. United States Geological Survey Professional Papers #93, #164.

Hanshaw, B.B., and Hill, G.A., 1969, Geochemistry and hydrodynamics of the Paradox Basin region, Utah, Colorado and New Mexico: Chemical Geology, v. 4, p. 263-294.

Hasiotis, S.T., 2002. Continental Trace Fossil Short Course Number 51. SEPM, Tulsa, Oklahoma, p. 132.

Hazel, J.E., Jr., 1994, Sedimentary response to intrabasinal salt tectonism in the upper Triassic Chinle Formation, Paradox Basin: USGS National Survey 2000.

Howell, E.R., and Blakey, R.C., 2013, Sedimentological constraints on the evolution of the Cordilleran arc: New insights from the Sonsela Member, Upper Triassic Chinle Formation, Petrified Forest National Park (Arizona, USA): Geological Society of America Bulletin, v. 125, p. 1349-1368.

Hudec, M.R. and Jackson, M.P.A., 2007, Terra infirma: Understanding salt tectonics: Earth Science Reviews, v. 82, p. 1–28.

Ingersoll, Raymond V., Thomas F. Bullard, Richard L. Ford, Joel P. Grimm, John D. Pickle, and Steven W. Sares. 1984, The Effect of Grain Size on Detrital Modes: A Test of the Gazzi-Dickinson Point-Counting Method: Journal of Sedimentary Research, v. 54, p. 103–16.

Kent, D.V., and Tauxe, L., 2005, Corrected Late Triassic Latitude for Continents Adjacent to the North Atlantic: Science, v. 307, p. 240-244.

Kluth, C.F., and DuChene, H.R., 2008, Late Pennsylvanian and Early Permian Structural Geology and Tectonic History of the Paradox Basin and Uncompahgre Uplift, Colorado and Utah, in W.S. Houston, L.L. Wray, and P.G. Moreland, eds., The Paradox Basin Revisited – New Developments in Petroleum Systems and Basin Analysis: RMAG 2009 Special Publication– The Paradox Basin, p. 178-197.

Lawton, T.F., 1994, Tectonic setting of Mesozoic sedimentary basins, Rocky Mountain region, United States, in Caputo, M.V., Peterson, J.A., and Franczyk, K.J., eds., Mesozoic Systems of the Rocky Mountain Region, USA: Denver, Colorado, Society for Sedimentary Geology, Rocky Mountain Section, p. 1-25.

Lawton, T. F., and Buck, B. J., 2006, Implications of diapir-derived detritus and gypsic paleosols in Lower Triassic strata near the Caste Valley salt wall, Paradox Basin, Utah: Geology, v. 34, p. 885-888.

Lucas, S.G., Heckert, A. B., Estep, J.W., and Andgerson, O.J., 1997, Stratigraphy of the upper Triassic Chinle Group, Four Corners Region: New Mexico Geological Society Guidebook, 48th Field Conference p. 81-107.

Mack, G. H., and K. A. Rasmussen, 1984, Alluvial-fan sedimentation of the Cutler Formation (Permo-Pennsylvanian), near Gateway, Colorado: Geological Society of America Bulletin, v. 95, p. 109–116.

Martz, J.W., Irmis, R.B., and Milner, R.C., 2014, Lithostratigraphy and biostratigraphy of the Chinle Formation (upper Triassic) in souther Lisbon Valley, southeastern Utah, in MacLean, J.S., Biek, R.F., and Huntoon, J.E., eds, Geology of Utah's Far South: Utah Geological Association Publication 43, p. 397-448.

Matthews, W.J., Hampson, G.J., Trudgill, B.D., and Underhill, J.R., 2007, Controls on fluviolacustrine reservoir distribution and architecture in passive salt-diapir provinces: Insights from outcrop analogs: AAPG Bulletin, v. 91, p.1367-1403.

McFarland, J.C., 2016, Structural and Stratigraphic Development of a Salt-Diapir Shoulder, Gypsum Valley, Colorado [M.S. Thesis] El Paso, University of Texas at El Paso, p. 107.

Miall, A.D., 1978, Facies types and vertical profile models in braided river deposits: A summary *in* Miall, A.D., ed., Fluvial Sedimentology: Canadian Society of Petroleum Geologists Memoir, v. 5, p. 597-604.

Miall, A. D., 1996, The geology of fluvial deposits: Sedimentary facies, basin analysis, and petroleum geology: Berlin, Springer-Verlag.

Miall, A.D., and Arush, M., 2001, Cryptic sequence boundaries in braided fluvial successions: Sedimentology, v. 48, p. 971-985.

Ohlen, H.R. and Mcintyre, L.B., 1965, Stratigraphy and tectonic features of the Paradox Basin, four corners area. AAPG Bulletin, v.49, p. 2020–2040.

Parrish, J.M., and Good, S.C., 1987, Preliminary report on vertebrate and invertebrate fossil occurrences, Chinle Formation (Upper Triassic), southeastern Utah: in Campbell, J.A., ed., Geology of Cataract Canyon and Vicinity: Four Corners Geological Society, Tenth Field Conference Guidebook, p. 109-115.

Pipiringos, G.N., and O'Sullivan, R.B.,1978, Principal unconformities in Triassic and Jurassic rocks: western interior United States –preliminary report USGS pp 1035-A 29.

Powel, J.W., 1876, Report on the geology of the eastern portion of the Uinta Mountains: U.S. geol. And Geog. Survey Terr., 2d div. p. 53, 68-69.

Prochnow, S.J., 2005, Paleosols as an Indicator of Ancient Landscapes, Climates and Stratal Response during the Triassic: The Salt Anticline Region of Utah, [PhD Dissertation] Waco, Baylor University, p. 130.

Prochnow, S.J, Atchley, S.C., Boucher, T.E, Nordt, L.C., and Hudec M.R, 2006, The influence of salt withdrawal subsidence on palaeosol maturity and cyclic fluvial deposition in the Upper Triassic Chinle Formation: Castle Valley, Utah: Sedimentology, v. 53, p. 1319-1345.

Riggs, N.R., Reynolds, S.J., Linder, P.J., Howell, E.R., Barth, A.P., Parker, W.G., and Walker, J.D., 2013, The early Mesozoic Cordilleran arc and Late Triassic paleotopography: The detrital record in Upper Triassic sedimentary successions on and off the Colorado Plateau: Geosphere, v. 9, p. 602-613.

Shanley, K.W. and McCabe, P.J., 1994, A perspective on the sequence stratigraphy of continental strata of continental strata: AAPG Bulletin, v. 78, p. 544-568.

Shawe, D.R., Simmons, G.C. and Archbald, N.L., 1968, Stratigraphy of Slick Rock District and vicinity San Miguel and Dolores Counties, CO: U.S. Geol. Survey Prof. Paper 576-A.

Shock, A.L., 2012, Origin and implication of Permian and Triassic Diagenetic Caprock adjacent to diapiric salt walls, Paradox Basin, Utah [M.S. thesis]: Las Cruces, New Mexico State University, p. 105.

Stevenson, G.M., and Baars, D.L., 1986, The Paradox: a pull-apart basin of Pennsylvanian age, in J.A. Peterson, ed., Paleotectonics and Sedimentation in the Rocky Mountain Region, United States: AAPG memoir 41, p. 513-539.

Stewart, J.H., Poole, F.G., and Wilson, R.F., 1972, Stratigraphy and Origin of the Chinle Formation and Related Upper Triassic Strata in the Colorado Plateau Region: United States Geological Survey Special Paper 691, p. 336.

Stokes, W.L., and Phoenix, D.A.,1948, Geology of the Egnar-Gypsum Valley area, San Miguel and Montrose Counties, Colorado: United States Geological Survey Oil and Gas Inv., Prelim. Map 93.

Trudgill, B.D., and Paz, M., 2009, Restoration of Mountain Front and Salt Structures in the Northern Paradox Basin, SE Utah, in W.S. Houston, L.L. Wray, and P.G. Moreland, eds., The Paradox Basin Revisited – New Developments in Petroleum Systems and Basin Analysis: RMAG 2009 Special Publication – The Paradox Basin, p. 132-177.

Trudgill, B.D, 2011, Evolution of salt structures in the northern Paradox Basin: controls on evaporate deposition, salt wall growth and supra-salt stratigraphic architecture: Basin Research, v. 23, p.208-238.

Warren, J., 1999. Evaporites: Their Evolution and Economics: Blackwell Science, Oxford. P. p. 438.

Worrall, D.M., and Snelson, S., 1989, Evolution of the northern Gulf of Mexico, with emphasis on Cenozoic growth faulting and the role of salt *In*: Bally, A., Palmer, A. (Eds.), The Geology of North America—An Overview. Geological Society of America, Boulder, Colorado, p. 97–138 (v. A).

Appendix 1

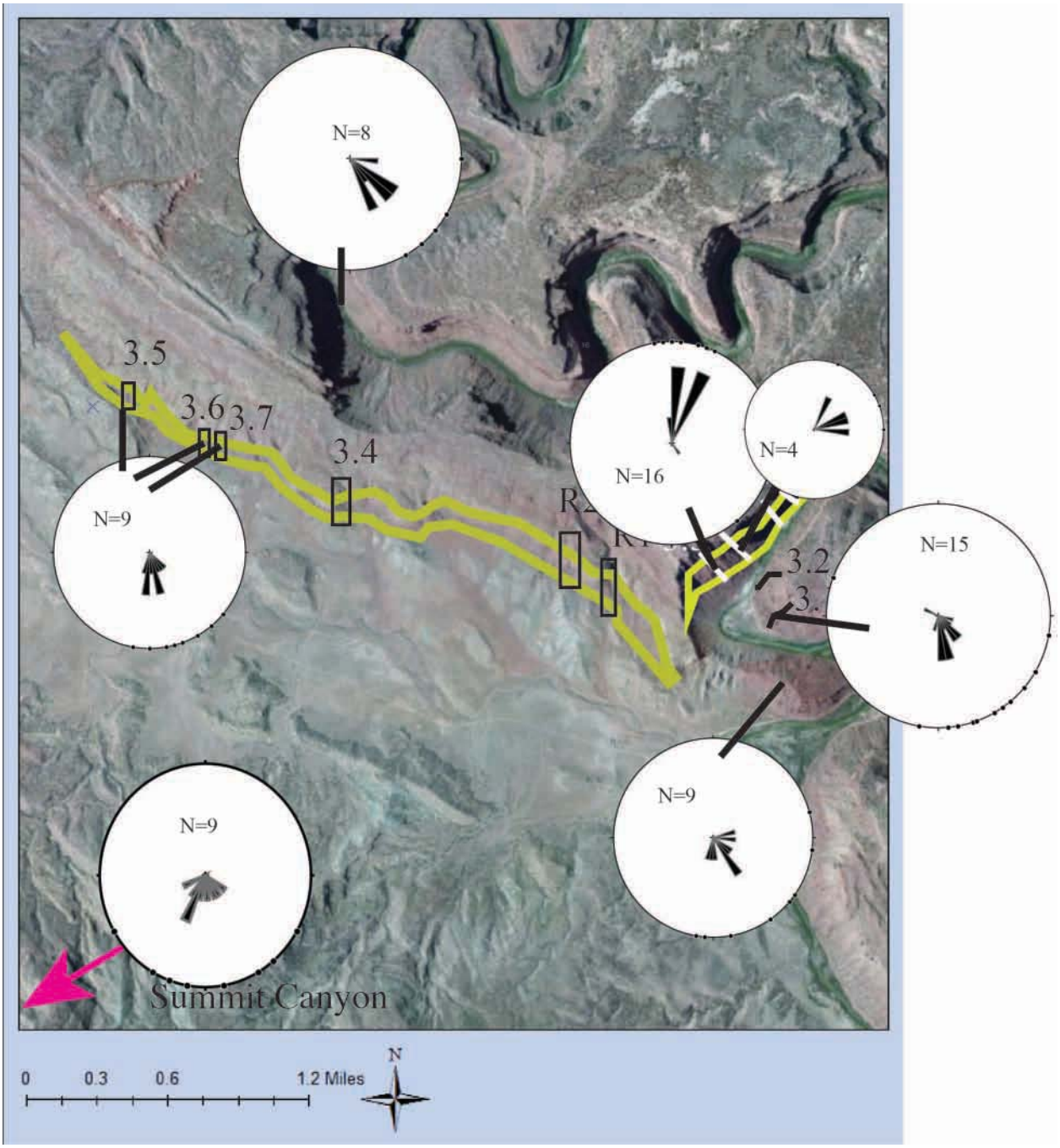

Paleocurrent Data for Chinle Formation

Appendix 2

Locations of Stratigraphic Sections in Bridge Canyon and the Box Canyon Transect

			Sandstones			
Coordinates						Grains
X	Y	Dist from diapir	Slot	ID	PetroFacies	Quartz
685226.63	4226101.61	0.55	1	BMS1	1.00	150
684795.573,	4225564.287	0.64	2	GVEH6	3.00	135
684855.243	4225659.27	0.83	3	S3S2	3.00	113
685080.77	4225880.82	0.20	4	S4S3	1.00	123
685033.980,	4225581.731	0.80	5	S5S5	2.00	110
x	x	x	10	GVEH3	x	168
684737.425,	4225151.435	0.25	19	GVEH5	3.00	124
681651.908	4226501.77	0.01	4	3.5.4	4.00	120
		12.00	7	3.8.1	5.00	141
		12	8	3.8.2	5.00	136
		12	9	3.8.4	5.00	132
		12	10	3.8.5	5.00	158
		12	11	3.8.6	5.00	130
		12	12	3.8.7	5.00	122
			13	3.8.8	5.00	154
682752	4227191	1.30	15	3.9.4	4.00	124
682752	4227191	1.30	16	3.9.5	4.00	124
682941	4226559	0.83	18	3.10.1	4.00	101
685226.63	4226101.61	1.30	24	BMS1	1.00	136
685435.202,	4225035.139	0.50	7	10.3-9	3.00	120
685435.202,	4225035.139	0.50	8	10.3-14	3.00	137
685435.202,	4225035.139	0.50	11	10.1-4	3.00	154
685435.202,	4225035.139	0.50	15	10.1-3	3.00	101
			Conglomerates			Grains
			Slot	ID	PetroFacies	Quartz
684666.532	4225478.39	0.48	2	3.3.4	6.00	61
684666.532	4225478.39	0.48	3	3.3.12	6.00	54
682141.333	4226287.4	0.01	5	3.7.4	6.00	39
682141.333	4226287.4	0.01	6	3.7.11	6.00	48
			22	GvEH4	6.00	57

			Carbonate			clay
Feldspar	Mica	Volcanics	Grains	Mud/opqu	Chert	Iron/opaque
65	7	6	15	21	3	38
59	17	0	0	44	1	0
55	26	0	0	44	4	0
60	18	15	4	32	0	23
44	16	4	12	29	0	19
69	2	10	4	11	0	18
19	2	0	0	2	45	0
33	20	15	22	34	35	16
44	2	2	9	22	13	0
54	3	4	22	14	12	0
40	3	1	33	9	18	0
37	8	5	11	15	32	0
51	5	9	9	36	14	0
36	13	16	41	27	24	0
39	2	8	34	10	22	0
43	5	5	5	16	55	0
44	14	3	45	28	23	0
27	6	7	2	58	13	7
59	13	6	0	26	32	3
47	8	15	20	27	27	3
46	1	0	46	8	10	1
51	14	15	18	22	32	1
19	8	3	5	30	5	15
			Carbonate			clay
Feldspar	Mica	Volcanics	Grains	Mud/opqu	Chert	Iron/opaque
19	8	0		17	2	44
17	4	0		17	7	42
8	0	0		22	5	29
4	1	0		4	0	0
14	5	1	20	55	4	

		rhombic				
Quartz Overg	Calcite	Dolomite	Void Filling	Isopachous	Sec. Porosity	Dissolution
15	0	39	dolo	dolo and clay	5	yes
11	14	29	dolo	dolo	1	yes
24	20	25	dolo and calc	calcite and d	13	yes
17	19	24	calcite	calcite and d	4	yes
11	15	45	dolo and calc	dolo and clay	3	yes
45	0	15	dolo	dolo	2	yes
45	0	48	dolo	dolo	62	yes
27	34	8	calcite	dolo and clay	48	yes
20	3	10	dolo	calcite	59	yes
50	6	11	dolo	calcite	60	yes
23	5	17	dolo	calcite	66	yes
30	1	7	dolo	calcite	64	yes
15	2	12	dolo	calcite	57	yes
20	1	11	dolo	calcite	49	yes
14	20	25	calcite and d	calcite	35	yes
24	69	28	calcite	dolo	8	yes
23	0	12	dolo	dolo and clay	51	yes
12	44	31	calcite and d	dolo and clay	33	yes
6	7	68	dolo and calc	clay	0	yes
10	37	39	dolo and calc	dolomite	14	yes
6	0	61	dolo	dolomite	6	yes
12	9	30	dolo and calc	dolomite	11	yes
1	33	141	dolo and calc	dolo	3	yes
		rhombic				
Quartz Overg	Calcite	Dolomite	Void Filling	Isopachous	Sec. Porosity	Dissolution
	27	134	calcite and d	dolo	10	yes
4	20	121	calcite and d	dolo and clay	50	yes
1	221	10	calcite	calcite	18	n
0	53	150	calcite and dolo		4	replaceme
	27	100	calcite and d	dolomite	24	y

Diagenesis	Percent Grai	Percent Poro	Percent Cem	Total	Depositional	Lithology
Compaction		Percent Porosity			Depositional	Quartz %
yes	69.2%	1.37%	29.40%	100.00%	FA2	60.71%
yes	82.3%	0.32%	17.36%	100.00%	FA2	53.13%
yes	74.7%	4.01%	21.30%	100.00%	FA2	48.35%
yes	74.3%	1.18%	24.48%	100.00%	FA2	48.81%
yes	69.1%	0.96%	29.90%	100.00%	FA1	51.16%
yes	76.7%	0.58%	22.67%	100.00%	FA1	63.64%
yes	55.3%	17.87%	26.80%	100.00%	FA1	88.02%
yes	67.7%	11.65%	20.63%	100.00%	FA1	55.56%
yes	71.7%	18.15%	10.15%	100.00%	FA2	66.09%
yes	64.7%	16.67%	18.61%	100.00%	FA2	58.37%
yes	66.3%	20.06%	13.68%	100.00%	FA2	60.55%
yes	69.6%	19.05%	11.31%	100.00%	FA2	67.52%
yes	73.6%	17.48%	8.90%	100.00%	FA2	54.17%
yes	75.9%	14.58%	9.52%	100.00%	FA2	47.84%
yes	72.4%	10.26%	17.30%	100.00%	FA2	62.35%
yes	66.2%	2.09%	31.68%	100.00%	FA1	70.75%
yes	71.7%	13.90%	14.44%	100.00%	FA1	55.89%
yes	62.8%	9.68%	27.57%	100.00%	FA1	53.27%
yes	76.4%	0.00%	23.60%	100.00%	FA2	61.76%
yes	71.9%	3.81%	24.25%	100.00%	FA1	55.68%
yes	77.0%	1.86%	21.12%	100.00%	FA3	59.27%
yes	82.9%	2.98%	14.09%	100.00%	FA1	60.78%
yes	47.0%	0.82%	52.20%	100.00%	FA1	61.99%
Diagenesis	Percent Grai	Percent Poro	Percent Cem	Total	Depositional	Lithology
Compaction						Quartz %
n?	33.2%	3.11%	63.66%	100.00%	FA1	58.88%
n?	29.5%	14.88%	55.65%	100.00%	FA1	61.62%
n	21.0%	5.10%	73.94%	100.00%	FA1	59.46%
n?	21.6%	1.52%	76.89%	100.00%	FA1	84.21%
n?	50.8%	7.82%	41.37%	100.00%	FA1	39.10%
	% Grains		%Porosity		%cement	
		40-49%		0-5%		0-10%
		50-59%		5.1-10%		10.1-20%
		60-69%		10.1-15%		20.1-30%
		70-79%		15.1-20%		30.1-40%
		80-100%		>20%		>40%

Based off Grain %				of Cement %	
Feldspar%	Lithic %	Total	hematite	Calcite Cement %	Calcite
25.79%	13.49%	100.00%	10.58%	14.02%	0.00%
23.05%	23.83%	100.00%	0.00%	25.93%	4.52%
22.73%	28.93%	100.00%	0.00%	28.99%	6.43%
23.81%	27.38%	100.00%	6.87%	22.89%	5.67%
20.47%	28.37%	100.00%	6.23%	16.67%	4.92%
26.14%	10.23%	100.00%	5.26%	0.00%	0.00%
9.90%	2.08%	100.00%	0.00%	0.00%	0.00%
11.83%	32.62%	100.00%	4.40%	40.00%	9.34%
18.88%	15.02%	100.00%	0.00%	9.09%	1.13%
23.18%	18.45%	100.00%	0.00%	8.96%	1.92%
18.35%	21.10%	100.00%	0.00%	11.11%	1.78%
15.81%	16.67%	100.00%	0.00%	2.63%	0.33%
21.25%	24.58%	100.00%	0.00%	6.90%	0.71%
14.12%	38.04%	100.00%	0.00%	3.13%	0.32%
15.79%	21.86%	100.00%	0.00%	33.90%	6.10%
17.00%	12.25%	100.00%	0.00%	57.02%	18.45%
16.73%	27.38%	100.00%	0.00%	33.96%	0.00%
12.62%	34.11%	100.00%	2.27%	46.81%	14.29%
21.69%	16.54%	100.00%	0.84%	8.33%	1.97%
17.80%	26.52%	100.00%	0.85%	41.57%	10.48%
18.55%	22.18%	100.00%	0.32%	0.00%	0.00%
16.67%	22.55%	100.00%	0.28%	17.31%	2.51%
11.11%	26.90%	100.00%	4.16%	17.37%	9.14%
Based off Grain %					
Feldspar%	Lithic %	Total		Calcite Cement %	
17.76%	23.36%	100.00%		13.17%	
17.17%	21.21%	100.00%		10.70%	
10.81%	29.73%	100.00%		84.67%	
7.02%	8.77%	100.00%		26.11%	
8.97%	51.92%	100.00%		21.26%	
				5/18/20165/18/20	0-25%
					25-50%
					>50%

of cement%	
Dolomite Cement%	Dolomite
36.45%	10.86%
53.70%	9.35%
36.23%	8.04%
28.92%	7.16%
50.00%	14.75%
19.23%	4.39%
51.61%	16.84%
9.41%	2.20%
30.30%	3.76%
16.42%	3.53%
37.78%	6.05%
18.42%	2.30%
41.38%	4.24%
34.38%	3.54%
42.37%	7.62%
23.14%	7.49%
22.64%	3.80%
32.98%	10.06%
80.95%	19.10%
43.82%	11.05%
89.71%	19.30%
57.69%	8.38%
74.21%	39.06%

Dolomite Cement%
65.37%
64.71%
3.83%
73.89%
78.74%

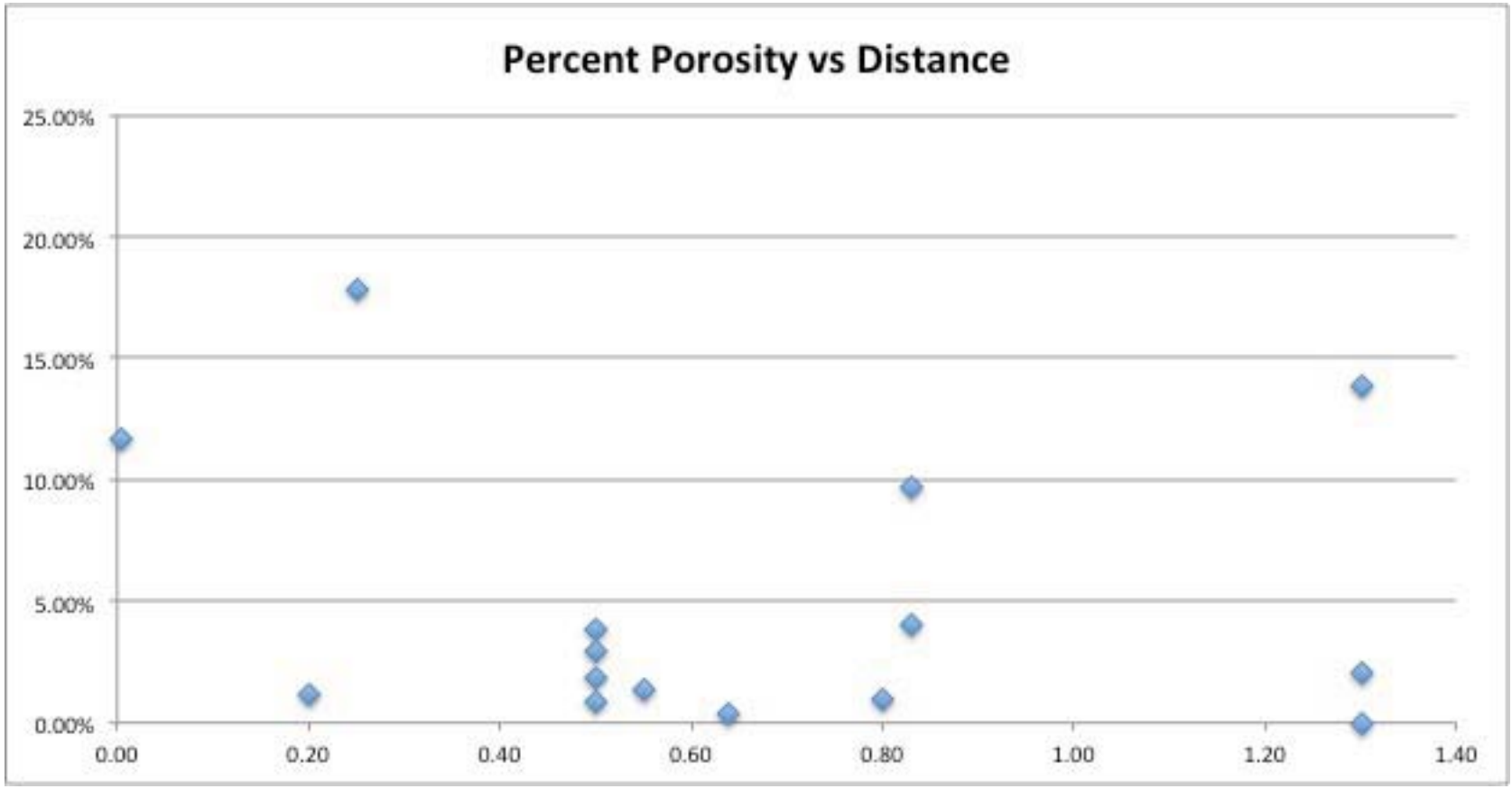
Percent Porosity vs Distance
25.00%
20.00%
15.00%
10.00%
5.00%
0.00%
0.00
0.20
0.40
0.60
0.80
1.00
1.20
1.40

Appendix 3

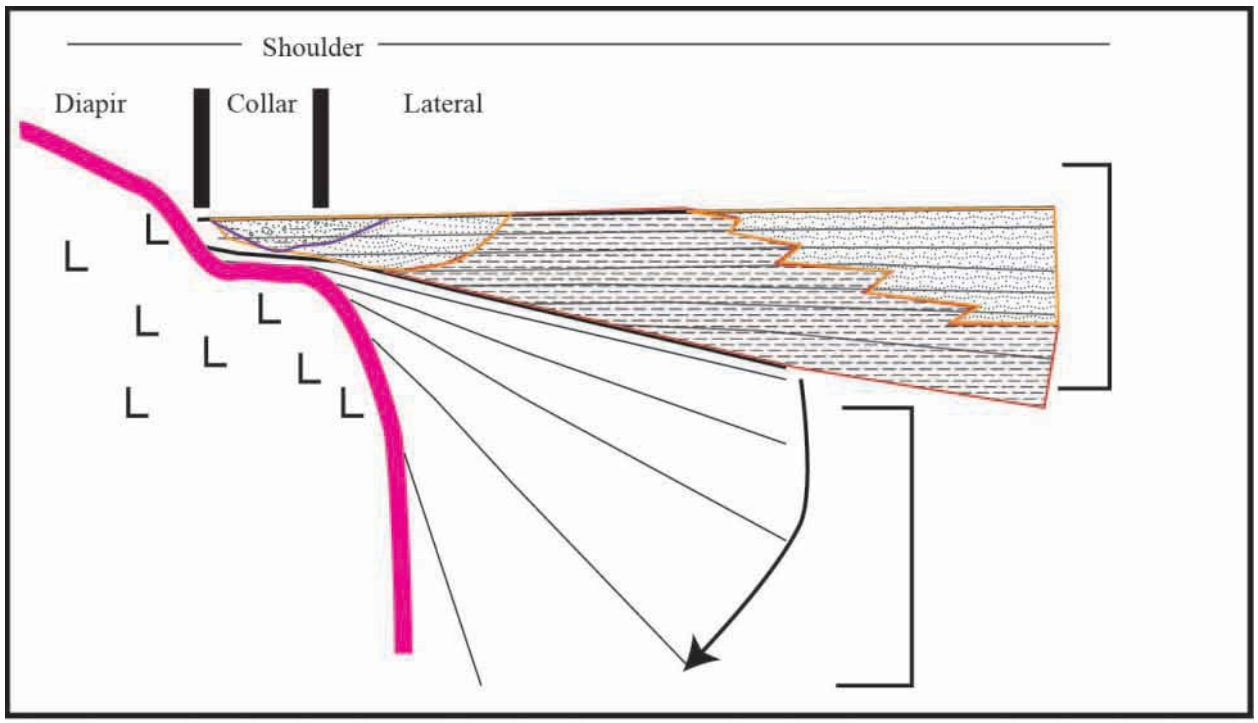

This model represents the interactions of fluvial systems against diapir margins, two sequences are pictured. As the fluvial system fills in the basin, and deposition is greater than subsidence, rivers can begin to erode the edge of the passively rising diapir, the beds thicken toward the basin and thin towards the diapir. When the subsidence of the basin outpaces deposition then strata will become tilted and eroded, creating angular unconformities between sequences.

Appendix 4

Locations of Sections

		X	Y	Distance from Diapir
	3.3	684666.532	4225478.39	0.48
S4		684771.087	4225597.71	0.68
S2		684855.243	4225659.27	0.83
S3		685080.77	4225880.82	0.20
S1		685226.63	4226101.61	1.30
	3.5	681651.908	4226501.77	0.00
	3.6	682041.032	4226315.82	0.01
	3.7	682141.333	4226287.4	0.01
	3.4	682780.988	4225956.31	0.02
R1		683981.91	4225626.87	0.25
R2		683786.924	4225736.62	0.26
	3.9	682752	4227191	1.30
Summit				12.00
3.10.		682941	4226559	

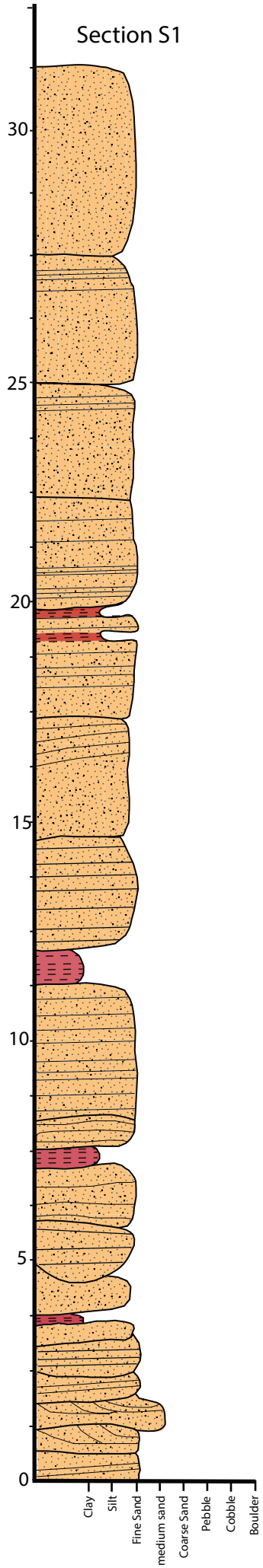
Section S1
30
25
20
15
10
5
0
Clay
Silt
Fine Sand
medium sand
Coarse Sand
Pebble
Cobble
Boulder

Section 54

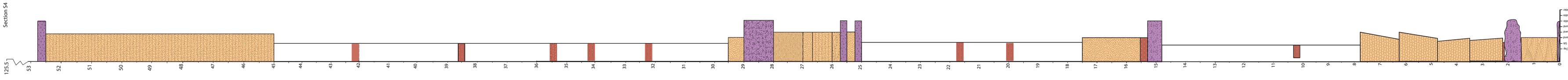
125,5
53
52
51
50
49
48
47
46
45
44
43
42
41
40
39
38
37
36
35
34
33
32
31
30
29
28
27
26
25
24
23
22
21
20
19
18
17
16
15
14
13
12
11
10
9
8
7
6
5
4
3
2
1
0
Clay
Silt
Fine sand
Medium sand
Coarse sand
Rubble
Cobble
Boulder

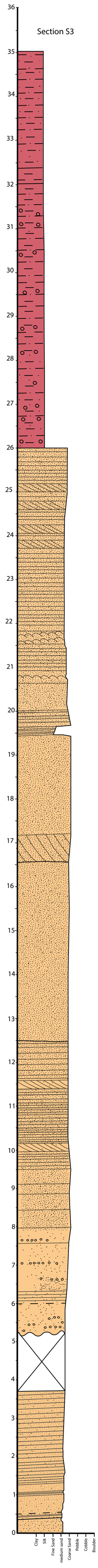
Section S3
36
35
34
33
32
31
30
29
28
27
26
25
24
23
22
21
20
19
18
17
16
15
14
13
12
11
10
9
8
7
6
5
4
3
2
1
0
Clay
Silt
Fine Sand
medium sand
Coarse Sand
Pebble
Cobble
Boulder

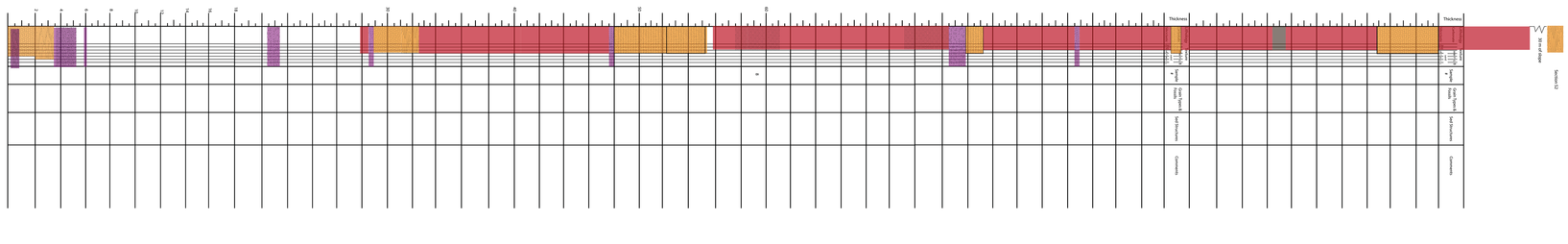
Section 12
Stratigraphic
Thickness
Thickness
Thickness
Grain Size
Sand
Silt
Clay
Sand Sorting
Poorly
Moderately
Well
Sand Structures
Comments

Section 3.5

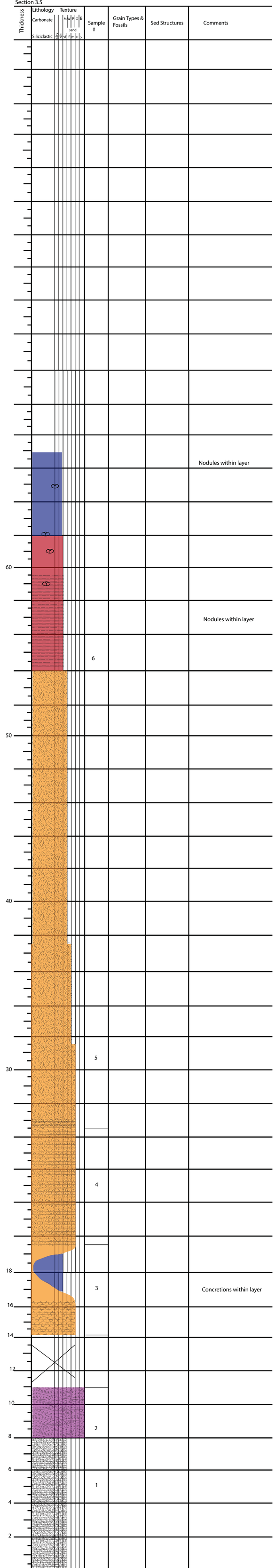
Thickness
Lithology
Carbonate
Siliciclastic
Texture
cl
si
vf
f
m
c
vc
W
W
P
G
B
sand
Sample #
Grain Types & Fossils
Sed Structures
Comments
Nodules within layer
Nodules within layer
6
5
4
3
Concretions within layer
2
1
60
50
40
30
18
16
14
12
10
8
6
4
2

Section 3.4

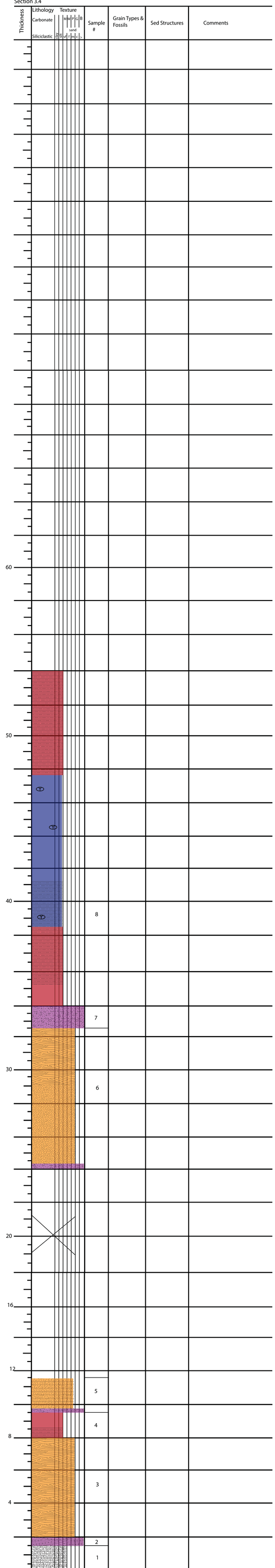
Thickness
Lithology
Carbonate
Siliciclastic
Texture
cl
si
vf
f
m
c
vc
W
P
G
B
sand
Sample #
Grain Types & Fossils
Sed Structures
Comments
60
50
40
30
20
16
12
8
4
8
7
6
5
4
3
2
1

Section 3.6

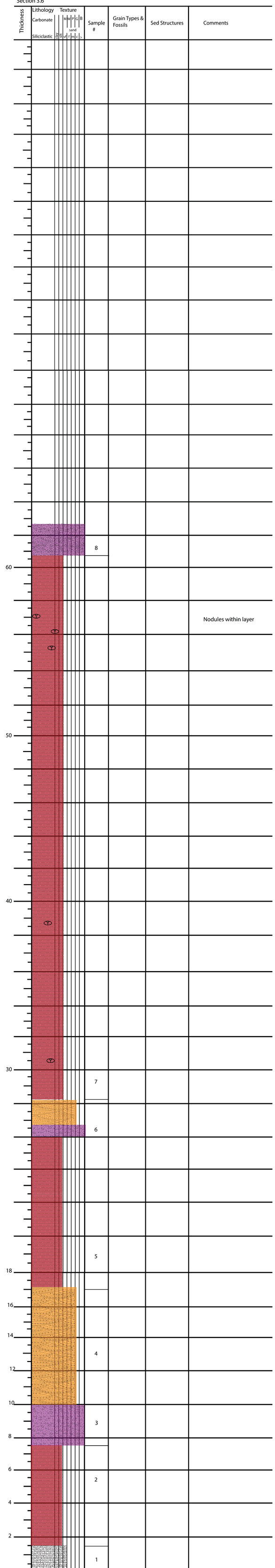
Thickness
Lithology
Carbonate
Siliciclastic
Texture
cl
si
vf
f
m
c
vc
M
W
P
G
B
sand
Sample #
Grain Types & Fossils
Sed Structures
Comments
60
50
40
30
18
16
14
12
10
8
6
4
2
8
7
6
5
4
3
2
1
Nodules within layer

Section 3.7

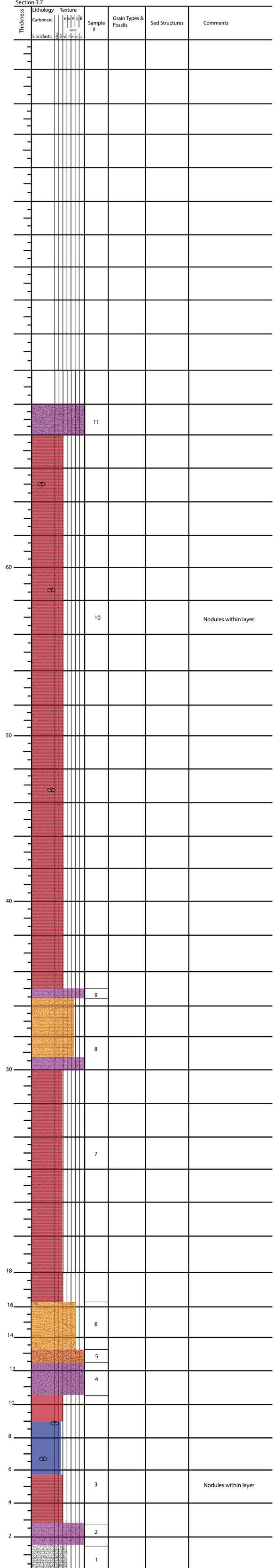
Thickness
Lithology
Carbonate
Siliciclastic
Texture
M W P G B
sand
cl si vf f m c
Sample #
Grain Types & Fossils
Sed Structures
Comments
60
50
40
30
18
16
14
12
10
8
6
4
2
11
10
Nodules within layer
9
8
7
6
5
4
3
Nodules within layer
2
1

Section R2

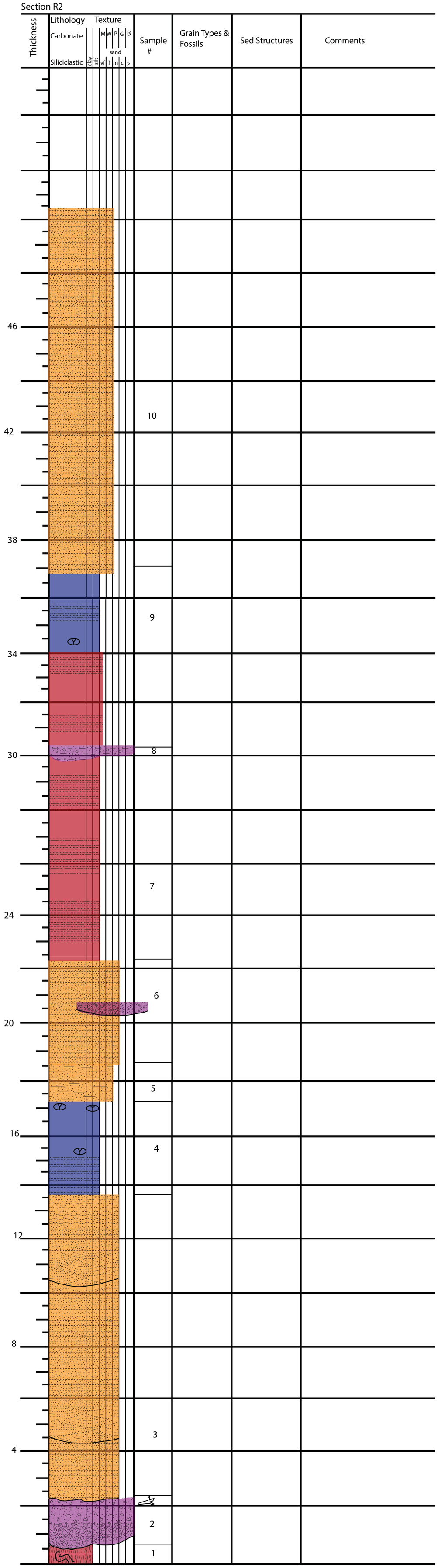
Thickness
Lithology
Carbonate
Siliciclastic
Texture
clay
silt
vf
f
m
c
>
M
W
P
G
B
sand
Sample #
Grain Types & Fossils
Sed Structures
Comments
46
42
38
34
30
24
20
16
12
8
4
10
9
8
7
6
5
4
3
2
1

Section R1

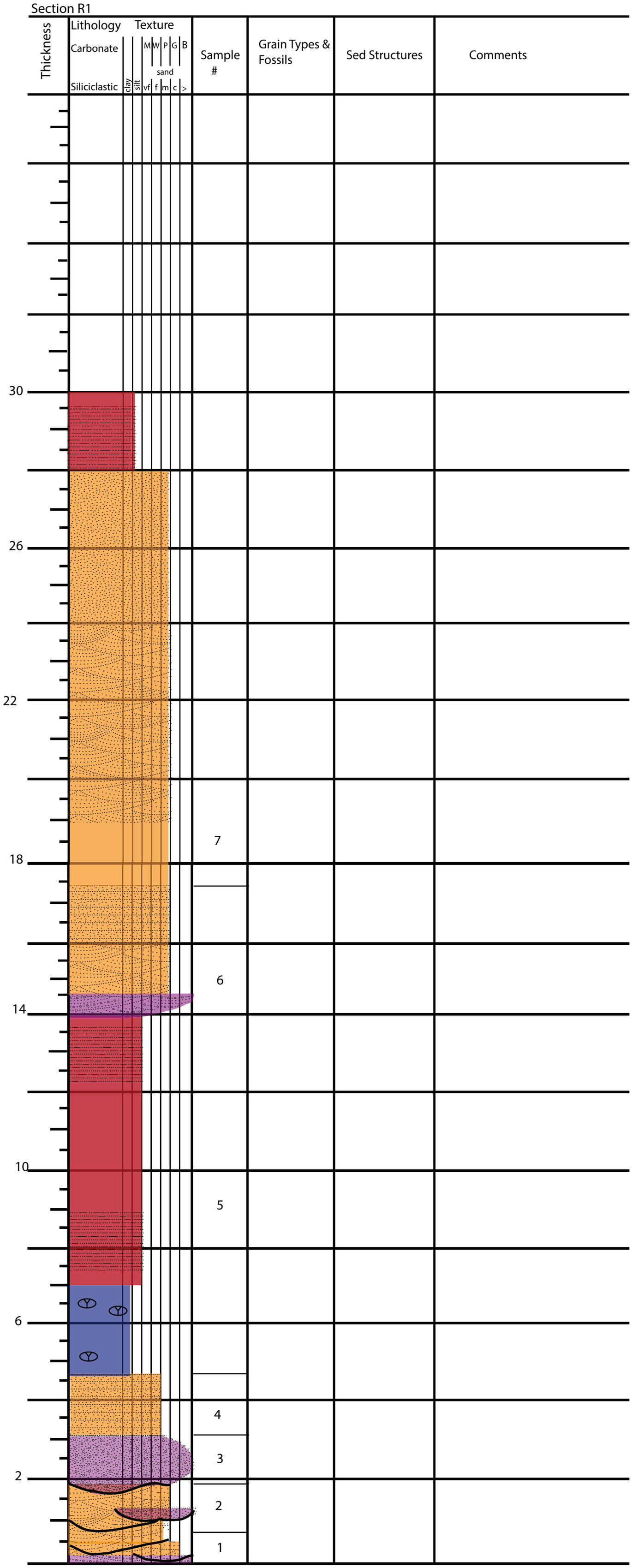
Thickness
Lithology
Carbonate
Siliciclastic
Texture
clay
silt
vf
f
m
c
>
sand
M
W
P
G
B
Sample #
Grain Types & Fossils
Sed Structures
Comments
30
26
22
18
14
10
6
2
7
6
5
4
3
2
1

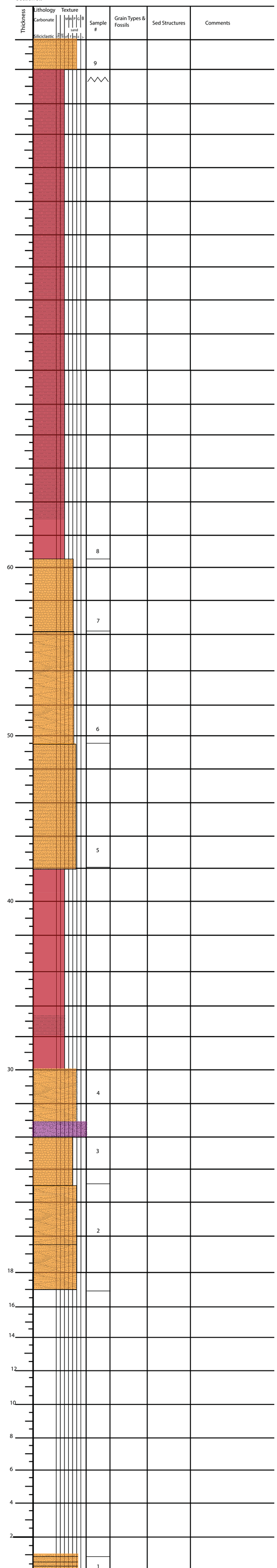
Thickness
Lithology
Carbonate
Siliciclastic
Texture
M W P G B
sand
vf f m c
Sample #
Grain Types & Fossils
Sed Structures
Comments
9
8
7
6
5
4
3
2
1
60
50
40
30
18
16
14
12
10
8
6
4
2

Summit Canyon Section 3.8

Thickness	Lithology: Carbonate / Siliciclastic	Texture: cl / si / vf / f / m / c / vc / B (sand)	Sample #	Grain Types & Fossils	Sed Structures	Comments
60						
50						
40						
30			7			
18			6			
16			5			
14			4			
12						
10			3			
8						
6			2			2. 4m upper medium grained, well sorted sandstone, medium bedded
4						
2			1			1. 2m Medium bedded, lower medium g sandstone, very well sorted

Vita

Elizabeth Anne (Liz) Heness was born March 30th 1990, in Wilkes-Barre Pennsylvania. The youngest of three children from Robert and Cynthia Heness, she graduated from Pittston Area Senior High School in 2008. Then graduated from Luzerne County Community College in 2010 with an Associate Degree in General Studies. She went on to pursue a Bachelor's of Science at Kutztown University of Pennsylvania. At Kutztown, Liz engaged in clubs on campus and undergraduate research. Holding an active role in Kutztown's Geology Club and Environmental Action Club for three years, she helped set up the annual Earth Day Celebration and engaged in group hikes all over southeastern Pennsylvania. As an undergraduate she presented research at three Geological Society of America (GSA) meetings on research in the Salton Sea, CA and Towle, South Africa. The 2012 GSA meeting is where she met Dr. Richard Langford who presented her with a SEPM best poster award in sedimentology. She received a dual BS degree in Geology and Environmental Science/Geology in May of 2013 then began her Masters of Science degree at University of Texas at El Paso (UTEP) with Dr. Richard Langford as her adviser. At UTEP she is secretary of Sigma Gamma Epsilon-Alpha Lambda chapter and an active member of UTEP's AAPG chapter. Within SGE she has volunteered with Girl Scouts and elementary schools around El Paso to teach them about fossils and other aspects of geology. She has received grants from Four Corners Geological Society and scholarships from West Texas Geological Society, SIPES Foundation. As a graduate student she worked as a teaching assistant for Sedimentology and Stratigraphy, Field Camp in Death Valley along with many other positions, held a summer internship with Chevron and, a research internship with Penn State.

Permanent address: 42 Main St. Inkerman
Pittston, PA, 18640

This thesis/dissertation was typed by Elizabeth Heness.